



People's Democratic Republic of Algeria
وزارة التعليم العالي والبحث العلمي
Ministry of Higher Education and Scientific Research
– جامعة الشهيد شيخ العربي التبسي تبسة –
Echahid Cheikh Larbi Tebessi University – Tebessa
معهد المناجم
Mining Institute
قسم المناجم والجيوتكنولوجيا
Department of mines and geotechnology
A dissertation submitted in partial fulfilment of the requirement
for the award of the degree of Master in mining engineering



Option: Geotechnics

**Investigation of Compression and Recompression
Indices in Clayey Soil Using Factorial Design
Techniques.**

By:

Hamla Chiheb Eddine

Dissertation committee:

Benghazi Zied	Chairman	MCB	Echahid Cheikh Larbi Tebessi University – Tebessa
Berrah Yacine	Supervisor	MCA	Echahid Cheikh Larbi Tebessi University – Tebessa
Brahmi Serhane	Examiner	MCB	Echahid Cheikh Larbi Tebessi University – Tebessa
Kerbati Nour Rahouadja	Examiner	MAB	Echahid Cheikh Larbi Tebessi University – Tebessa

2023/2024



Année universitaire : 2023/2024

Tébessa le : 06/06/2024


Lettre de soutenabilité

Noms et prénoms des étudiants : **Hamla Chiheb Eddine**

Niveau : 2^{ème} année Master Option : Géotechnique

Thème: Investigation of compression and recompression indices using factorial design techniques.

Nom et prénom de l'encadreur : **Berrah Yacine.**

Chapitres réalisés	Signature de l'encadreur
Chapter 1: Geological, hydrogeological and climatic conditions.	
Chapter 2: Overview on soil compressibility and parameter's predictive methods.	
Chapter 3: Geotechnical data investigation.	
Chapter 4: Experimental Design and Data Analysis in Predictive Modeling.	



الجمهورية الجزائرية الديمقراطية الشعبية

وزارة التعليم العالي و البحث العلمي

جامعة العربي التبسي - تبسة

مقرر رقم 477 مؤرخ في 09 جوان 2024

يتضمن الترخيص بمناقشة مذكرة الماستر

إن مدير جامعة العربي التبسي بتبسة،
بموجب القرار الوزاري رقم 318 و المؤرخ في 05 ماي 2021 المتضمن تعيين السيد "قواسمية عبد الكريم" مديرا
لجامعة العربي التبسي - تبسة.
و بمقتضى المرسوم التنفيذي رقم : 12-363 مؤرخ في 8 أكتوبر 2012، يعدل ويتم المرسوم التنفيذي رقم 09
- 08 المؤرخ في : 04 جانفي 2009 و المتضمن إنشاء جامعة العربي التبسي بتبسة،
و بمقتضى المرسوم التنفيذي رقم 08-265 المؤرخ في 17 شعبان عام 1429 الموافق 19 غشت سنة 2008 الذي
يحدد نظام الدراسات للحصول على شهادة الليسانس وشهادة الماستر وشهادة الدكتوراه. لاسيما المادة 9 منه،
و بموجب القرار رقم 362 المؤرخ في 09 جوان 2014 الذي يحدد كفاءات إعداد ومناقشة مذكرة الماستر. لاسيما المادة
منه.

- وبموجب القرار رقم 1380 المؤرخ في 09 أوت 2016 و المتضمن تأهيل مؤسسات التعليم العالي لضمان التكوين لنيل
شهادة الماستر اختصاص جيوتقني بعنوان السنة الجامعية 2023/2024،
و بموجب المقرر رقم 477 المؤرخ في 09 جوان 2024، و المتضمن تعيين لجنة مناقشة مذكرة الماستر.
و بعد الاطلاع على مقرر تعيين لجنة مناقشة مذكرة الماستر المؤرخ في 09 جوان 2024
يقرر ما يأتي:

المادة الأولى: يُرخصُ للطالب (ة) حملة شهاب الدين، المولود (ة) 2001/09/26 بتبسة. بمناقشة مذكرة الماستر
والموسومة بـ

Investigation of Compression and Recompression Indices in Clayey Soil Using

Factorial Design Techniques

المادة 2: يكلف رئيس قسم المناجم و الجيوتكنولوجيا. بتنفيذ هذا المقرر الذي يسلم نسخة عنه إلى الطالب المعني
بالمناقشة وأعضاء لجنة المناقشة فور توقيعه، وبضمن نشره عبر فضاءات المؤسسة المادية والرقمية.

المادة 3: تُحفظ نسخة عن هذا المقرر ضمن الملف البيداغوجي للطالب المعني وينشر في النشرة الرسمية لجامعة

العربي التبسي

حُرر ب تبسة، في 09 جوان 2024

عن المدير، وبتفويض منه

مدير معهد المناجم



مقرر رقم: 496 مؤرخ في 08 جوان 2024

يتضمن تعيين لجنة مناقشة مذكرة الماجستير

أن مدير جامعة العربي التبسي بتبسة.

- بموجب القرار الوزاري رقم 318 و المؤرخ في 05 ماي 2021 المتضمن تعيين السيد "فواسمية عبد الكريم" مديرا لجامعة العربي التبسي - تبسة،
- بموجب المرسوم التنفيذي رقم 12 / 363 مؤرخ في 8 أكتوبر 2017. يعطل ويتم المرسوم التنفيذي رقم 09 - 08 المؤرخ في 04 حانفي 2009 و المتضمن
اسم جامعة العربي التبسي بتبسة.
- وبمقتضى المرسوم التنفيذي رقم 08-265 المؤرخ في 17 شعبان عام 1429 الموافق 19 غشت سنة 2008 الذي يحدد نظام الدراسات للحصول على شهادة الليسانس
وشهادة الماجستير وشهادة الدكتوراه. لاسيما المادة 9 منه.

- وبموجب القرار رقم 362 المؤرخ في 09 جوان 2014 الذي يحدد كفاءات إعداد ومناقشة مذكرة الماجستير. لاسيما المادتان 10 و 11 منه.

- وبموجب القرار رقم 1080 المؤرخ في 13 أكتوبر 2015 والمتضمن تأهيل ماستر الفروع ذات تسجيل وطني بجامعة تبسة.

- بموجب القرار رقم 375 المؤرخ في 15 جوان 2020 المعدل للمحق القرار 1080 المؤرخ في 13 أكتوبر 2015 والمتضمن تأهيل ماستر الفروع ذات تسجيل وطني بجامعة
تبسة. اختصاص جيوتقي

وبعد الاطلاع على محضر المجلس العلمي لمعهد المناجم المؤرخ في 12 جانفي 2024

يقرر ما يأتي:

المادة الأولى: تُعيّن بموجب هذا المقرر لجنة مناقشة مذكرة الماجستير المحضرة من طرف الطالب:

حملة شهاب الدين. المولود (5) 2001/09/26 بتبسة.

والموسومة ب

Investigation of Compression and Recompression Indices in Clayey Soil Using Factorial Design Techniques

والمسجل (5) بمعهد المناجم

المادة 2: تتشكل اللجنة المشار إليها في المادة الأولى من الأعضاء الآتي ذكرهم:

رقم	الاسم واللقب	الرتبة	مؤسسة الانتماء	الصفة
1	بن غازي زياد	أستاذ محاضر ب	جامعة العربي التبسي - تبسة	رئيسا
2	براح ياسين	أستاذ محاضر - أ	جامعة العربي التبسي - تبسة	المؤطر
3	كرياطي نور	أستاذ مساعد- ب	جامعة العربي التبسي - تبسة	ممتحنا
4	براهمي سرحان	أستاذ محاضر ب	جامعة العربي التبسي - تبسة	ممتحنا

المادة 3: يكلف رئيس قسم المناجم والجيوتكنولوجيا بتنفيذ هذا المقرر الذي يُسلم نسخة عنه إلى كل من الطالب المعني والمشرف على المذكرة وأعضاء لجنة المناقشة فور توقيعه

المادة 4: تحفظ نسخة عن هذا المقرر في الملف البيداغوجي للطلاب المعني. وينشر في النشرة الرسمية لجامعة العربي التبسي.

حُرر ب تبسة، في:

عن المدير، وبتفويض منه

مدير معهد المناجم



الجمهورية الجزائرية الديمقراطية الشعبية
وزارة التعليم العالي والبحث العلمي

مؤسسة التعليم العالي : جامعة الشهيد الشيخ العربي التبسي - تبسة

تصريح شرفي
خاص بالالتزام بقواعد النزاهة العلمية لانجاز بحث

أنا الممضي أدناه،

السيد (ة) ..حصوله...دكتوراه...الدرجة...العلمية...الدرجة...العلمية...الدرجة...العلمية...
الحامل لبطاقة التعريف الوطنية رقم : 1.5.6.1.0.2.0.7.4... و الصادرة بتاريخ 2023/12/30.....
المسجل بمعهد...البحوث...قسم...العلوم...البيئية...البيئية...
و المكلف بانجاز أعمال بحث (مذكرة التخرج، مذكرة ماستر، مذكرة ماجستير، أطروحة دكتوراه)، عنوانها :
Investigation of compression and recompression indices using.....
factorial design techniques.....

أصرح بشرفي أنني ألتزم بمراعاة المعايير العلمية و المنهجية و معايير الأخلاقيات المهنية و النزاهة الأكاديمية
المطلوبة في انجاز البحث المذكور أعلاه.

09 جوان 2024

التاريخ:.....



UNIVERSITÉ LARBI TEBESSI - TEBESSA

INSTITUT des Mines

تبريسا في 2024/2024



جامعة العربي التبسي-تبسة

معهد المناجم

رقم: 539/ج.ع.ت.م.م/2024

رفع التحفظات

اسم و لقب الأستاذ المناقش: جريجور جرجان
عنوان المذكرة: Investigation of compression and recompression
Indices in clayey soil using factorial design techniques.

الطلبة:

1- حمالة شهاب ليريش

2-

التخصص: جريجور جرجان، القسم: المناجم والجيولوجيا

موافق على وضع المذكرة في المكتبة بعد إجراء التصحيح المطلوب

موافق على وضع المذكرة في المكتبة و هي معفية من التصحيح

إمضاء الأستاذ المناقش

Acknowledgment

I express my deep gratitude and my sincere thanks to my supervisor

Dr. BERRAH YACINE for his confidence, his support and his understanding, his sense of scientific appreciation, his rigor for a job well done, his relevant suggestions in research and above all his availability.

I thank all the professors of Mining Department.

I would like to thank all those who directly or indirectly contributed to the realization of this dissertation.

DEDICATIONS

This modest work is the fruit of several years of hard work and tireless sacrifices; I dedicate it to:

To my dear mother and my dear father.

To all my brothers, who are always by my side when I need them.

To all my family and loved ones.

To my dear friends who contributed massively to the success of my student life and who were my second family and who helped me during my university period.

To all the group of geotechnical engineering 2024, as well as all the groups of the department. Finally, to all those I love, those who love me and respect me from near or far.



Hamla Chiheb Eddine

Abstract

The compressibility of clayey soils is a crucial aspect of geotechnical engineering, particularly in Tebessa province where settlement issues are prevalent. This dissertation investigates soil compression indices using full factorial design (FFD) techniques embedded within the well-known design of experiment (DoE) methodology. Physical and mechanical data has been collected from the studied area, including geological and hydrogeological studies, theoretical frameworks, numerical simulation and advanced statistical methods. The study employs various statistical predictive tools to accurately define compression and recompression indices (C_c and C_s), as well as the overconsolidation ratio (OCR). Principal Component Analysis (PCA) and regression analysis distill complex data sets into meaningful insights. The DoE methodology, including FFD and Response Surface Methodology (RSM), facilitates systematic investigation and optimization of experimental conditions to obtain the best-fit predictive models with high correlation coefficients R of 0.85 up to 0.93 for all different obtained models, it is concluded from this investigation that the main input parameters C_c , C_s and OCR are dependent parameters yielded high correlation to Atterberg limits void ration and dry unit weight and initial vertical stress. For the validation step in this investigation, samples were prepared from the studied area and analyzed in a soil mechanics laboratory to obtain the target parameters for model dependency. The obtained results aligned accurately with those issue from models using the mentioned methodology. Numerical simulations using finite element analysis confirmed very close settlement results compared to those calculated using the predictive models for the compression indices of the studied soil.

Keywords: Compressibility, Soil compression indices, Geotechnical data, OCR, optimization.

Résumé

La compressibilité des sols argileux est un aspect crucial de l'ingénierie géotechnique, en particulier dans la province de Tébessa où les problèmes de tassement sont répandus. Cette thèse étudie les indices de compression du sol à l'aide de techniques de plan factoriel complet intégrées à la méthodologie bien connue du plan d'expérience. Des données physiques et mécaniques ont été collectées dans la zone étudiée, notamment des études géologiques et hydrogéologiques, des cadres théoriques, des simulations numériques et des méthodes statistiques avancées. L'étude utilise divers outils statistiques prédictifs pour définir avec précision les indices de compression et de recompression (C_c et C_s), ainsi que le taux de surconsolidation. L'analyse en composantes principales (ACP) et l'analyse de régression distillent des ensembles de données complexes en informations significatives. La méthodologie conception d'expériences, y compris la méthodologie plan factoriel complet et la méthodologie de surface de réponse, facilite l'investigation systématique et l'optimisation des conditions expérimentales pour obtenir les modèles prédictifs les mieux adaptés avec des coefficients de corrélation élevés R de 0,85 à 0,93 pour tous les différents modèles obtenus, conclut-on. Cette étude selon laquelle les principaux paramètres d'entrée C_c , C_s et OCR sont des paramètres dépendants a donné une forte corrélation avec les limites d'Atterberg, le taux de vides, le poids unitaire sec et la contrainte verticale initiale. Pour l'étape de validation de cette enquête, des échantillons ont été préparés dans la zone étudiée et analysés dans un laboratoire de mécanique des sols afin d'obtenir les paramètres cibles pour la dépendance au modèle. Les résultats obtenus s'alignent avec précision sur ceux issus des modèles utilisant la méthodologie mentionnée. Les simulations numériques par analyse par éléments finis ont confirmé des résultats de tassement très proches de ceux calculés à l'aide des modèles prédictifs des indices de compression du sol étudié.

Mots clés : Compressibilité, Indices de compression du sol, Données géotechniques, OCR, optimisation.

ملخص

تُعد قابلية انضغاط التربة الطينية جانباً مهماً في الهندسة الجيوتقنية، وخاصة في ولاية تبسة حيث تنتشر مشاكل الاستقرار. تبحث هذه الأطروحة في مؤشرات ضغط التربة باستخدام تقنيات التصميم العامل الكامل المدمجة ضمن منهجية التصميم التجريبي المعروفة. تم جمع البيانات الفيزيائية والميكانيكية من المنطقة المدروسة، بما في ذلك الدراسات الجيولوجية والهيدرولوجية، الأثر النظرية، المحاكاة العددية والأساليب الإحصائية المتقدمة. تستخدم الدراسة أدوات إحصائية تنبؤية متنوعة لتعريف مؤشرات الانضغاط وإعادة الانضغاط (Cc) و (Cs) بدقة، بالإضافة إلى نسبة التراكب الزائد. تقوم تحليل المكونات الرئيسية والتحليل النحاري بتبسيط مجموعات البيانات المعقدة إلى رؤى مفيدة. تتيح منهجية، بما في ذلك ومنهجية استجابة السطح، التحقيق المنهجي وتحسين الظروف التجريبية للحصول على نماذج تنبؤية بأفضل مالءة ومعاملات ارتباط عالية تتراوح بين 0.85 و 0.93 لجميع النماذج المختلفة التي تم الحصول عليها. في خطوة التحقق في هذا التحقيق، تم تحضير عينات من المنطقة المدروسة وتحليلها في مختبر ميكانيكا التربة للحصول على المعلومات المستهدفة للاعتماد على النموذج. تطابقت جميع التحقق بدقة مع النماذج التي تم الحصول عليها باستخدام المنهجية المذكورة. أكدت المحاكاة العددية باستخدام تحليل العناصر المحدودة نتائج الاستقرار القريبة جداً مقارنة بتلك المحسوبة باستخدام النماذج التنبؤية لمؤشرات الانضغاط للتربة المدروسة.

الكلمات المفتاحية: قابلية الانضغاط، مؤشرات ضغط التربة، بيانات الجيوتكنيك، OCR، تحسين.

Contents

General Introduction	1
Chapter I: Overview on soil compressibility and parameter's predictive tools.	
I.1. Introduction	4
I.2. Consolidation	4
I.2.1. One dimensional consolidation test	5
I.2.2. Compression & recompression indices discussion and prediction in literature	7
I.2.2.1. Compression Index	7
I.2.2.2. Recompression Index	8
I.2.2.3. Prediction and Modeling	8
I.3. Design of experiments	10
I.3.1. Brief history of design experiments	11
I.3.2. The main uses of DOE	12
I.3.3. DOE techniques	13
I.3.3.1. Randomized complete block design	13
I.3.3.2. Factorial design	15
I.3.3.3. Response surface methodology	17
I.3.3.4. Taguchi	19
I.4. Statistics uses	22
I.4.1. Principal component analysis	22
I.4.1.1. Historical overview and basic concepts	22
I.4.1.2. Mathematical formulation	23
I.4.1.3. Applications of PCA in geotechnical engineering	23
I.4.2. Regressions	24

I.4.2.1. Historical overview and basic concepts	25
I.4.2.2. Types of Regression Models	25
I.4.2.3. Applications of regression analysis in geotechnical engineering	28
I.4.3. Finite element analysis	29
I.4.3.2. Methodologies for Predicting Soil Properties using Finite Element Analysis (FEA)	29
I.5. Conclusion	31
Chapter II: Geological, hydrogeological and climatic conditions.	
II.1. Introduction	33
II.2. Overview	33
II.3. Geographic location	34
II.4. Geology	35
II.4.1. Lithostratigraphy of Tebessa region	37
II.4.1.1. Secondary	37
II.4.1.1.1. Trias	37
II.4.1.2. Lower and middle cretaceous	38
II.4.1.2.1. Aptien	38
II.4.1.2.2. Albien	38
II.4.1.2.3. Vraconian	38
II.4.1.3. Upper cretaceous	38
II.4.1.1.3.1. Cenomanian	38
II.4.1.1.3.2. Turonian	38
II.4.1.1.3.3. Emscherian	39

II.4.1.1.3.4. Campanian	39
II.4.1.1.3.5. Maastrichtian	39
II.4.1.2. Tertiary	39
II.4.1.2.1. Paleocene	39
II.4.1.2.2 Eocene	39
II.4.1.2.3. Miocene	39
II.4.1.3. Quaternary	39
II.4.2. Tectonic	40
II.5. Hydrogeology	42
II.5.1. General description	43
II.5.2. Boundary Conditions Maps	43
II.5.3. Piezometry	45
II.5.3.1. Inventory of water points	45
II.5.3.2. Establishment of a piezometric map	46
II.6. Climatic	48
II.6.1. Climate type	48
II.6.2. Precipitations	49
II.6.2. Temperatures	51
II.7. Conclusion	51
Chapter III: Geotechnical data investigation.	
III.1. Introduction	52
III.2. Presentation of geotechnical soil data in the region studied	52
III.2.1. Implementation of boreholes	53

III.3. Identification and classification of the soils studied	56
III.3.1. Granulometry of the soils studied (grain size)	56
III.3.2. Atterberg limits	59
III.4. Tests and results	60
III.5. Conclusion	76
Chapter IV: Experimental design and data analysis in predictive modeling.	
IV.1. Introduction	77
IV.2. Materials and methods	77
IV.2.1. Principal component analysis	77
IV.2.2. Design of experiments	80
IV.2.2.1. Input and output parameters	81
IV.3. DOE and data implementation	83
IV.4. Results and discussion	85
IV.4.1. Full factorial design	85
IV.4.2. Response surface methodology	93
IV.4.3. Optimisation	100
IV.4.4. Overconsolidation ration and preconsolidation pressure predicting	102
IV.4.5. Validation of the equations	107
IV.4.5.1. Settlement calculation	108
IV.4.5.2. Plaxis Modeling	108
IV.4.5.2.1. Data Introduction	109
IV.4.5.2.1.1. The geometric model	109
IV.4.5.2.1.2. Material properties	110
IV.4.5.2.2. Mesh Generation	112
IV.4.5.2.3. Phasing	113

IV.4.5.2.4. Output	113
IV.4.5.2.5. Curves	115
IV.4.6. Results interpretation	116
IV.4.6.1. Predictive Equations and Validation	116
IV.4.6.2. Settlement Analysis	116
IV.4.6.3. Plaxis Simulation	116
IV.4.6.4. Comparison of Results	117
IV.5. Conclusion	118
General Conclusion	120

List of figures

Figure 1: (a) typical consolidation apparatus, (b) a fixed ring cell, (c) a floating ring cell.	6
Figure 2: C_c and C_s indices.	7
Figure 3: DOE application in scientific research.	12
Figure 4: Examples of RCBD experimental design.	14
Figure 5: A two-factor factorial experiment, with the response (y) shown at the corners.	15
Figure 6: A two-factor factorial experiment with interaction.	16
Figure 7: a- A factorial experiment without interaction, b- A factorial experiment with interaction.	17
Figure 8: A three-dimensional response surface showing the expected yield (η) as a function of x_1 and x_2 .	18
Figure 9: A contour plot of a response surface.	19
Figure 10: Example of Taguchi DOE for $K_{in} = 3$, $K_{out} = 2$, 23 full factorial inner array, 22 full factorial outer array.	21
Figure 11: Simple linear regression model.	26
Figure 12: Multiple linear regression model.	26
Figure 13: Polynomial regression model.	27
Figure 14: Logistic regression model.	27
Figure 15: Geographic location of the studied area.	35
Figure 16: Geological map shows the distribution of different soil and rock formations in the Tebessa region.	36
Figure 17: Schematic section of the geological formations of Tebessa region.	36
Figure 18: Synthetic stratigraphic column of the Tebessa region.	37
Figure 19: Tectonic sketch of the Tebessa region.	41

Figure 20: Hydrogeological section across the Tebessa plain.	43
Figure 21: Map of boundary conditions of the study area.	44
Figure 22: Map of boundary conditions of the study area.	45
Figure 23: The inventory map of wells on the plain (Bekkaria-Tebessa-Hammamet-Morsott).	46
Figure 24: piezometric map.	47
Figure 25: Simplified map of the climatic zones of Eastern Algeria.	49
Figure 26: Interannual variation of precipitation at the Tébéssa station (1972/2012).	50
Figure 27: Monthly temperature distribution 1972/2012.	51
Figure 28: Implementation of boreholes in the studied area.	53
Figure 29: Logs of representative surveys taken in the study area	54
Figure 30: LPC classification of fine soils, the gray dot identifies the clay of the study area.	56
Figure 31: GTR soil classification with $D_{max} < 50\text{mm}$. Source: NF P 11-300.	57
Figure 32: Projection of measurements of (LL and PI) soils studied on Casagrande abacus.	59
Figure 33: Sample 1 location (UTM: zone 32, easting 416801, and northing 3916741).	61
Figure 34: Sample 2 location (UTM: zone 32, easting 415225, and northing 3920853).	62
Figure 35: Paraffined and weighed samples.	64
Figure 36: Washing the samples through a 0.4mm sieve.	66
Figure 37: Portion of the moist soil sample in the cup of the Casagrande.	67
Figure 38: Portion of the moist soil sample in the cup of the Casagrande.	68
Figure 39: Determination of moisture content.	68

Figure 40: Liquid limit for sample 1 (LL= 66.2).	70
Figure 41: Liquid limit for sample 2 (LL= 64.5).	70
Figure 42: Sample trimming.	71
Figure 43: Sample saturation.	72
Figure 44: Set the loading frame with a loading platform.	73
Figure 45: The loads are applied using air pressure via a computer.	74
Figure 46: $e - \log(P)$ curve for sample 1.	76
Figure 47: $e - \log(P)$ curve for sample 2.	76
Figure 48: Scree plot of the data.	81
Figure 49: The variables circle of correlation.	82
Figure 50: Definition of different parameters in full factorial design.	83
Figure 51: Definition of different parameters in RSM.	83
Figure 52: Select the most effect factors for compression index.	84
Figure 53: Select the most effect factors for recompression index.	85
Figure 54: Pareto chart for C_c .	86
Figure 55: Pareto chart for C_s .	86
Figure 56: Predicted response versus actual for compression index.	89
Figure 57: Predicted response versus actual for recompression index.	89
Figure 58: Response surface 3D representing the compressibility index (C_c) vs dry unit weight γ_d and water content w .	90
Figure 59: Response surface 3D representing the compressibility index (C_c) vs liquid limit LL and the void ratio e_0 .	90

Figure 60: Response surface 3D representing the swelling index (C_s) vs dry unit weight and void ratio e_0 .	91
Figure 61: Response surface 3D representing the swelling index (C_s) vs saturation degree S_r and water content w .	92
Figure 62: Predicted response versus actual for compression index.	96
Figure 63: Predicted response versus actual for recompression index.	96
Figure 64: Response surface 3D representing the compressibility index (C_c) vs dry unit weight γ_d and water content w .	97
Figure 65: Response surface 3D representing the compressibility index (C_c) vs liquid limit LL and void ratio e_0 .	98
Figure 66: Response surface 3D representing the swelling index (C_s) vs water content w and liquid limit LL.	98
Figure 67: Response surface 3D representing the swelling index (C_s) vs liquid limit LL and void ratio e_0 .	99
Figure 68: Maximization of the responses.	103
Figure 69: Minimization of the responses.	104
Figure 70: Predicted response versus actual for OCR.	107
Figure 71: Response surface 3D representing the OCR vs liquid limit LL and void ratio e_0 .	108
Figure 72: Response surface 3D representing the OCR vs swelling index C_s and void ratio e_0 .	108
Figure 73: General settings.	111
Figure 74: The geometric model.	112
Figure 75: Material properties of the soil.	113
Figure 76: Model of adding material properties.	113
Figure 77: Surface load $\Delta P = 150\text{kPa}$.	114

Figure 78: Surface load applied.	114
Figure 79: Mesh generation.	115
Figure 80: Vertical displacement $U_z = 13.54\text{cm}$ for sample 1.	116
Figure 81: Vertical displacement $U_z = 10.32\text{cm}$ for sample 2.	116
Figure 82: Vertical displacement curve for sample 1.	117
Figure 83: Vertical displacement curve for sample 2.	117

List of tables

Table 4: Empirical correlations for the compression ratio.	9
Table 5: Empirical correlations for the recompression ratio.	10
Table 6: Example of RCBD experimental design for $k = 2$, $L_1 = 3$, $L_2 = 4$, $N = 12$, nuisance factor X_1 , primary factor X_2 .	14
Table 7: Taguchi designs synoptic table.	21
Table 1: Average monthly precipitation (mm) at Tebessa (1972/2012).	49
Table 2: Wet years during the period (1972-2012).	50
Table 3 : Température moyenne mensuelle 1972/2012.	51
Table 8: Synthesis of soil geotechnical characteristics of the study area.	52
Table 9: Fine Soil Classification (GTR) Standard NF P 11 – 300.	56
Table 10: Water content results.	61
Table 11: Unit weight results.	63
Table 12: Liquid limit results for sample 1.	67
Table 13: Liquid limit results for sample 2.	67
Table 14: Oedometer test results for sample 1.	72
Table 15: Oedometer test results for sample 2.	73
Table 16: Needed results of all tests.	75
Table 17: Eigenvalue table and accumulated proportion of principal component analysis of 193 data samples.	78
Table 18: Factor loadings correlations between variables and factors	78
Table 19: Summary statistics of the collected data set.	82
Table 20: Factors for response study.	82
Table 21: Results of ANOVA model for compression index.	87
Table 22: Results of ANOVA model for recompression index.	88
Table 23: Regression statistics for compression index.	88
Table 24: Regression statistics for recompression index.	89
Table 25: Model fit summary for C_c .	93
Table 26: Model fit summary for C_s .	94
Table 27: ANOVA for response surface quadratic model for compressibility index.	94
Table 28: ANOVA for response surface quadratic model for swelling index.	95

Table 29: Regression statistics for recompression index.	96
Table 30: Regression statistics for recompression index.	96
Table 31: Factors for response study.	103
Table 32: Model fit summary for Cc.	103
Table 33: ANOVA for response surface quadratic model for OCR.	104
Table 34: Regression statistics for OCR.	104
Table 35: Obtained results from the equations	107
Table 36: Comparison between calculated and predicted results.	108
Table 37: Settlement results.	108
Table 38 : Finale settlement results.	117

List of Indices

γ_d	Dry unit weight
γ_h	Wet unit weight
w	Water content %
F_f	Fine friction < 0,08mm
F_c	Fine friction < 0,02mm
LL	Liquid limit
PI	Plasticity index
e_0	Initial void ratio
D_{max}	Maximum diameter
A	Activity ($I_p / < \text{fraction } 0,02\mu\text{m}$)
VBS	Methylene blue value
C_c	Compression index
C_s	Recompression / Swelling index
P_c	Preconsolidation pressure
P_s	Swelling pressure
OCR	Overconsolidation ratio
$CaCo_3$	Percentage of Calcium Carbonate
Gypse	Gypsum percentage
RSM	Response surface methodology
FFD	Full factorial design
CCD	Centrale composite design

General introduction

Understanding the compressibility of sediments and deposits, such as clays and fine-grained soils, is a cornerstone of geotechnical engineering. Compressibility reflects the relationship between void ratio and effective stress due to loads transmitted from foundations. Given that settlement is heavily influenced by compressibility, accurately defining compression and recompression indices through oedometer tests is paramount. Despite their reliability, these tests are time-intensive, require undisturbed samples, and incur significant costs. In Tebessa province, settlement issues are prevalent, often causing significant structural damage or functional impairment due to differential settlements. This master's dissertation aims to investigate compressibility in Tebessa area using a combined approaches that includes sample collection, laboratory testing, data collection, numerical modeling, and statistical analysis.

Statistical methods are crucial in geotechnical investigations, aiding in data identification treatment, analysis, categorization and decision-making. In this study, statistical tools such as Principal Component Analysis (PCA) and regression analysis are employed to distill complex datasets into meaningful insights and establish relationships between variables affecting soil compression parameters especially those findings in literature that highly correlate to the chosen input parameter. The Design of Experiments (DoE) methodology is integral to this study, facilitating a systematic investigation of factors affecting soil compression parameters. By using factorial design and Response Surface Methodology (RSM), we efficiently explore interactions between multiple variables such as unit weights, void ratio, moisture content, Atterberg limits and fraction of fines and some others as input physical parameters simple to achieve in laboratory, related to output parameters such as compression indices and overconsolidation ratio.

The Full Factorial Design (FFD) approach comprehensively examines all possible combinations of factors and their levels, providing a robust framework for identifying significant factors and their interactions, leading to a thorough understanding of soil compressibility. RSM is used to optimize experimental conditions and develop predictive

models, fitting a surface to the experimental data to identify optimal conditions for minimal soil compression and establish a prediction equation for future scenarios.

Accurate data collection and treatment are fundamental to the success of this study. Geotechnical data regarding soil properties, environmental conditions, and loading scenarios are meticulously gathered and processed to ensure the reliability and validity of the results. The materials and methods section outlines the systematic approach taken in this research, covering the implementation of DoE, FFD, and RSM techniques, along with optimization and validation processes. The prediction equations derived from the experimental data are validated through simulation and settlement estimation, ensuring their practical applicability, where Finite Element Analysis (FEA) is utilized to simulate clayey soil behavior under different loading conditions, visualizing stress distribution and deformation patterns to complement empirical data.

To accomplish this work, the dissertation has been meticulously structured into four comprehensive chapters, general introduction and conclusion as follows:

- **Chapter 1:** Presents the theoretical foundations necessary for understanding soil compressibility phenomena, then covers advanced statistical methods, including Principal Component Analysis (PCA), the design of experiments (DoE) methodology, with a use the Full Factorial Design (FFD) and Response Surface Methodology (RSM) for optimizing experimental conditions and developing predictive models.
- **Chapter 2:** This chapter provides an in-depth overview of the studied area, starting with a description of its geographical location and environmental setting. It then delves into the geological characteristics, including stratigraphy, hydrogeological, hydrological and climatic context.
- **Chapter 3:** outlines the systematic approach to data collection and classification. It describes the procedures for gathering geotechnical data, including soil sampling and lab testing. The chapter details the classification of the collected data based on soil type and properties. Laboratory testing methods are comprehensively

discussed, with a focus on oedometer tests for determining soil compressibility and Atterberg limits for assessing soil plasticity.

- **Chapter 4:** presents the results obtained from the analysis of the collected data. It includes detailed models and equations derived from statistical and numerical analyses, illustrating the relationships between various soil properties and their compression indices. The chapter also discusses the validation of these models using independent datasets and numerical simulations. The accuracy and reliability of the predictive models are evaluated through comparison with observed settlement and finite element analysis results.

Chapter I:

**Overview on Soil Compressibility
and Parameter's Predictive Tools.**

I.1. Introduction

In the realm of geotechnical studies, the phenomena of consolidation and settlement pose significant challenges in ensuring the stability of structures built upon soils. Understanding the intricate processes of soil behavior under load is essential for engineers and researchers to devise effective solutions for mitigating potential risks associated with consolidation and settlement (Yune, C. Y., & Olgun, C. G. 2016). Over the years, researchers have turned to the power of statistical analysis and advanced programming techniques to delve deeper into these phenomena, offering insights that inform the design and implementation of robust engineering solutions (Naqvi, M. W. et al 2023). This introduction sets the stage to explore how research endeavors have harnessed the tools of statistics and programming to tackle the complexities of consolidation and settlement in geotechnical engineering. Through rigorous analysis and innovative computational methods, researchers have endeavored to enhance our understanding and management of these critical aspects, thereby contributing to the advancement and sustainability of infrastructure worldwide.

I.2. Consolidation

All soils are compressible, in that they undergo volume changes when they are subjected to changes in the stresses applied to them. The resulting compressions can be particularly large when the drainage is not impeded, but their magnitudes are of engineering significance only when reference is made to the deformations which are tolerable for a given type of structure. The magnitude and rate of the deformation depend on the type of soil and on the nature of the applied loads. The introduction of Terzaghi's consolidation theory (Terzaghi, 1923), is considered by many to be the birth of modern soil mechanics. Since then, a great number of contributions have been made. All of these have attempted to improve the capability of predicting the magnitude and rate of settlement and the rate of excess pore pressure dissipation by introducing more refined soil models and less restricted assumptions on the parameters describing these models (Naqvi, M. W. et al 2023). The availability of electronic computing facilities has relatively recently created a boom in the application of numerical techniques, among which the finite element method has proved to be a most versatile and useful tool (Zienkiewicz, O. C., & Taylor, R. L.

2005). Methods to determine the relevant soil parameters in the laboratory and in the field have also been improved, although the progress in this respect has not kept pace with the analytical techniques. Most recently, attempts have also been made to employ probabilistic techniques, because one of the inherent difficulties in achieving more accurate predictions of the settlement process lies in the variability of the soil parameters. (Balasubramaniam, A. S., & Brenner, R. P. 1981).

I.2.1. One dimensional consolidation test

The one-dimensional consolidation test, called the Oedometer test, serves to determine various parameters including C_c , C_s , C_a , C_v , and m_v (Budhu, M. 2010). Additionally, it allows for the calculation of hydraulic conductivity, k_z , based on the gathered data. The apparatus and procedures for conducting the test are elaborated in XP P 94-090-1. In this test, a soil disk is contained within a rigid metal ring and positioned between two porous stones immersed in water within a cylindrical vessel, shown in Figure 1. A metal load platen mounted on top of the upper porous stone transmits the applied vertical stress (vertical total stress) to the soil sample. Both the platen and the upper porous stone can vertically displace within the ring as the soil settles under the applied stress. The ring containing the soil sample may be either secured to the vessel by a collar or left unrestrained. Incremental loads, including unloading sequences, are applied to the platen, and the settlement of the soil at fixed intervals under each load increment is gauged using a displacement gauge. Each load increment persists until soil settlement stabilizes and excess pore water pressure dissipates, typically within 24 hours for most soils but possibly longer for certain types like montmorillonite. Load increments are doubled, and the ratio of each increment to the previous one is termed the load increment ratio (LIR), traditionally set at LIR=1. To determine C_s , the soil sample undergoes unloading using a load decrement ratio of 2 relative to the current load. (Das, B. M., & Sobhan, K. 2012; Budhu, M. 2010).

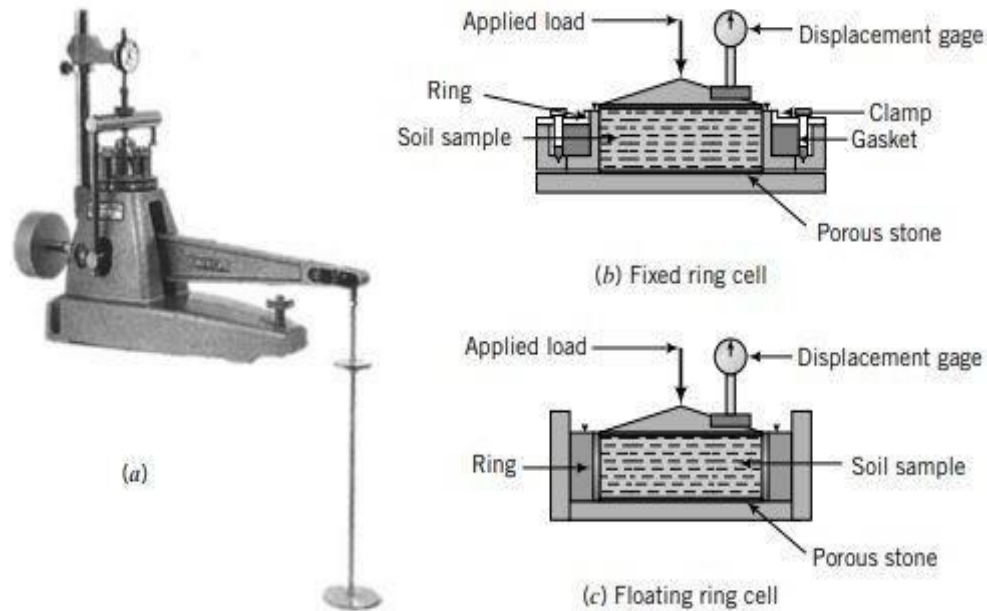


Figure 1: (a) typical consolidation apparatus, (b) a fixed ring cell, (c) a floating ring cell. (Budhu, M. 2010).

Upon completion of the Oedometer test, the apparatus is disassembled, and the water content of the sample is determined. It is advisable to reduce the pressure on the soil sample to a minimal level before disassembly. This precaution is necessary because complete removal of the final consolidation load can result in a negative excess pore water pressure equivalent to the final consolidation pressure. Such negative pressure may induce water influx into the soil, elevating its water content. Consequently, the calculated final void ratio derived from the ultimate water content would be inaccurate (Das, B. M., & Sobhan, K. 2012; Been, K., & Sills, G. C. 1981).

The data obtained from the one-dimensional consolidation test are as follows:

1. Initial height of the soil, H_0 , which is fixed by the height of the ring.
2. Current height of the soil at various time intervals under each load (time–settlement).
3. Water content at the beginning and at the end of the test, and the dry weight of the soil at the end of the test.

Now have to use these data to determine C_c and C_s , because they are the coefficients with which this dissertation is concerned. Once the void ratio–pressure curve

(e - $\log(p)$) plotted, the slope of the loading part is the C_c coefficient, while the slope of the unloading part is C_s .

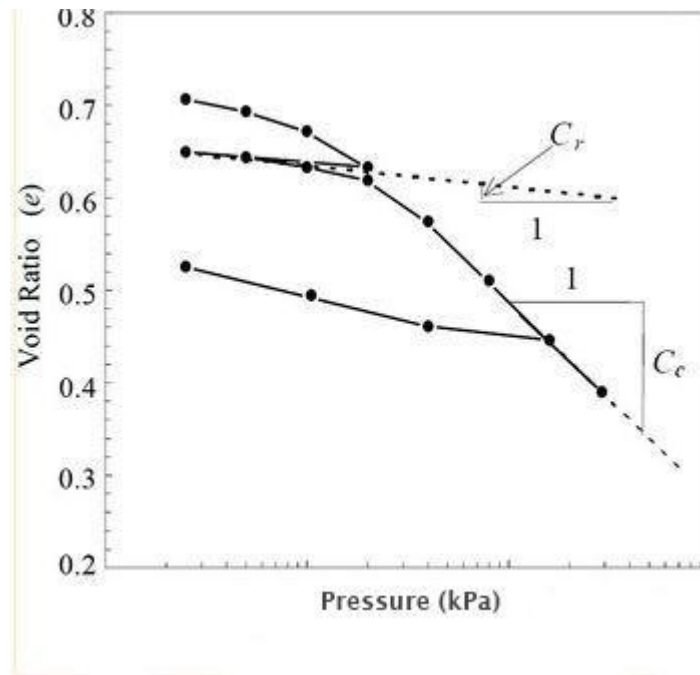


Figure 2: C_c and C_s indices.

I.2.2. Compression and recompression indices discussion and prediction in literature

The compression and recompression indexes are crucial parameters in geotechnical engineering, particularly in the analysis of soil behavior under various loads and conditions. The literature highlights the importance of accurately predicting these indexes to ensure the stability and safety of structures built on or in soil.

I.2.2.1. Compression Index (C_c)

- The compression index (C_c) is a measure of the compressibility of a soil under a given load. It is a critical parameter in predicting the settlement of structures on or in soil (Alzabeebee, S., & Al-Taie, A. 2022; Kim, Y. et al 2022; Erzin, Y. 2020; Kurnaz, T. F. et al 2016; Gunduz, Z., & Arman, H. 2007).

- The C_c is influenced by various soil properties, including the initial void ratio, liquid limit, natural water content, and plasticity index (Erzin, Y. 2020; Gunduz, Z., & Arman, H. 2007).
- Researchers have employed various methods to predict the C_c , including regression analysis and robust optimization models. These methods have shown promise in improving the accuracy of predictions compared to traditional empirical formulas (Erzin, Y. 2020; Gunduz, Z., & Arman, H. 2007).

I.2.2.2. Recompression Index (Cr)

- The recompression index (C_r) is another important parameter that describes the soil's behavior during the recompression phase after a previous load has been removed. It is essential for understanding the long-term settlement behavior of structures (Alzabeebee, S., & Al-Taie, A. 2022; Kim, Y. et al 2022; Erzin, Y. 2020; Kurnaz, T. F. et al 2016; Gunduz, Z., & Arman, H. 2007).
- The C_r is also influenced by soil properties, but its relationship with these properties is less well understood compared to the C_c . This is reflected in the lower correlation coefficients (R^2) reported for C_r predictions using regressions (Kurnaz, T. F. et al 2016).
- The literature suggests that the C_r is more challenging to predict accurately due to the complex interactions between soil properties and the recompression process (Kurnaz, T. F. et al 2016).

I.2.2.3. Prediction and Modeling

- Techniques like design of experiments, regression analysis, and principal component analysis could potentially be employed to explore the complex relationships between the input parameters and the compression/recompression indexes, and to identify the most influential factors (Long, T. 2023; Erzin, Y. 2020).
- The development of accurate models for predicting the compression and recompression indexes is crucial for the design and analysis of structures in soil. Researchers have employed various approaches, including neural network and robust optimization models, to improve the accuracy of predictions (Erzin, Y. 2020; Kurnaz, T. F. et al 2016).

- These models have been shown to be effective in reducing the uncertainty associated with the measurements of input parameters and in improving the overall accuracy of predictions (Erzin, Y. 2020).

- The literature highlights the need for further research in this area to better understand the relationships between soil properties and the compression and recompression indexes, as well as to develop more robust and accurate prediction models (Alzabeebee, S., & Al-Taie, A. 2022; Kim, Y. et al 2022; Erzin, Y. 2020; Kurnaz, T. F. et al 2016; Gunduz, Z., & Arman, H. 2007).

Table 1: Empirical correlations for the compression ratio (Ameratunga, J., et al 2016).

Correlation	Comments	References
$C_c = 0.009 (LL-10)$	Undisturbed clay of sensitivity less than 4. Reliability $\pm 30\%$	Terzaghi and Peck (1948)
$C_c = 0.007 (LL-10)$	Remoulded clay	Skempton (1944)
$C_c = 0.0046 (LL-9)$	Sao Paulo, Brazil clays	Cozzolino (1961)
$C_c = 0.0186 (LL-30)$	Soft silty Brazilian clays	Cozzolino (1961)
$C_c = 0.01 (LL-13)$	All clays	USACE (1990)
$C_c = 0.008 (LL-8.2)$	Indiana soils	Lo and Lovell (1982)
$C_c = 0.21 + 0.008 LL$	Weathered & soft Bangkok clays	Balasubramaniam and Brenner (1981)
$C_c = 0.30 (e_0 - 0.27)$	Inorganic silty clay	Hough (1957)
$C_c = 1.15(e_0 - 0.35)$	All clays	Azzouz et al. (1976)
$C_c = 0.75(e_0 - 0.50)$	Soils of very low plasticity	Azzouz et al. (1976)
$C_c = 0.4(e_0 - 0.25)$	Clays from Greece & parts of US	Azzouz et al. (1976)
$C_c = 0.141G_s^{1.2} \left(\frac{1+e_0}{G_s}\right)^{2.382}$	90 samples; Bowles (1988) suggests e_0 be less than 0.8	Rendon-Herrero (1980)
$C_c = 0.256 + 0.43(e_0 - 0.84)$	Brazilian clays	Cozzolino (1961)
$C_c = 0.54 (e_0 - 0.35)$	All clays	Nishida (1956)
$C_c = 0.22 + 0.29 e_0$	Weathered and soft Bangkok clays	Balasubramaniam and Brenner (1981)
$C_c = 0.575 e_0 - 0.241$	French clays	Balasubramaniam and Brenner (1981)

Table 2: Empirical correlations for the recompression ratio (Ameratunga, J., et al 2016).

Soil type	Correlation	References
Marine clays of southeast Asia	$CR = 0.0043 w_n$	Azzouz et al. (1976)
	$CR = 0.0045 LL$	Balasubramaniam and Brenner (1981)
Bangkok clays	$CR = 0.00463LL - 0.013$	Balasubramaniam and Brenner (1981)
	$CR = 0.00566 w_n - 0.037$	
French clays	$CR = 0.0039 w_n + 0.013$	Balasubramaniam and Brenner (1981)
Indiana clays	$CR = 0.0249 + 0.003 w_n$	Lo and Lovell (1982)
	$CR = 0.0294 + 0.00238 LL$	
	$CR = 0.0125 + 0.152e_0$	
Indiana clays	$CR = 0.2037(e_0 - 0.2465)$	Goldberg et al. (1979)
Clays from Greece & parts of US	$CR = 0.002 (LL + 9)$	Azzouz et al. (1976)
	$CR = 0.14(e_0 + 0.007)$	
	$CR = 0.003 (w_n + 7)$	
	$CR = 0.126(e_0 + 0.003LL - 0.06)$	
Chicago clays	$CR = 0.208 e_0 + 0.0083$	Azzouz et al. (1976)
Inorganic & organic clays and silty soils	$CR = 0.156 e_0 + 0.0107$	Elnaggar and Krizek (1970)

I.3. Design of experiments

Predicting soil properties accurately is inherently challenging due to the complex and heterogeneous nature of soil. Traditional empirical methods often lack the precision and efficiency required for reliable predictions, leading to uncertainties in design and construction processes (Kurmi, P. et al 2023). In recent years, there has been a growing interest in applying advanced statistical methodologies, particularly Design of Experiments (DOE), to enhance the accuracy and efficiency of soil property prediction in geotechnical engineering (Kumar, V. et al 2023).

Design of Experiments offers a systematic approach for planning, conducting, and analyzing experiments to efficiently explore the effects of various factors on the response of interest. By strategically selecting experimental factors and levels, DOE enables researchers to optimize experimental designs, reduce the number of required experiments, and identify significant factors affecting the response variable (Kumar, V. et al 2023). When combined with sophisticated statistical software such as Design Expert, DOE

becomes a powerful tool for predictive modeling and optimization in geotechnical engineering.

I.3.1. Brief history of design experiments

The history of Design of Experiments (DOE) can be traced back to the early 20th century, with significant contributions from pioneering statisticians and scientists who laid the foundation for modern experimental design methodologies. While the concept of experimentation dates back much further, the systematic approach to planning and analyzing experiments emerged during the early development of statistical theory. Sir Ronald A. Fisher (1890–1962): Fisher, a British statistician and geneticist, is often credited as the father of modern experimental design. In the 1920s and 1930s, Fisher developed the principles of randomized experiments and analysis of variance (ANOVA). His seminal works, including "The Design of Experiments" (1935), introduced revolutionary concepts such as randomization, replication, and factorial designs. Fisher's contributions laid the groundwork for DOE and established its fundamental principles. (Durakovic, B. 2017).

Even though DOE tools are not new, their use in scientific domains such as product/process quality improvement, product optimization, and services has grown significantly during the last 20 years. Trainings and new, user-friendly statistical software packages, both commercial and non-commercial, made a major contribution to the expansion of DOE in this period's study. Figure 3 depicts the use of DOE worldwide and in a range of scientific fields between 1920 and 2018 (Durakovic, B. 2017).

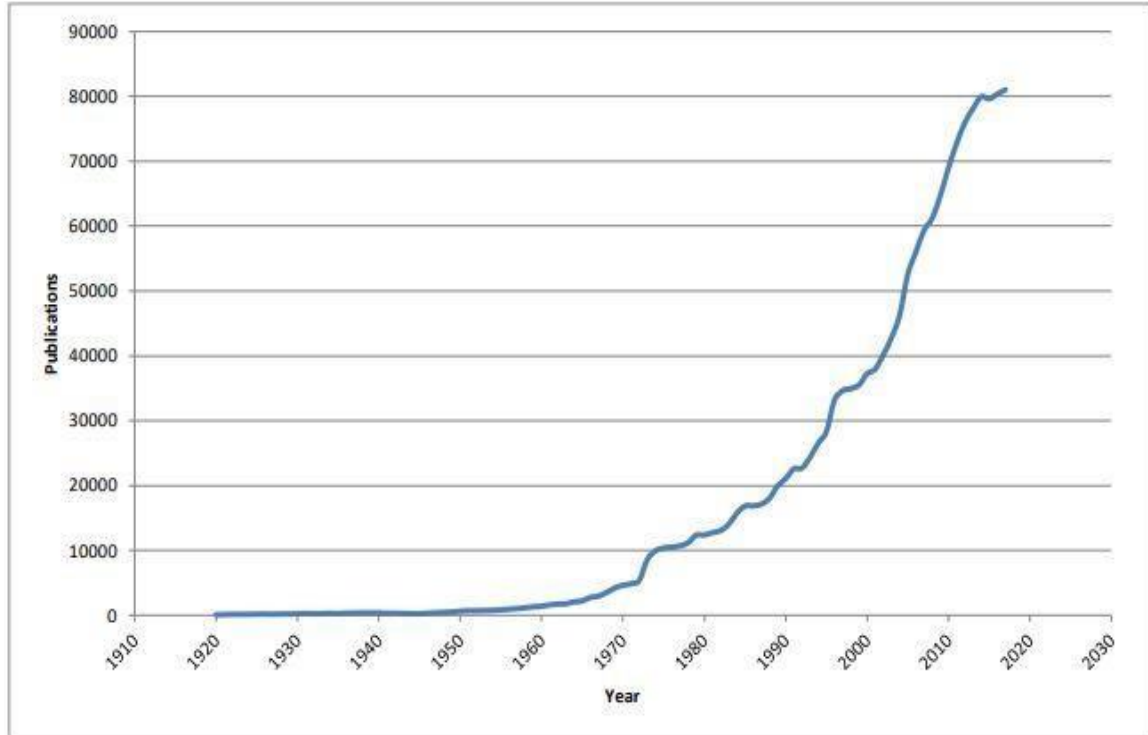


Figure 3: DOE application in scientific research (Durakovic, B. 2017).

Experimental design methods have been widely applied in a variety of disciplines. Experimentation may be viewed as part of the scientific process and one method for learning how systems or processes work. In general, learning is accomplished by a series of actions that include making conjectures about a process, conducting experiments to generate data from the process, and then using the information from the experiment to build new conjectures, which lead to new experiments, and so on.

I.3.2. Main uses of DOE

An experiment's design is a versatile instrument that can be applied in a variety of contexts to determine key input variables and the relationships between them and the outputs (response variable). Regression analysis is essentially what DOE is, and it may be applied in a variety of contexts (Telford, J. K. 2007) (Durakovic, B. 2017). The following design types are frequently utilized:

- Comparison: This is one factor in multiple comparisons using t-test, Z-test or F-test to choose the best option.

- Variable Screening: These are typically two-level factorial designs designed to select from a number of important factors (variables) that influence the performance of a response (output).
- System Optimization: Transfer functions can be used to optimize by moving the experiment to the optimal setting of the variables. In this way, the performance of the response can be improved.
- Robust Design: Focus on reducing variation in a system or process (response) without eliminating its causes. The rugged design was developed by Dr. Genichi Taguchi, who made the system robust to noise (environmental factors and uncontrollable factors are considered noise).

I.3.3. DOE techniques

In this section some DOE techniques are presented and discussed. The list of the techniques considered is far from being complete since the aim of the section is just to introduce the reader into the topic showing the main techniques which are used in practice.

I.3.3.1. Randomized complete block design

Randomized Complete Block Design (RCBD) is a DOE technique based on blocking. In an experiment there are always several factors which can affect the outcome. Some of them cannot be controlled, thus they should be randomized while performing the experiment so that on average, their influence will hopefully be negligible. Some other are controllable (Emerson, R. W., & Cavazzuti, M. 2017). RCBD is useful when we are interested in focusing on one particular factor whose influence on the response variable is supposed to be more relevant. We refer to this parameter with the term primary factor, design factor, control factor, or treatment factor. The other factors are called nuisance factors or disturbance factors. Since we are interested in focusing our attention on the primary factor, it is of interest to use the blocking technique on the other factors, that is, keeping constant the values of the nuisance factors, a batch of experiments is performed where the primary factor assumes all its possible values. To complete the randomized block design such a batch of experiments is performed for every possible combination of the nuisance factors. Let us assume that in an experiment there are k controllable factors X_1, \dots, X_k and one of

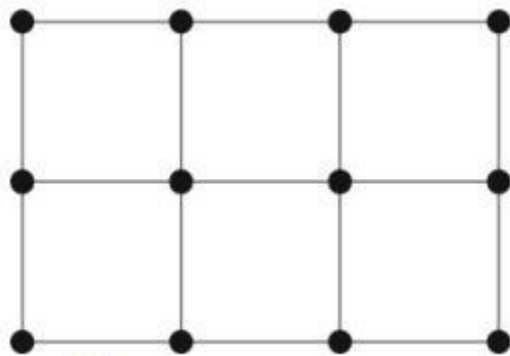
them, X_k , is of primary importance. Let the number of levels of each factor be L_1, L_2, \dots, L_k . If n is the number of replications for each experiment, the overall number of experiments needed to complete a RCBD (sample size) is $N = L_1 \cdot L_2 \cdot \dots \cdot L_k \cdot n$. In the following we will always consider $n = 1$. Let us assume: $k = 2, L_1 = 3, L_2 = 4$, X_1 nuisance factor, X_2 primary factor, thus $N = 12$. Let the three levels of X_1 be A, B , and C , and the four levels of X_2 be α, β, γ , and δ . The set of experiments for completing the RCBD DOE is shown in table 3. Other graphical examples are shown in figure 4.

Table 3: Example of RCBD experimental design for $k = 2, L_1 = 3, L_2 = 4, N = 12$, nuisance factor X_1 , primary factor X_2 (Emerson, R. W., & Cavazzuti, M. 2017).

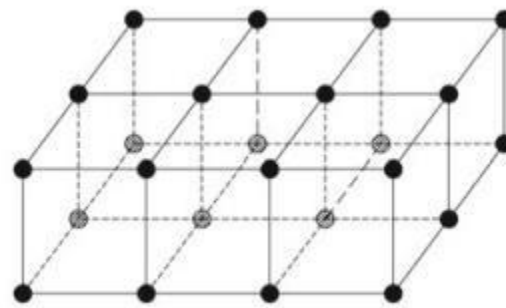
Experiment Number		Factor Level	
		X_1	X_2
Block 1	1	A	α
	2	A	β
	3	A	γ
	4	A	δ
Block 2	5	B	α
	6	B	β
	7	B	γ
	8	B	δ
Block 3	9	C	α
	10	C	β
	11	C	γ
	12	C	δ

\Rightarrow

		X_2			
		$A\alpha$	$A\beta$	$A\gamma$	$A\delta$
X_1	B	$B\alpha$	$B\beta$	$B\gamma$	$B\delta$
	C	$C\alpha$	$C\beta$	$C\gamma$	$C\delta$



(a) $k = 2, L_1 = 4, L_2 = 3, N = 12$



(b) $k = 3, L_1 = 4, L_2 = 2, L_3 = 3, N = 24$

Figure 4: Examples of RCBD experimental design (Emerson, R. W., & Cavazzuti, M. 2017).

I.3.3.2. Factorial design

Numerous experiments entail exploring the impacts of multiple factors. Typically, factorial designs prove to be the most effective for such investigations. With a factorial design, every complete trial or replication (repetition of the entire experiment) of the experiment scrutinizes all conceivable combinations of the factor levels. For instance, if there are 'a' levels of factor A and 'b' levels of factor B, each replication encompasses all 'ab' treatment combinations. When factors are organized within a factorial design, they are commonly referred to as being crossed (Montgomery, D. C. 2017; Durakovic, B. 2017).

The influence of a factor is defined as the change in response caused by changes in the level of the factor. This is often called the 'main effect' because it refers to the main factor of interest in the experiment. For example, consider the simple experiment in Figure 5. This is a two-factor experiment, with both design factors at two levels. We call these values "low" and "high" and label them "-" and "+" respectively. The main effect of factor A in this two-level design can be thought of as the difference between the mean response at low levels of A and the mean response at high levels of A (Montgomery, D. C. 2017), numerically, this is

$$A = \frac{40 + 52}{2} - \frac{20 + 30}{2} = 21$$

That is, increasing factor A from the low level to the high level causes an average response increase of 21 units. Similarly, the main effect of B is

$$B = \frac{30 + 52}{2} - \frac{20 + 40}{2} = 11$$

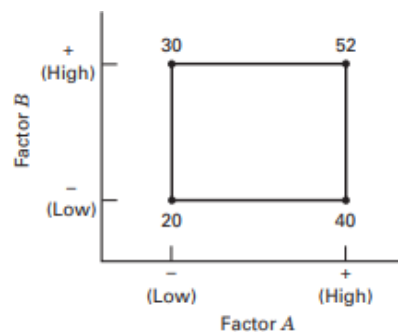


Figure 5: A two-factor factorial experiment, with the response (y) shown at the corners (Montgomery, D. C. 2017).

In certain experiments, we might observe that the variation in response between the levels of one factor isn't consistent across all levels of the other factors. In such instances, there exists an interaction between the factors. For instance, contemplate the two-factor factorial experiment depicted in Figure 6. At the low level of factor B (or B-), the effect of A is

$$A = 50 - 20 = 30$$

And at the high level of factor B (or B+), the A effect is

$$A = 12 - 40 = -28$$

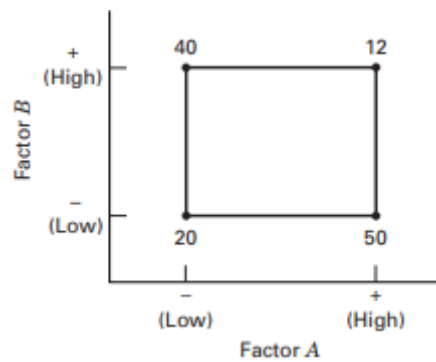


Figure 6: A two-factor factorial experiment with interaction (Montgomery, D. C. 2017).

Because the effect of A depends on the level chosen for factor B, we see that there is interaction between A and B. The magnitude of the interaction effect is the average difference in these two A effects, or $AB = (-28 - 30)/2 = -29$. Clearly, the interaction is large in this experiment. These ideas may be illustrated graphically. Figure 7-a plots the response data in Figure 5 against factor A for both levels of factor B. Note that the B- and B+ lines are approximately parallel, indicating a lack of interaction between factors A and B. Similarly, Figure 7-b plots the response data in Figure 6. Here we see that the B- and B+ lines are not parallel. This indicates an interaction between factors A and B (Montgomery, D. C. 2017; Durakovic, B. 2017).

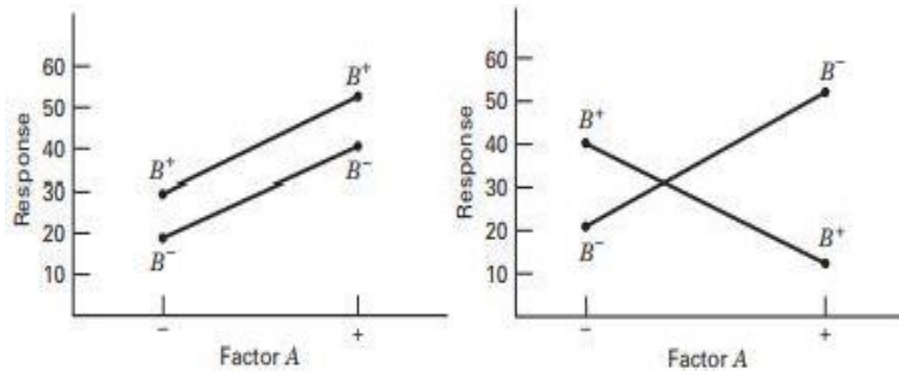


Figure 7: a- A factorial experiment without interaction, b- A factorial experiment with interaction (Montgomery, D. C. 2017).

Factorial experiments involving multiple factors (A, B, ..., K) and two levels ("low" and "high") can present challenges due to their complexity. As the number of factors increases, so does the number of possible combinations. For example, a 2-level design with 9 factors results in 512 combinations, imposing significant demands on experimentation and data analysis. Conducting experiments with multiple factors requires substantial resources, materials, and time, rendering them both time-consuming and expensive. Moreover, maintaining consistent experimental conditions across a large number of experiments poses an additional challenge in multiple factorial designs (Durakovic, B. 2017; Emerson, R. W., & Cavazzuti, M. 2017).

To address the challenges associated with multiple factor factorial designs, various approaches can be considered, depending on the specific circumstances. These approaches may include Full Factorial Design 2^k (which the used method in this dissertation and will be explained more lately) or Fractional Factorial Design 2^{k-p} . Here, the number '2' denotes the number of levels, 'k' represents the number of factors, and 'p' signifies the fraction size of the full factorial employed (Durakovic, B. 2017; Emerson, R. W., & Cavazzuti, M. 2017).

I.3.3.3. Response surface methodology

Response Surface Methodology (RSM) encompasses a set of mathematical and statistical tools tailored for modeling and analyzing problems where multiple variables influence a response of interest, with the aim of optimizing this response. For instance, consider a

problem where a geotechnical engineer aims to determine the optimal levels of (x_1) and (x_2) to minimize the yield (y) of a certain process (like settlement) (Montgomery, D. C. 2017; Myers, R. H. et al 2016). In this case, the process yield is a function of the levels of x_1 and x_2 , say

$$y = f(x_1, x_2) + c$$

Where 'c' represents the noise or error observed in the response y . If we denote the expected response by $E(y) = f(x_1, x_2) = \eta$, then the surface represented by

$$\eta = f(x_1, x_2)$$

Is called a response surface.

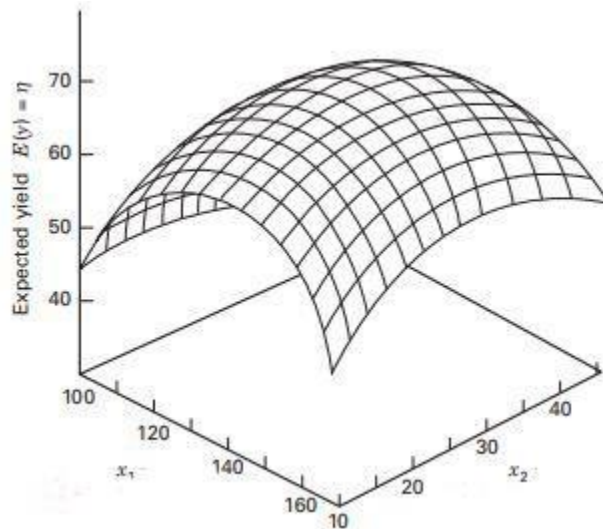


Figure 8: A three-dimensional response surface showing the expected yield (η) as a function of x_1 and x_2 (Montgomery, D. C. 2017).

We usually represent the response surface graphically, such as in Figure 8, where η is plotted versus the levels of x_1 and x_2 . To help visualize the shape of a response surface, we often plot the contours of the response surface as shown in Figure 9. In the contour plot, lines of constant response are drawn in the x_1, x_2 plane. Each contour corresponds to a particular height of the response surface.

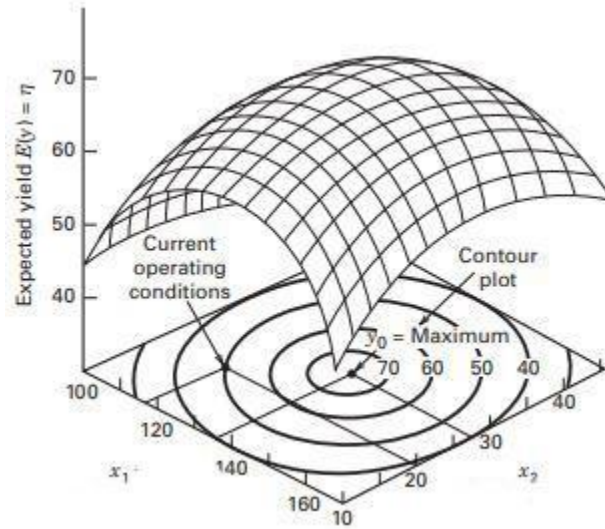


Figure 9: A contour plot of a response surface (Montgomery, D. C. 2017).

In most RSM problems, the form of the relationship between the response and the independent variables is unknown. Thus, the first step in RSM is to find a suitable approximation for the true functional relationship between y and the set of independent variables. Usually, a low-order polynomial in some region of the independent variables is employed. If the response is well modeled by a linear function of the independent variables, then the approximating function is the ‘first-order model’ (Montgomery, D. C. 2017).

$$y = \beta_0 + \beta_1 x_1 + \dots + c \quad (1)$$

If there is curvature in the system, then a polynomial of higher degree must be used, such as the ‘second-order model’

$$y = \beta_0 + \sum_{i=1}^k \beta_i x_i + \sum_{i=1}^k \beta_{ii} x_i^2 + c \quad (2)$$

Almost all RSM problems use one or both of these models. Of course, it is unlikely that a polynomial model will be a reasonable approximation of the true functional relationship over the entire space of the independent variables, but for a relatively small region they usually work quite well (Montgomery, D. C. 2017; Myers, R. H. et al 2016).

I.3.3.4. Taguchi (Robust Design)

Robust parameter design (RPD) is an approach to product realization activities that focuses on choosing the levels of controllable factors (or parameters) in a process or a product to

achieve two objectives: (1) to ensure that the mean of the output response is at a desired level or target and (2) to ensure that the variability around this target value is as small as possible. When an RPD study is conducted on a process, it is usually called a 'process robustness study'. The general RPD problem was developed by a Japanese engineer, Genichi Taguchi, and introduced in the United States in the 1980s (Emerson, R. W., & Cavazzuti, M. 2017). Taguchi proposed an approach to solving the RPD problem based on designed experiments and some novel methods for analysis of the resulting data. His philosophy and technical methods generated widespread interest among engineers and statisticians, and during the 1980s his methodology was used at many large corporations. These techniques generated controversy and debate in the statistical and engineering communities. The controversy was not about the basic RPD problem, which is an extremely important one, but rather about the experimental procedures and the data analysis methods that Taguchi advocated. Extensive analysis revealed that Taguchi's technical methods were usually inefficient and, in many cases, ineffective. Consequently, a period of extensive research and development on new approaches to the RPD problem followed. From these efforts, response surface methodology (RSM) emerged as an approach to the RPD problem that not only allows us to employ Taguchi's robust design concept but also provides a sounder and more efficient approach to design and analysis (Montgomery, D. C. 2017; Le, T. H., & Shin, S. 2018).

An important aspect of Taguchi's approach was his notion that certain types of variables cause variability in the important system response variables (Montgomery, D. C. 2017; Villa, A. et al 2012).

Let us consider a problem with five parameters ($k = 5$), three of which are controllable ($K_{in} = 3$) and two uncontrollable ($K_{out} = 2$), and let us consider two-levels. Full factorial experimental designs for the inner and the outer arrays. Assume full factorial designs for simplicity, even though they are never taken into consideration by the Taguchi method. Therefore, we must perform a full 2^2 factorial design (outer array) for each sample of the 2^3 inner array. We can graphically represent the situation as in Figure 10.

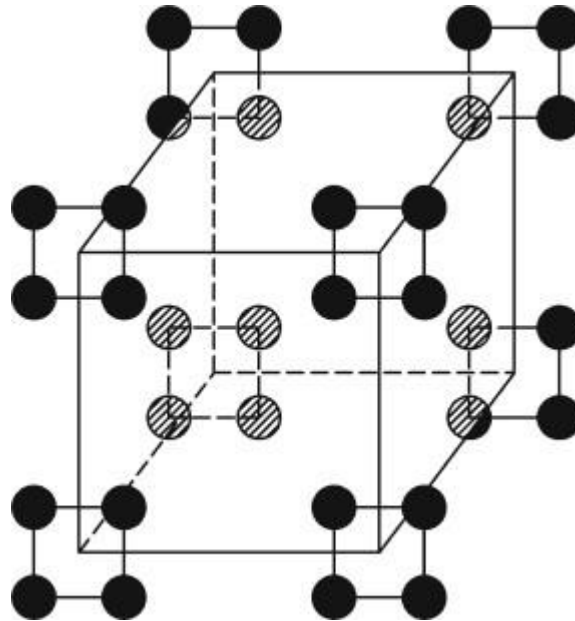


Figure 10: Example of Taguchi DOE for $K_{in} = 3$, $K_{out} = 2$, 23 full factorial inner array, 22 full factorial outer array (Emerson, R. W., & Cavazzuti, M. 2017).

Table 4: Taguchi designs synoptic table (Emerson, R. W., & Cavazzuti, M. 2017).

Number of variables	Number of levels			
	2	3	4	5
2, 3	L4	L9	LP16	L25
4	L8	L9	LP16	L25
5	L8	L18	LP16	L25
6	L8	L18	LP32	L25
7	L8	L18	LP32	L50
8	L12	L18	LP32	L50
9, 10	L12	L27	LP32	L50
11	L12	L27	N/A.	L50
12	L16	L27	N/A.	L50
13	L16	L27	N/A.	N/A.
14, 15	L16	L36	N/A.	N/A.
from 16 to 23	L32	L36	N/A.	N/A.
from 24 to 31	L32	N/A.	N/A.	N/A.

The Taguchi orthogonal arrays, are individuated in the literature with the letter L, or LP for the four-level ones, followed by their sample size. Suggestions on which array to use depending on the number of parameters and on the numbers of levels, as summarized in Table 4.

I.4. Statistics uses

Geotechnical engineering involves the analysis and design of structures built upon or within the ground. Soil and rock mechanics play a pivotal role in the stability and performance of such structures. Compression and swelling indexes are fundamental properties that govern the behavior of soils under load and environmental changes. Predicting these indexes accurately is essential for ensuring the safety and longevity of geotechnical projects. This part shows some statistical methods used for predicting soil properties, and contributing to advancements in geotechnical engineering practices.

I.4.1. Principal component analysis

Principal Component Analysis (PCA) stands as one of the cornerstone techniques in the field of multivariate statistics and data analysis. It is aiming to simplify the complexity of high-dimensional datasets while preserving essential information. Over the past century, PCA has emerged as a versatile tool with applications spanning across diverse disciplines, including but not limited to engineering. The proliferation of data in today's digital age has accentuated the need for effective methods to analyze and interpret complex datasets. Traditional statistical approaches often struggle to cope with the sheer volume and dimensionality of modern datasets, leading to computational inefficiencies and interpretation challenges. In this context, PCA offers a compelling solution by transforming high-dimensional data into a lower-dimensional space, where underlying patterns and structures can be more easily discerned. (Elhaik, E. 2022).

I.4.1.1. Historical overview and basic concepts: The roots of PCA can be traced back to the early 20th century, with the pioneering work of Karl Pearson and Harold Hotelling in the field of multivariate statistics. Pearson introduced the concept of principal components in 1901 as a method for summarizing the variability in datasets with multiple variables. Hotelling further formalized PCA in the 1930s, laying the groundwork for its widespread adoption in statistical analysis and data science.

At its core, PCA seeks to identify the principal components (PCs) of a dataset, which are orthogonal linear combinations of the original variables (Jackson, J. E. 2005). The first principal component captures the maximum variance in the data, with subsequent

components capturing decreasing amounts of variance. Each principal component is a linear combination of the original variables, weighted by coefficients known as loadings (Jackson, J. E. 2005).

I.4.1.2. Mathematical formulation: Mathematically, PCA can be formulated as an eigenvalue problem, where the objective is to find the eigenvectors and eigenvalues of the covariance matrix of the dataset. Let X be an $n \times p$ matrix representing the dataset, where n is the number of observations and p is the number of variables. The covariance matrix Σ is computed as $\Sigma = (1/n) X^T X$. The eigenvectors and eigenvalues of Σ are then calculated, and the principal components are derived from the eigenvectors. (Beattie, J. R., & Esmonde-White, F. W. 2021; Abdi, H., & Williams, L. 2010). Where eigenvectors are the directions in which the data exhibit the most variability. Each eigenvector corresponds to a principal component, while eigenvalues represent the amount of variance captured by each principal component. Larger eigenvalues correspond to principal components with greater variability.

Geometrically, PCA can be visualized as a rotation of the original coordinate system to align with the directions of maximum variance in the data. The first principal component corresponds to the direction of maximum spread, while subsequent components capture orthogonal directions of decreasing variability. PCA effectively identifies a new set of axes (principal components) such that the data are maximally spread out along these axes, facilitating dimensionality reduction and visualization (Ivosev, G., 2008).

I.4.1.3. Applications of PCA in geotechnical engineering: Principal Component Analysis (PCA) has found extensive applications across various domains, leveraging its capability to reduce data dimensionality, extract meaningful features, and uncover underlying patterns in complex datasets. It has diverse range of applications where PCA has demonstrated efficacy, spanning fields such as data compression, feature extraction, pattern recognition, financial analysis and a lot. Principal Component Analysis (PCA) offers several valuable applications in geotechnical engineering, aiding in the characterization of soil behavior, site investigation, risk assessment, and quality control, below are some key applications of PCA in geotechnical engineering:

a- **Soil Characterization:** PCA can be employed to analyze large datasets comprising soil properties such as grain size distribution, plasticity index, shear strength, permeability, and compressibility. By reducing the dimensionality of soil data, PCA facilitates the identification of dominant factors influencing soil behavior and classification. PCA aids in the interpretation of complex relationships between soil properties, enabling engineers to categorize soils into meaningful groups and predict their engineering behavior (Fox, G. A., & Metla, R. 2005).

b- **Risk Assessment:** PCA assists in evaluating uncertainties and variability in soil parameters, which are critical for assessing the stability, settlement, and performance of engineering structures. By identifying key factors contributing to soil variability, PCA aids in quantifying risk levels associated with geotechnical hazards such as landslides, liquefaction, and slope instability. PCA-based risk assessment techniques inform decision-making processes by highlighting potential failure modes, design vulnerabilities, and mitigation strategies (Yu, J., et al 2021).

c- **Interpretation and Visualization:** PCA enables the visualization of complex geotechnical datasets in reduced-dimensional spaces, facilitating data interpretation and communication. Scatter plots, biplots, and three-dimensional visualizations generated from PCA results provide insights into soil variability, correlations between parameters, and spatial patterns. Interpretation of PCA results helps engineers and stakeholders understand soil characteristics, site conditions, and geological processes, guiding decision-making and risk management efforts (Niedoba, T. 2014).

I.4.2. Regressions

Regression analysis serves as a foundational statistical technique that enables researchers, analysts, and practitioners to model and understand relationships between variables. With its roots tracing back to the early 19th century, regression analysis has evolved into a versatile tool widely used across various disciplines, including economics, finance, marketing, engineering, environmental science, healthcare, and social sciences. By quantifying the relationship between one or more predictor variables and a response

variable, regression analysis facilitates hypothesis testing, prediction, and decision-making based on empirical evidence.

I.4.2.1. Historical overview and basic concepts: The origins of regression analysis can be traced back to the pioneering work of Sir Francis Galton in the late 19th century. Galton introduced the concept of regression to the mean while studying the heritability of traits in plants and animals. However, the formalization of regression analysis as a statistical technique is often attributed to Sir Francis Ysidro Edgeworth and Karl Pearson in the early 20th century. Since then, regression analysis has undergone significant development, with contributions from eminent statisticians such as Ronald Fisher, Jerzy Neyman, and Egon Pearson.

Key concepts and terminology in regression analysis include:

- **Dependent Variable:** The variable being predicted or explained by the independent variables. It is denoted as Y or the response variable.
- **Independent Variables:** The variables used to predict or explain the variation in the dependent variable. They are denoted as X_1, X_2, \dots, X_p or predictor variables.
- **Regression Equation:** The mathematical relationship between the dependent and independent variables, typically represented as $Y = \beta_0 + \beta_1 X_1 + \beta_2 X_2 + \dots + \beta_p X_p + \varepsilon$, where β_0 is the intercept, $\beta_1, \beta_2, \dots, \beta_p$ are the coefficients, and ε is the error term.
- **Coefficients:** The regression coefficients ($\beta_1, \beta_2, \dots, \beta_p$) represent the change in the dependent variable for a one-unit change in the corresponding independent variable, holding other variables constant.
- **Residuals:** The differences between the observed values of the dependent variable and the values predicted by the regression model. Residual analysis is essential for assessing model fit and identifying outliers or influential data points.

I.4.2.2. Types of Regression Models: Regression analysis encompasses various types of models, including:

- **Simple Linear Regression:** Involves a single independent variable and a linear relationship between the independent and dependent variables.

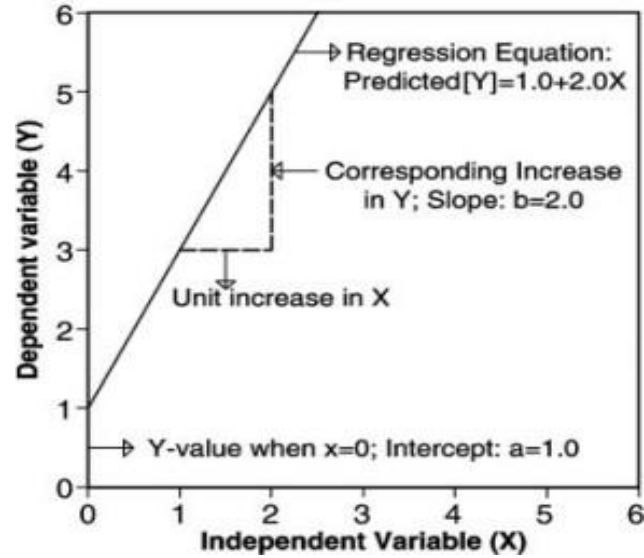


Figure 11: Simple linear regression model. (Zou, K. H. et al 2003).

- Multiple Linear Regression: Incorporates multiple independent variables to model the relationship with the dependent variable.

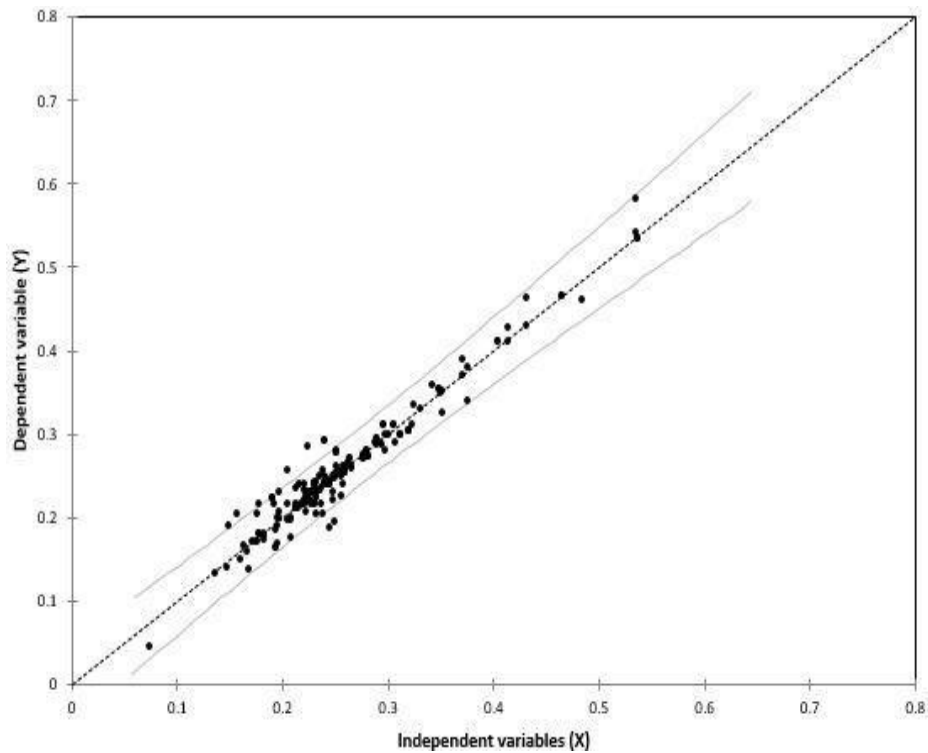


Figure 12: Multiple linear regression model.

- Polynomial Regression: Extends linear regression to capture nonlinear relationships by including polynomial terms of the independent variables. (Ostertagová, E. 2012).

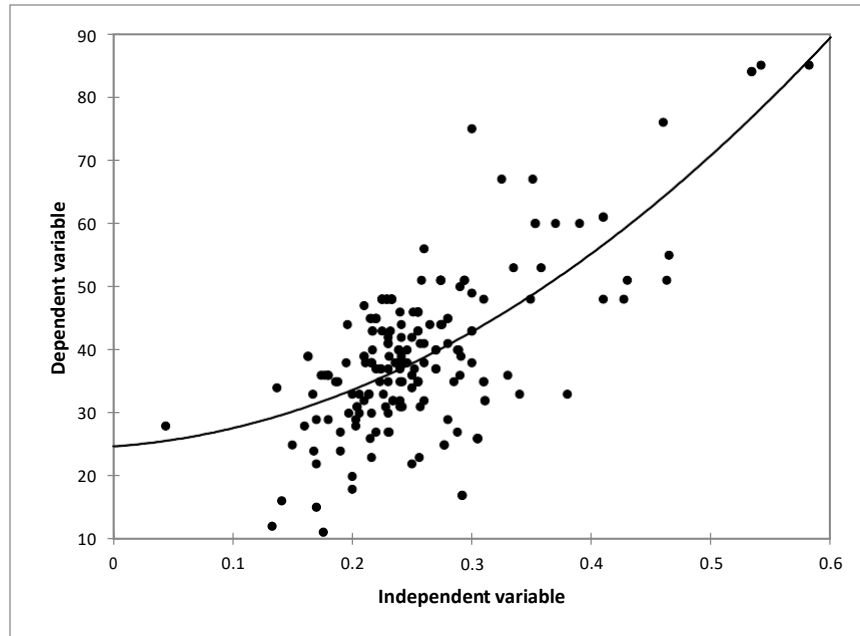


Figure 13: Polynomial regression model.

- Logistic Regression: Used for binary classification tasks, where the dependent variable is categorical (e.g., yes/no, success/failure, 0/1). (LaValley, M. P. 2008).

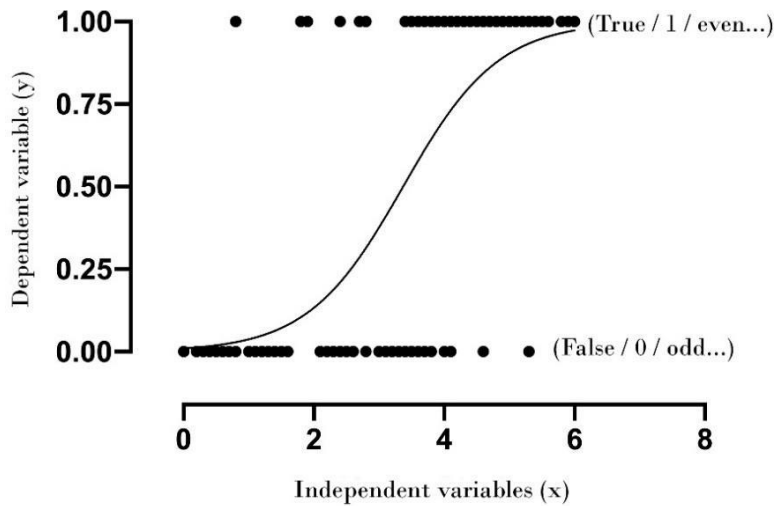


Figure 14: Logistic regression model.

I.4.2.3. Applications of regression analysis in geotechnical engineering:

Regression analysis finds several applications in geotechnical engineering, where it serves as a valuable tool for analyzing and modeling relationships between geotechnical parameters, predicting soil behavior, and guiding engineering decisions. Here are some key applications:

Soil Property Prediction: Regression analysis is utilized to predict important soil properties based on easily measurable parameters such as grain size distribution, Atterberg limits, and soil composition (Berrah, Y. et al 2022). By developing regression models, engineers can estimate properties like shear strength, permeability, and compressibility, (As will be discussed in this dissertation), which are crucial for designing foundations, slopes, and retaining structures.

Site Characterization: Geotechnical site investigation involves collecting data from various sources such as borehole logs, laboratory tests, and field observations. Regression analysis helps in integrating diverse datasets to characterize site conditions and subsurface properties. By modeling relationships between soil parameters and site characteristics, engineers can create predictive models to assess soil variability and identify potential geotechnical hazards (Fox, G. A., & Metla, R. 2005).

Slope Stability Analysis: Regression analysis is employed to assess factors contributing to slope instability and predict slope behavior under different conditions. By correlating slope geometry, soil properties, groundwater levels, and external forces, engineers can develop regression models to evaluate slope stability, identify potential failure mechanisms, and design appropriate stabilization measures (Khan, M. I., & Wang, S. 2021; Benz, T., & Nordal, S. 2010).

Ground Improvement Techniques: Regression analysis assists in evaluating the effectiveness of ground improvement techniques such as soil stabilization, compaction, and reinforcement. Engineers use regression models to quantify the relationship between treatment parameters (e.g., material properties, compaction energy) and improvements in soil strength and stability, aiding in the selection and optimization of ground improvement strategies. (Akan, R., Keskin, S. N., & Uzundurukan, S. 2015).

I.4.3. Finite element analysis

In recent decades, computational methods have revolutionized the field of geotechnical engineering, offering sophisticated tools for analyzing and predicting soil behavior. Among these methods, Finite Element Analysis (FEA) has emerged as a powerful numerical technique for simulating the mechanical behavior of soils and structures interacting with soil media (Benz, T., & Nordal, S. 2010). FEA allows engineers to model complex soil-structure systems, simulate various loading scenarios, and predict the response of soil under different conditions with remarkable accuracy (Benz, T., & Nordal, S. 2010).

Computational methods have revolutionized geotechnical engineering by providing powerful tools for simulating and analyzing complex soil-structure interactions. Finite Element Analysis (FEA), in particular, has gained prominence for its ability to model and predict soil behavior with high fidelity. By discretizing the soil domain into finite elements and applying appropriate constitutive models, FEA enables engineers to simulate a wide range of geotechnical problems, including settlement analysis (Which is the subject of this dissertation), slope stability assessment, and foundation design. Additionally, computational techniques such as finite difference methods, boundary element methods, and discrete element methods offer alternative approaches for studying soil mechanics and geotechnical phenomena. (Potts, D. M. et al 2001).

I.4.3.1. Methodologies for Predicting Soil Properties using Finite Element Analysis (FEA)

Predicting soil properties through Finite Element Analysis (FEA) involves a systematic approach that encompasses various methodologies tailored to the specific characteristics of the soil and the engineering problem at hand. This section outlines the key methodologies employed in predicting soil properties using FEA, including modeling approaches, boundary conditions and loading scenarios, and calibration and validation techniques (Tang, K., 2020).

a- Modeling Approaches: FEA offers flexibility in modeling soil-structure systems, allowing engineers to represent complex geometries, material properties, and loading conditions. The choice of modeling approach depends on factors such as the scale of the

analysis, the level of detail required, and the computational resources available. Common modeling approaches in geotechnical engineering include:

- **Continuum Models:** Ideal for macroscopic analysis of soil behavior, continuum models represent soil as a continuous medium characterized by material properties such as density, stiffness, and strength. Continuum models are suitable for simulating large-scale geotechnical problems such as slope stability analysis and embankment design.
- **Discrete Models:** Discrete models represent soil as a collection of discrete particles or elements connected by interaction forces. Discrete element methods (DEM) and lattice-based models fall under this category and are often used to study granular materials, soil-structure interaction at the microscale, and particle-scale phenomena such as particle crushing and rearrangement.
- **Coupled Models:** Coupled models integrate multiple physical phenomena such as soil deformation, groundwater flow, and heat transfer into a unified framework. These models enable the analysis of coupled processes such as consolidation, seepage, and thermal-mechanical interaction in geotechnical systems.

b- **Boundary Conditions and Loading Scenarios:** The selection of appropriate boundary conditions and loading scenarios is crucial for accurately predicting soil properties using FEA. Boundary conditions define the constraints imposed on the soil-structure system, while loading scenarios specify the applied loads and their distribution. Common boundary conditions and loading scenarios in geotechnical FEA include:

- **Boundary Conditions:** Fixed displacements, prescribed loads, symmetry conditions, and contact interfaces are examples of boundary conditions used to model interactions between soil and external structures or boundaries.
- **Loading Scenarios:** Loading scenarios vary depending on the engineering problem and may include static loads (e.g., gravity, applied forces), dynamic loads (e.g., seismic excitation), thermal loads, and environmental loads (e.g., changes in pore water pressure, temperature variations).

c- Calibration and Validation Techniques: Calibration and validation of FEA models are essential steps in ensuring the accuracy and reliability of predicted soil properties. Calibration involves adjusting model parameters to match observed behavior or laboratory test results, while validation involves comparing model predictions with field measurements or independent experimental data. Common calibration and validation techniques include:

- **Parameter Sensitivity Analysis:** Sensitivity analysis involves systematically varying model parameters to assess their influence on model predictions. Sensitivity analysis helps identify critical parameters and refine their values through calibration.
- **Comparative Analysis:** Comparative analysis involves comparing FEA predictions with analytical solutions, empirical correlations, or benchmark case studies to validate model accuracy and identify discrepancies.
- **Field Monitoring and Instrumentation:** Field monitoring programs involve installing sensors and instrumentation at project sites to measure soil behavior and validate FEA predictions. Field monitoring data provide valuable feedback for refining FEA models and improving their predictive capabilities.

I.5. Conclusion

In this chapter, we embarked on a journey to explore the comprehensive integration of statistical methodologies, including Principal Component Analysis (PCA), regression analysis, Finite Element Analysis (FEA), and Design of Experiments (DOE) using software like Design Expert, to solve problems in geotechnical engineering. Investigation into the fundamentals of each method is explained, recognizing their pivotal role in predicting the stability and safety of geotechnical engineering structures. Traditional methods of prediction, albeit valuable, were revealed to be limited in their capacity to capture the nuanced interactions between various soil properties and external factors. Hence, the integration of advanced statistical techniques emerged as a promising avenue for enhancing predictive accuracy and reliability.

We navigated through the landscape of statistical methodologies, recognizing PCA as a powerful tool for dimensionality reduction and variable selection. By distilling complex datasets into their essential components, PCA provided a streamlined framework for identifying key predictors influencing the obtained response. Leveraging regression analysis, then established robust models capable of quantifying the relationships between input parameters and output indexes. The flexibility of regression techniques, spanning from linear to nonlinear models, accommodated the intricacies of soil behavior with precision.

The incorporation of Finite Element Analysis (FEA) enriched our predictive capabilities by enabling the simulation of soil deformation and stress distribution under diverse loading scenarios. FEA served as the bridge between statistical models and real-world applications, offering insights into the mechanical responses of soils and informing engineering decisions with empirical evidence. Furthermore, the integration of Design of Experiments (DOE) using software like Design Expert facilitated systematic exploration of the design space, optimizing experimental designs and refining predictive models.

Chapter II:
Geological, Hydrogeological
and Climatic Conditions

II.1. Introduction

The geological study of the region reveals areas mainly composed of clays and marls. Key formations include the Lower Maastrichtian with gray marls and marl-limestones, the Paleogene with clay and gypsum, the Pliocene with red clays, and alluvial formations with clays, silty clays, sand, and silt. Core drillings confirm the presence of fine-grained soils, such as clayey and marl-clay formations, at shallow depths. These soils, despite small-scale variations, are homogeneous regionally and prone to volume changes due to water content fluctuations or external loading, leading to ground instability.

II.2. Overview

Knowledge of the geology and hydrogeology of an area is indispensable for geotechnical engineering as it forms the bedrock for informed decision-making in the design and construction of projects. Geotechnical engineers investigate into the geological characteristics of the area, examining the composition, properties, and structural arrangement of rocks and soils. This comprehension is pivotal in determining many parameters, as different geological conditions directly affect factors such as bearing capacities, shear strength, and compressibility (Arjwech, R., 2020), which is our subject here. Furthermore, understanding the geological context aids in assessing the stability of slopes, predicting and mitigating landslide risks, and designing support systems for tunnels and excavations (Legget, R. F. 1979). Hydrogeological considerations are essential, especially for projects involving underground structures, as engineers need to manage groundwater movements effectively through dewatering systems (Smith, D. K. 2021). Overall, geotechnical engineers leverage their knowledge of geology and hydrogeology to address challenges, select appropriate construction materials, and ensure the safety, durability, and environmental sustainability of infrastructure projects.

Emphasizing to the reader that, when encountering a geotechnical challenge, the primary and immediate consideration is directed towards the geological aspects. Recognizing the fundamental role of geology, the prioritization involves gaining a thorough understanding of the site's geological characteristics, including soil and rock composition, structural properties, and other relevant factors (Legget, R. F. 1979). This

emphasis on geology serves as the cornerstone for informed decision-making throughout the entire engineering process, influencing choices in overall project feasibility.

II.3. Geographic location

Tebessa is located in northeastern Algeria, positioned within the Tell Atlas Mountain range. It boasts a diverse geographical setting, encompassing mountains, plateaus, and a southern extension that reaches into the Sahara Desert. This strategic location contributes to a varied landscape, characterized by both scenic mountainous terrain and the arid expanses of the Sahara. With some altitudes ranging from 800m to 1600m.

The wilaya of Tebessa is limited by:

- From the north by the wilaya of SOUK AHRAS.
- The south by the wilaya of OUED SOUF.
- The EAST via the ALGERIAN-TUNISIAN borders.
- From the WEST by the two wilayas OUMELBOUAGHI and KHENCHELA.

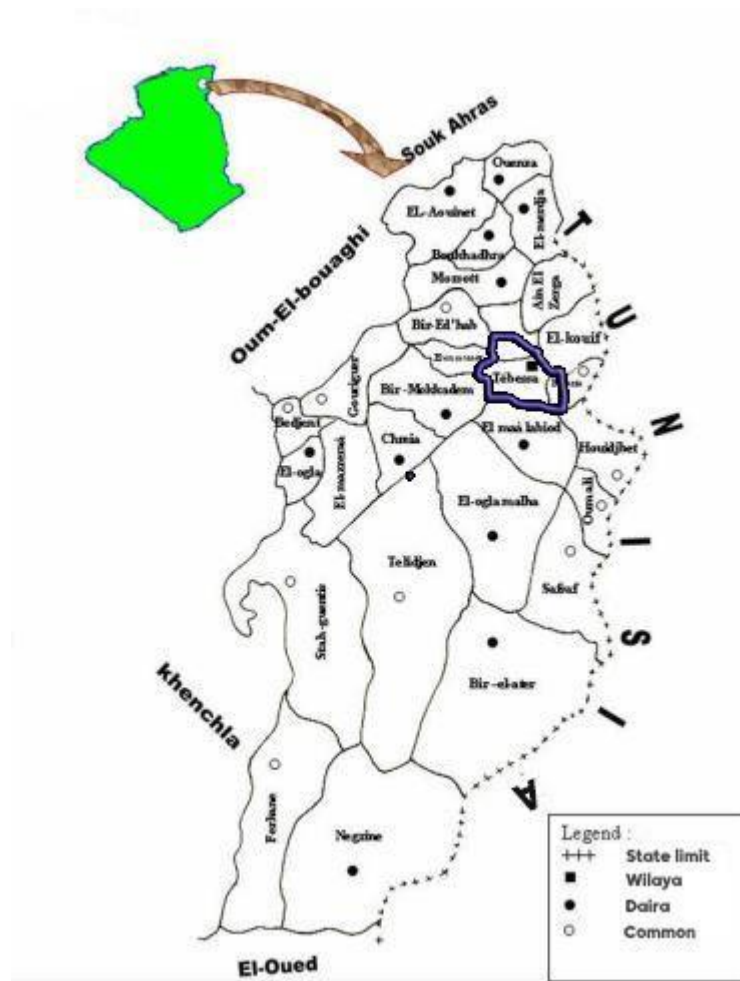


Figure 15: Geographic location of the studied area.

II.4. Geology

Tebessa region is part of the indigenous North-Aurèsian (Aurès Nememcha) structure of the Saharan Atlas (Durozoy 1956; Blès 1969; Vila 1974; Kowalski et al. 1997). The geological map (Figure 16) at a scale of 1/100000 shows the distribution and structure of the different lithologies in the region. It is primarily composed of:

- A Triassic diapiric formation dislocating overlying formations at the level of Djebel Djebissa.
- Carbonate formations represented by significant layers of marly limestone and marl of Cretaceous to Tertiary age. Some of these formations can be observed at the edges of Tebessa plain.

- An unconformity of important Mio-Plio-Quaternary alluvial deposits, overlying the previous formations and thus forms the filling of the depression, currently the plain. This formation is observable especially at the foothills of rugged reliefs. (Figure 17).

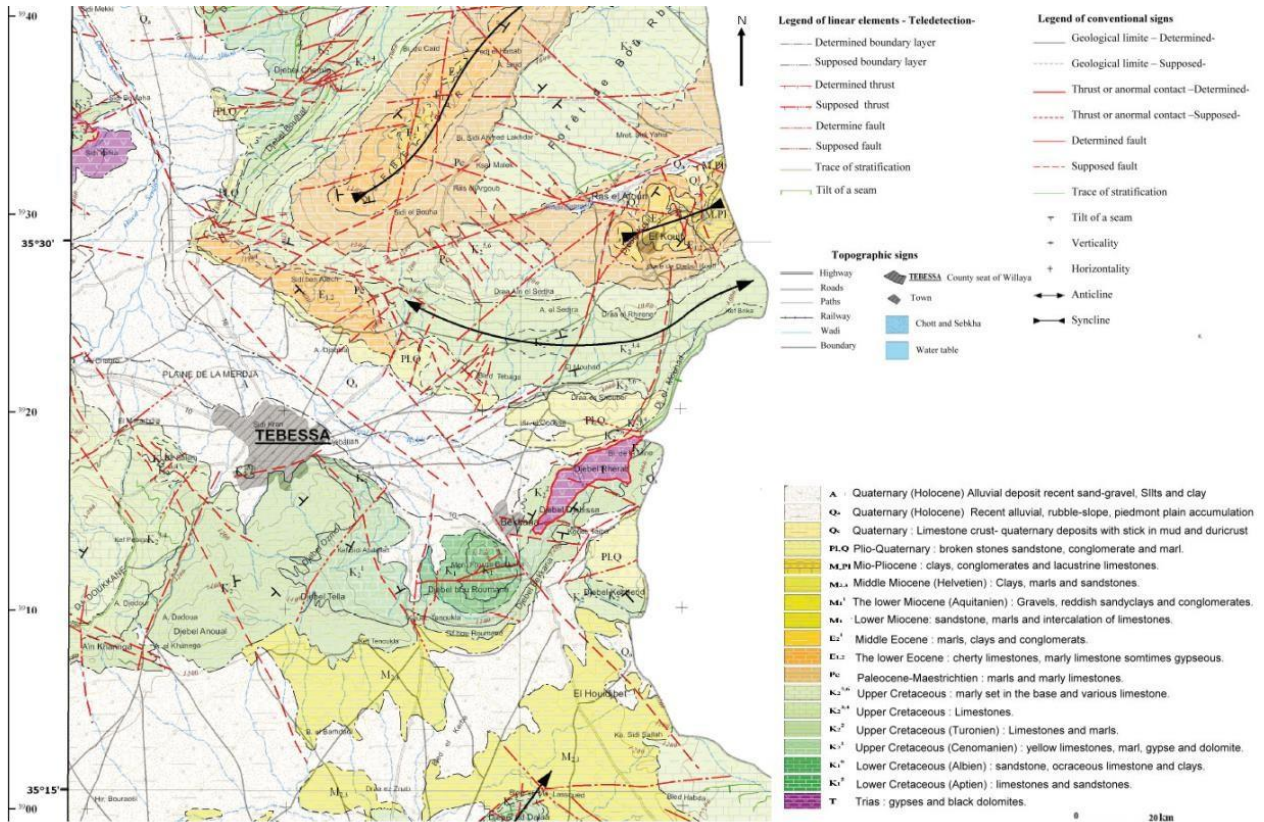


Figure 16: Geological map shows the distribution of different soil and rock formations in Tebessa region (extracted from the geological map, ANRH 2009)

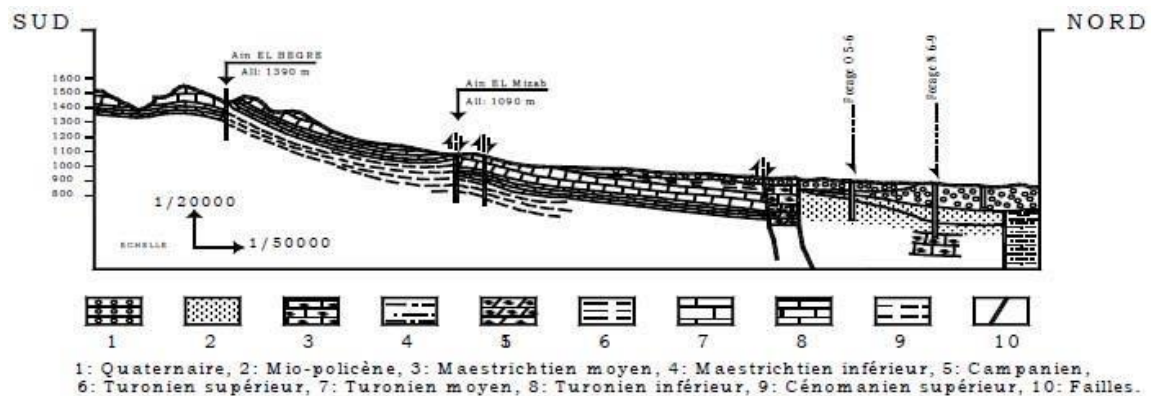


Figure 17: Schematic section of the geological formations of Tebessa region.

II.4.1. Lithostratigraphy of Tebessa region

The study of the stratigraphy of Tebessa region (Figure 18) is essentially based on the research work of several authors (Dubourdiou, 1949, 1956; Durozoy, 1956; Blés and Fleury 1970 and Vila J. M 1980 and 1994).

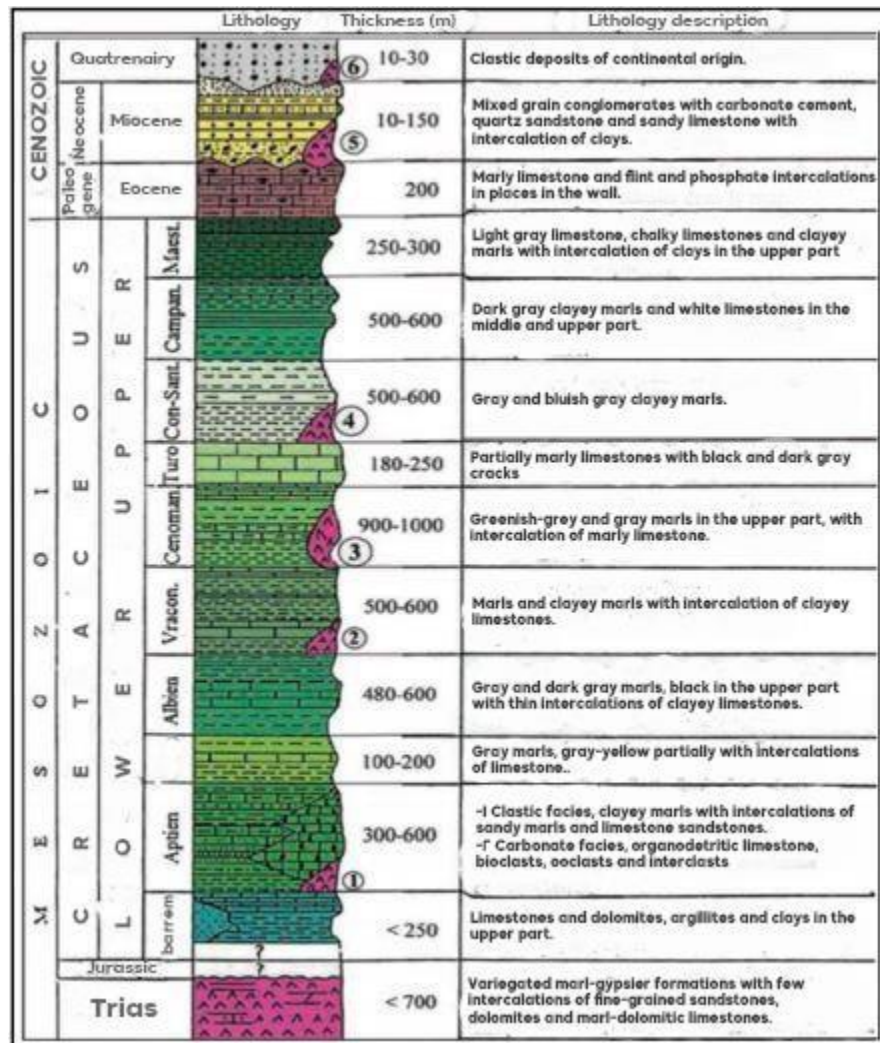


Figure 18: Synthetic stratigraphic column of the Tebessa region (Dubourdiou, 1956).

II.4.1.1. Secondary

II.4.1.1.1. Trias: The oldest known lands in the «diapir zone» of the Tebessa region. Belong to the Triassic. The Triassic outcrops in this region have since always been the subject of a Triassic. Special attention, due to their importance for exploration of mining

and oilfields. In North Eastern Algeria and Tunisia, the many diapirs are in Trias. However, the presence of salt is often confirmed at depth. (Bouzenoune, 1993).

In Tebessa region, the Triassic outcrops in the form of an extrusion and generally occupies the heart of anticlinal structures, with reefs at its apex in the Aptian and Albian (Masse and Chikhi-Aouimeur, 1982). These Triassic bodies have variable dimensions in the form of elliptical sections sometimes very stretched, on a strip-oriented NE-SW for approximately 80 km. The most outcrops the most important are those of Djebissa, Ouenza, Boukhadra, Mesloul, Boujaber, Hameimat North, Hameimat South and many other massifs.

II.4.1.1.2. Lower and middle Cretaceous

II.4.1.1.2.1. Aptien: It is formed by Orbitolines limestone banks, often brecciated at dolomitic or calcic cement. In the southern part of the Djebel Belkif, these limestones are encompassed in the diapiric Triassic, with a thickness exceeding 100 m.

II.4.1.1.2.2. Albien: It outcrops near Djebel Bouroumane where it is formed by limestone banks thick browns over a thickness of 90 m. These bases form a large part of the slopes averages of the western slope of Bouroumane. This floor is not located in the study area, perhaps because of the accentuated diapirism during this period, however according to the last article by Villa J-M. (2001) there is near Djebel Belkif.

II.4.1.1.2.3. Vraconian: It is well developed in the Bouroumane area and there are probably deep in the Hammamet ditch. This floor is characterized by a set of limestones and grayish calcareous marls in platelets, containing imprints of Ammonites.

II.4.1.1.3. Upper Cretaceous

II.4.1.1.3.1. Cenomanian: It crops out in the northwest part of the Hammamet ditch to the east of Djebel Essen, in the form of blue-violet marls intercalated with lumachelles.

II.4.1.1.3.2. Turonian: It is subdivided into two parts, the Lower Turonian and the Upper Turonian. The base of the Lower Turonian is represented by grayish marls and limestones, of which the thickness is around 60 m. The top of the Lower Turonian is represented by beige limestones which constitute the cliffs of Djebel Essen; Djebel Belkif,

kef Daheche, Djebel Tella (Ozmor Range). The Upper Turonian presents itself in gray marls, alternating with green marls with a thickness of approximately 150 m.

II.4.1.1.3.3. Emscherian: It is a thick and monotonous series of marls gray or green, containing in its upper part levels of lumachellic limestone over a thickness of 250 m.

II.4.1.1.3.4. Campanian: The Campanian (lower and upper) is characterized by a series of gray marls having a thickness of 200 m. The Middle Campanian present in the relief a new cornice between those of the Turonian and the Maastrichtian, it passes noticeably to the marly formations which make the passage between upper Campanian and Maastrichtian lower.

II.4.1.1.3.5. Maastrichtian: The lower Maastrichtian is represented by scree at the foot of the landforms. The Upper Maastrichtian is a powerful formation of massive white limestones well-bedded containing numerous Inocerames imprints. Their thickness is of the order from 80 to 100 m, but reaches 200 m southwest of Youkous (Hammamet).

II.4.1.2. Tertiary

II.4.1.2.1. Paleocene: Its base presents marls similar to that of the upper Maastrichtian, which is intercalated with phosphate layers towards the upper levels.

II.4.1.2.2. Eocene: Limestones with flint and others with nummulites characterize the lower and middle Eocene, near perimeters of the Tebessa region. Their thickness is 200 meters.

II.4.1.2.3. Miocene: Lower and middle Miocene deposits rest transgressive on the ancient formations (Albian-Senonian and even the Triassic).

At their base, the Miocene formations include conglomerates containing elements of varied limestone, gray flint, ferruginous pebbles and elements borrowed from the Triassic, testifying to diapiric activity (Bouzenoune, 1993)

II.4.1.3. Quaternary: The Quaternary deposits are of continental origin and are distributed in the lower parts of the reliefs and cover large areas (current plains and valleys).

They are made up of limestone crusts, scree silt, pebbles and pudding. The thickness of the quaternary varies between 10 and 30 m (Dubourdieu, 1956). Lithological formations that can be distinguished are the current formations.

The current and recent formations:

- Current Scree: They exist at the foot of all the large limestone reliefs, but they are confused, most of the time, with ancient scree.
- Travertines: They are deposited by the sources of Tebessa and Tenoukla.
- Current alluvium: They only rarely exist because, as a very general rule, valleys intersect the formations on which they flow. On the edges of the plain, they affect the appearance of torrential deposits.
- Recent silts: they are developed especially in the large valley of Wadi Kebir. In the Merdja of Tebessa, alluvial gypsum deposits are the subject of local exploitation.
- Limestone crusts: These are superficial deposits due to the evaporation of water loaded with limestone developed especially on old stony alluvium.

II.4.2. Tectonic and structural description:

Structurally, the territory in question occupies two geotectonic regions which differ by the age of their folded base and by the particularity of their structure (Figure 19).

These are Hypercinian platforms (North and center of the territory) and Antecambrian platforms (South) divided by the North Atlas fault (Saharan Flexure).

The territory of the Tebessa region is covered by large structures synclinals and anticlinals in NE-SW direction. These structures are clearly visible in particular on the Cheria plateau and at Dj Dyr.

In the El Ma-Labiod area, deeper structures are covered by the Continental Miocene, they are therefore before the Miocene and the distension phase that caused the collapse of the Tebessa-Morsott plain which is much further north behind Bekkaria.

Considering the terrain on Morsott's map, it is difficult to determine the age wrinkling; the only tertiary deposits, subsequent to the Eocene emergence, sublittoral attributed to the Tortonian are located at the heart of the Dj Dyr syncline, where they overcome without apparent unconformity the Lower Lutetian limestones. However, east of El Kouif, between the limit of the sheet and the Tunisian border, the same sands from the lower Miocene lie unconformably on Eocene limestones or Paleocene marls.

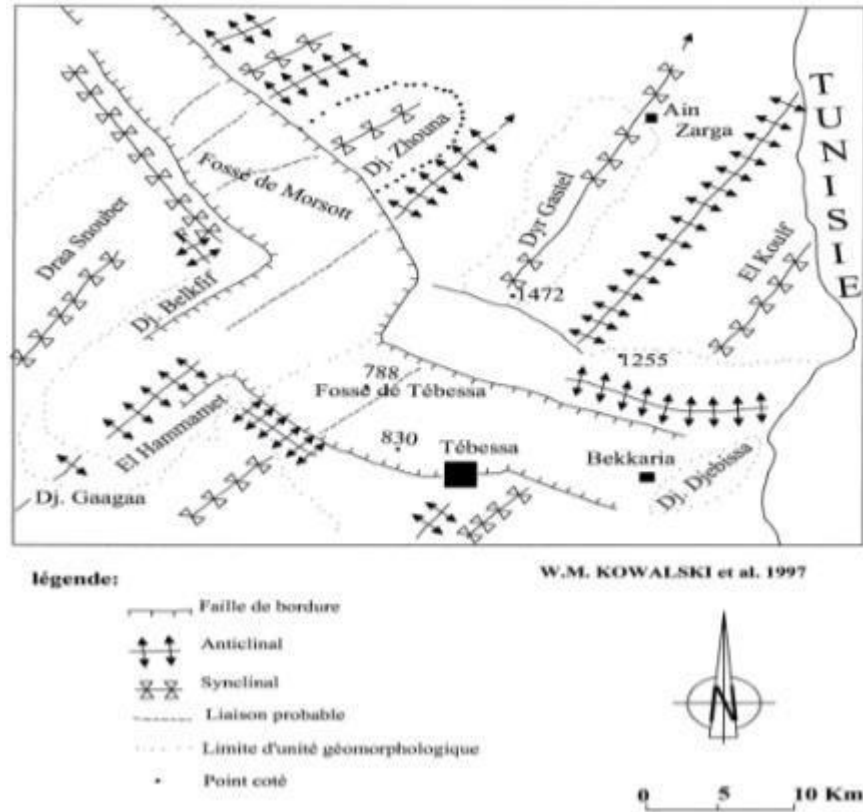


Figure 19: Tectonic sketch of the Tebessa region (Kowalski et al. 1997).

On the other hand, according to Dubourdieu. G (1949-1951; 1956 and 1959) further north (Boukhadra and Dj Ouenza sheets, as well as Dj Mesloul), the Miocene is discordant on all the terms of the Cretaceous series (Tebessa sheet) we also note, the discordant Miocene on Cretaceous terms. The folding of the region is therefore post-Lutetian. Lower and earlier than the Miocene and is undoubtedly responsible for the emergence of the region in the Middle Eocene (Dubourdieu, 1959).

A large NE-SW direction accident seems to cut and detach the plain of Tebessa, this is a reverse fault. The SE compartment overlaps the NW compartment, this is clearly visible at Dj Chemela between Morsott -Tebessa.

The SW continuation of this accident seems to drown in depth under the anticline by Cheria. On the edge of the plateau, it mainly affects the Turonian and does not appear pass upwards to the Maastrichtian limestone. This stacking of structures towards the depth is organized with a reduction in the radius of curvature and beyond a certain depth by the formation of a fault especially when the levels become competent at the level of the Turonian limestones. Towards the top, this accident is absorbed in the marls of Coniacian, Santonian and Lower Campanian. This is how the Maastrichtian of Cheria is not affected.

The axis of the large structures has a dip towards the SW, the highest point of the region is located to the SW of the Dj Dyr syncline with 1472 m.

The summits of the limestone reliefs at altitudes of 1000 to 1500m represent the witnesses of an ancient erosion surface, almost flat, but slightly left, culminating at the southern tip of Dj Dyr (from this point it slopes steadily towards the north and perpendicular to this direction, towards the N-W and the S-W).

This erosion surface, practically not deformed, is posterior to the folding and in particular to the continental post-lower Miocene tangential compressions: The sandy or conglomeratic formations of this level constitute, in fact, some summits of the same altitudes as those of the older surrounding formations which determine this surface. It also predates the formation of the Morsott ditch. Which clearly intersects with it.

II.5. Hydrogeology

Hydrogeology constitutes a very important tool for the knowledge of the elements allowing the definition of the characteristics of an aquifer; On the basis of maps and geological sections combined with the stratigraphic columns of the drillings carried out across the region, their depths, the altitude, and the measurement of piezometric levels, hydrogeological sections and piezometric maps were established in order to understand the mechanism of circulation of groundwater in the different aquifer systems and determine

the direction of water flow and thus define the existing relationships between the different systems.

II.5.1. General description

According to the work of (Djabri, 1987 and Rouabhia, 2004 and 2009); the aquifer system of the Tebessa plain is essentially formed by an alluvial mantle of Quaternary age; composed of limestone pebbles with a thickness varying between 10 and 400 m. The limestones of Turonians, Maestrichtians and Campanians constituting the reliefs on the North-East and South of the plain, also form important aquifers. (Hemali, 2020).

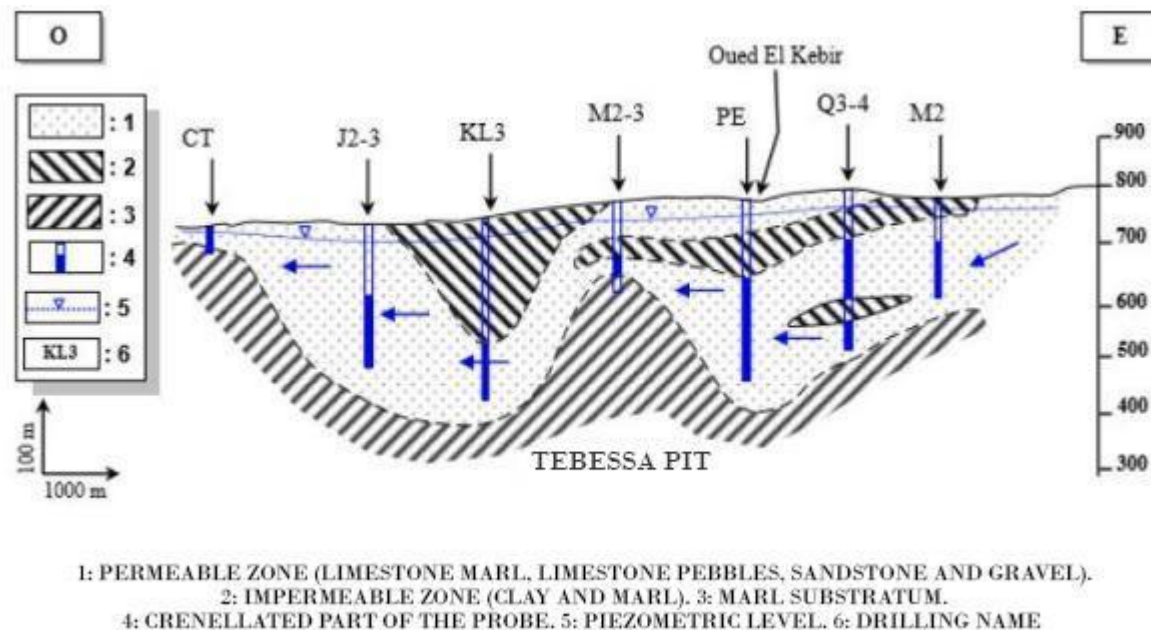


Figure 20: Hydrogeological section across Tebessa plain. (Hemali, 2020).

II.5.2. Boundary conditions maps

Figure 21 represents a summary of previous work (Djabri, 1987; Ghuerieb, 2011), which represents the boundary conditions characterizing the aquifer system of part from the studied area. The direction of flow of groundwater follows that of Oued El-Kebir which plays the role of drainage axis of the surface aquifer on a South-East North-West axis, the aquifer is characterized by a limit at incoming flow to the East, North and South-East. An outflow limit is located to the West. To the south, the eastern limit of inflow which

constitutes the most important limit in terms of recharge of the aquifer, because in this part the aquifer is in direct contact with the carbonate formations which also represents another system neighboring aquifer.

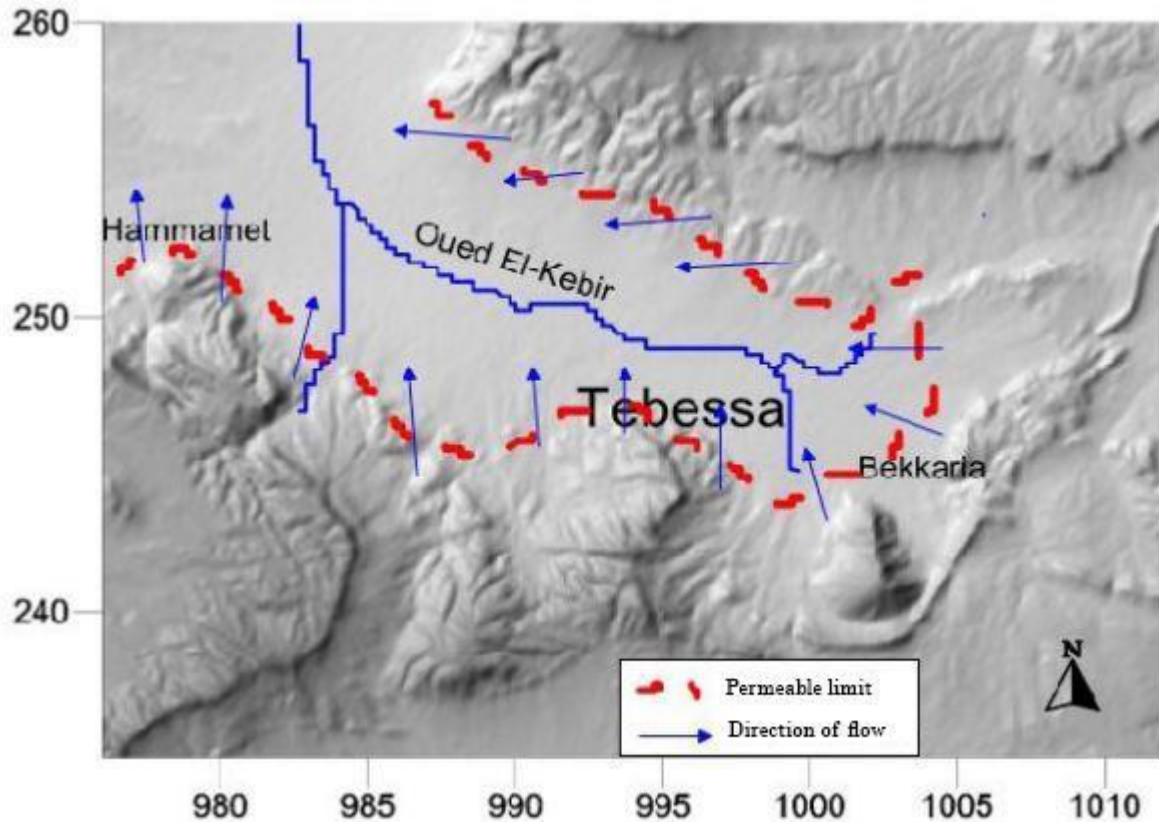


Figure 21: Map of boundary conditions of the study area (Hemali, 2020).

As for the other studied area, the general flow in East-West direction, part of this water converges towards Oued El-Kebir, which plays the role of drainage axis of the surface water table. The limestone formations located on the edges are cracked, thus ensuring recharge of the water table.

The water table is supplied via the north and south edges. To the east the aquifer is slightly recharged (Triassic), while to the west a partial recharge exists via the Turonian limestones. (Figure 22).

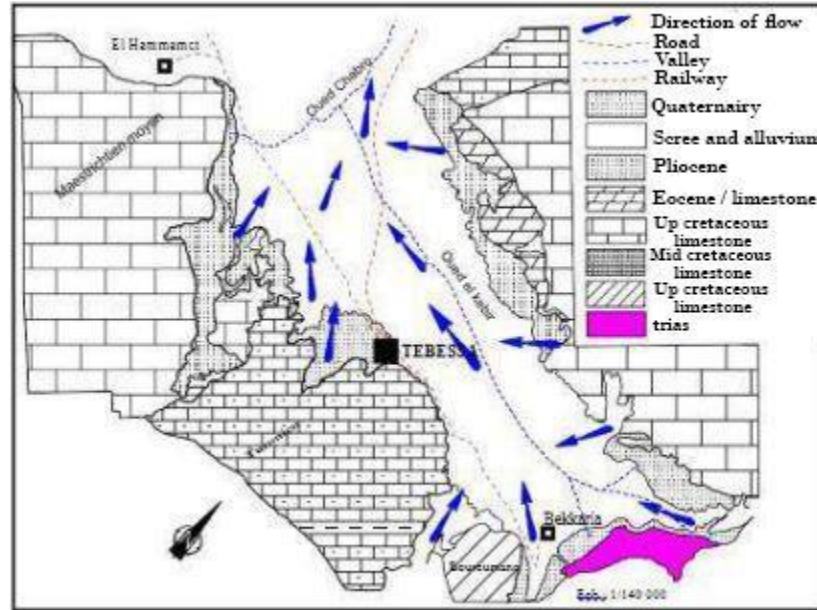


Figure 22: Map of boundary conditions of the study area (Djabri, 1987).

II.5.3. Piezometry

Piezometry is the measurement of depth of the surface of the groundwater table. This level is measured using an electrical probe. When the probe reaches the level of the air/water interface, electrical contact is established between two metal rods, triggering a sound and light signal.

II.5.3.1. Inventory of water points

It will be based on the readings carried out on the 36 domestic wells (Figure 23). The measurements a campaign was carried out during the month of March 2020.

The water points sampled for the establishment of piezometric maps are distributed as on the inventory map, they were dug according to the means available and which generally have no protection against surface water.

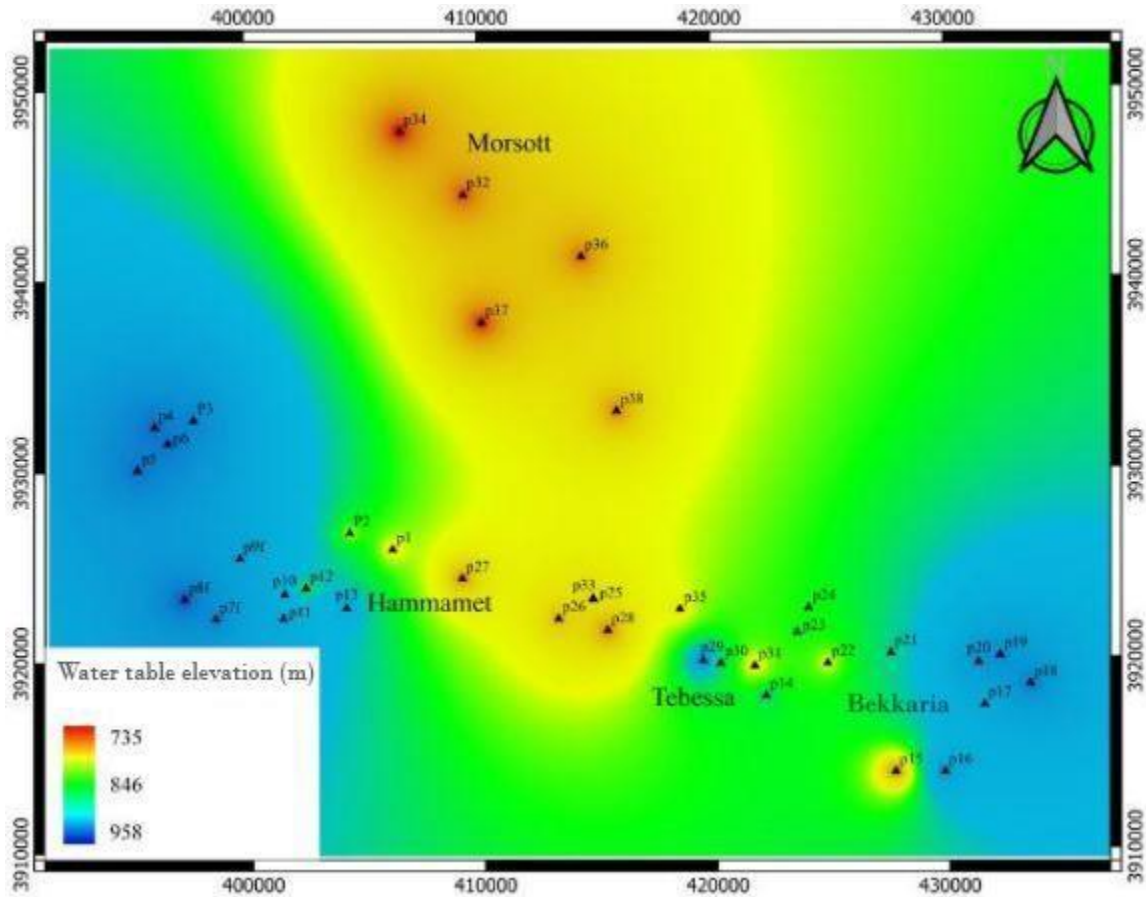


Figure 23: The inventory map of wells on the plain (Bekkaria-Tebessa-Hammamet-Morsott) (Fathi, B., & Smail, B. 2021).

II.5.3.2. Establishment of a piezometric map

Knowledge of the piezometric state by establishing the piezometric map for the plain in space is of great importance in the context of this study. For this reason, we carried out a piezometric campaign, in March 2020.

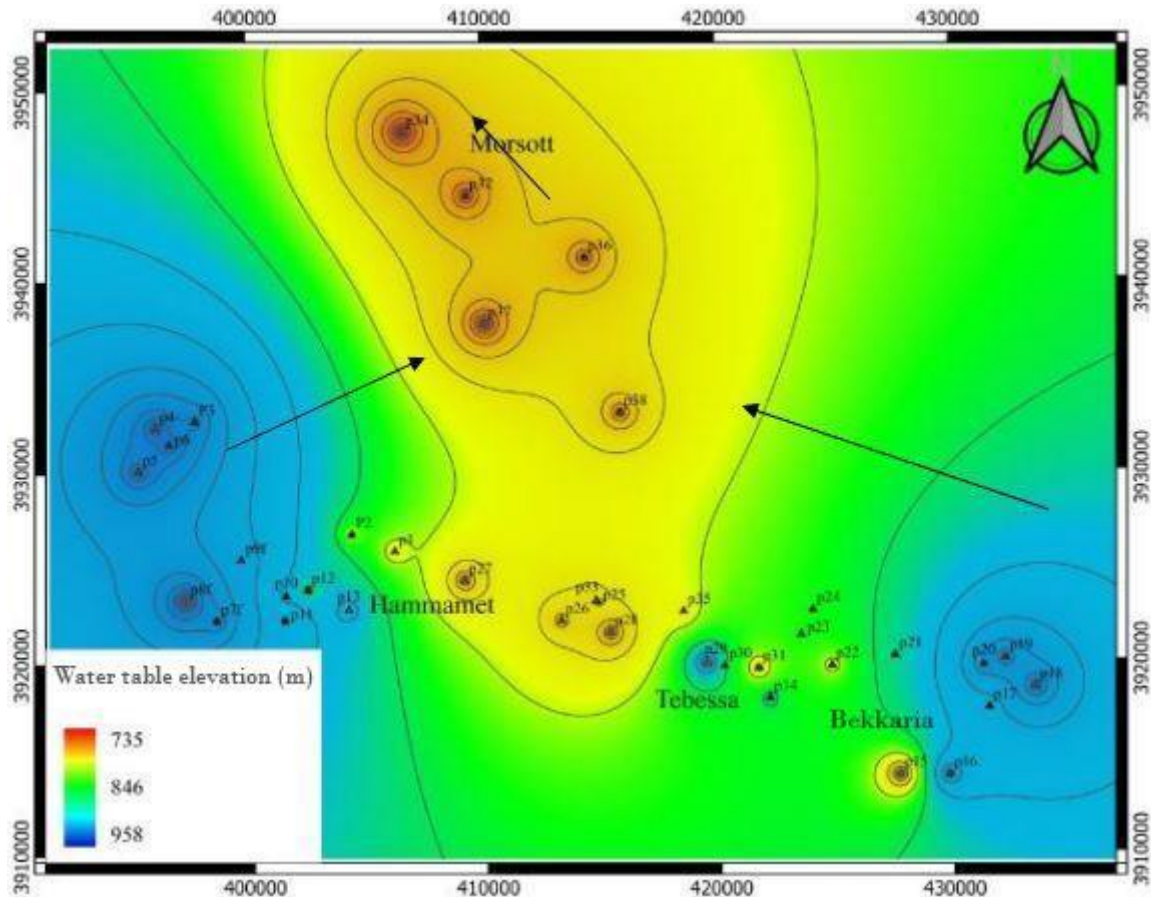


Figure 24: piezometric map (Fathi, B., & Smail, B. 2021).

The measurement of piezometric levels of 37 wells at the level of the Tebessa plain majority of wells are imperfect structures, distributed irregularly throughout the plain and which are largely used for irrigation and domestic needs; water depth in the wells is from 1.6 to 49.73m.

The piezometric map figure 24 allows to visualize a general flow from the South-South-East towards Ain Chabro wadi and then towards the North (Morsott) which confirms the direction of flow known in the region. A rapid flow noted in the South-South-East part with a hydraulic gradient estimated at 0.03 and in the South-East part a flow from a direction towards the North which can be explained by a lateral supply by the limestones of Maastrichtian of Hammamet with a less significant hydraulic gradient.

- Bekkaria zone: the curves are tight, and their spacing is considerable, with current lines in an East-West direction; which translates an area accumulation and drainage by Oued El-Kebir. The supply of this area comes from the edges of the plain.
- Tebessa zone: the piezometric curves are regularly spaced reflecting a zone of accumulation and drainage by El-Kebir wadi.
- Ain Chabro zone: the curves become spaced out and reflecting a groundwater accumulation zone.

II.6. Climatic

II.6.1. Climate type

Algeria, due to its geographical situation, is divided into three distinct climatic zones (figure 25), the first with a Mediterranean climate in the north, the second with a semi-arid climate towards the interior of the country (high plateaus), and finally an arid climate characterizing the vast Sahara.

The study region of Tebessa is part of the semi-arid domain, known for hot and dry summers and cold and humid winters. Thus, these widely varying hydroclimatic parameters greatly influence the swelling-shrinkage phenomenon of the clay formations on the surface.

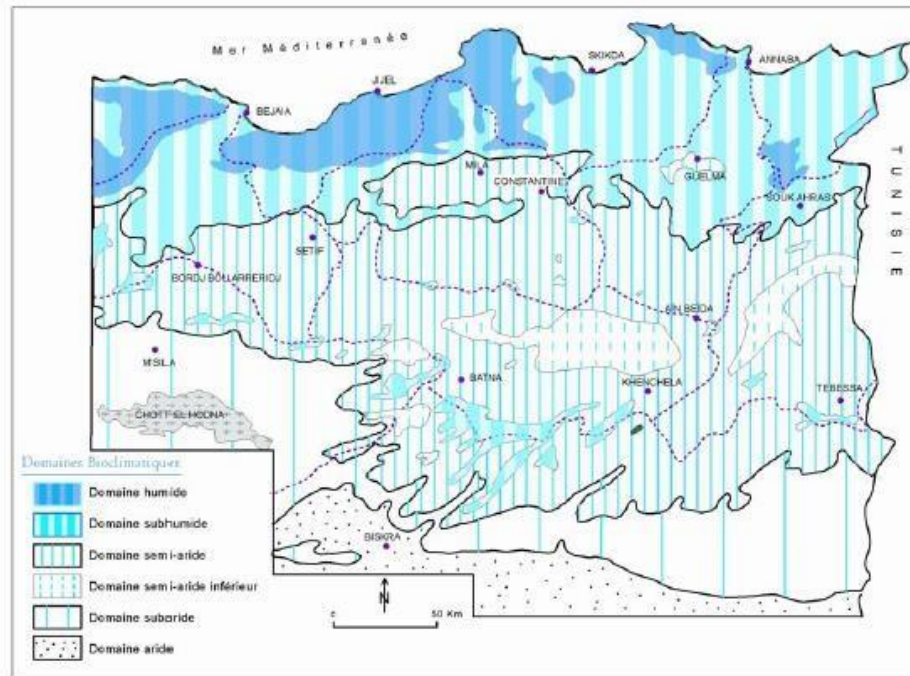


Figure 25: Simplified map of the climatic zones of Eastern Algeria (Based on Côte M., 1998).

II.6.2. Precipitations

The distribution of precipitation in time and space conditions the shape of the flows and the contributions to the water tables. Table 5 gives an overview of the distribution of monthly precipitation at Tebessa during the period (1972/2012).

Table 5: Average monthly precipitation (mm) at Tebessa (1972/2012).

Month	S	O	N	D	J	F	M	A	M	J	J	A
Precipitations	40.7	36.1	33.3	28.5	26.4	26.9	44.1	32.7	38.8	26.8	13.1	29.4

We note that the month of March and the month of September are the rainiest, reaching 44.1mm and 40.7mm respectively. Note that the rains in the summer season are exceptionally torrential and stormy and can in one or two days reach the average for the entire month. These summer rains, when they precipitate suddenly, have a notable erosive

effect on the interception surfaces (impact of drops of water on the ground which receives them) and cause a temperature difference and increase the humidity level in a way that cannot be neglected in a study which concerns the phenomenon of compressibility.

The analysis of the curve of interannual variations of precipitation over a period of 40 years (1972/2012) (Figure 26), shows that the year 1972 is the wettest with 634.7 mm/year, on the other hand the year 1997 is the driest with 207.4 mm/year. Note that the average annual rainfall module is around 376.9 mm/year.

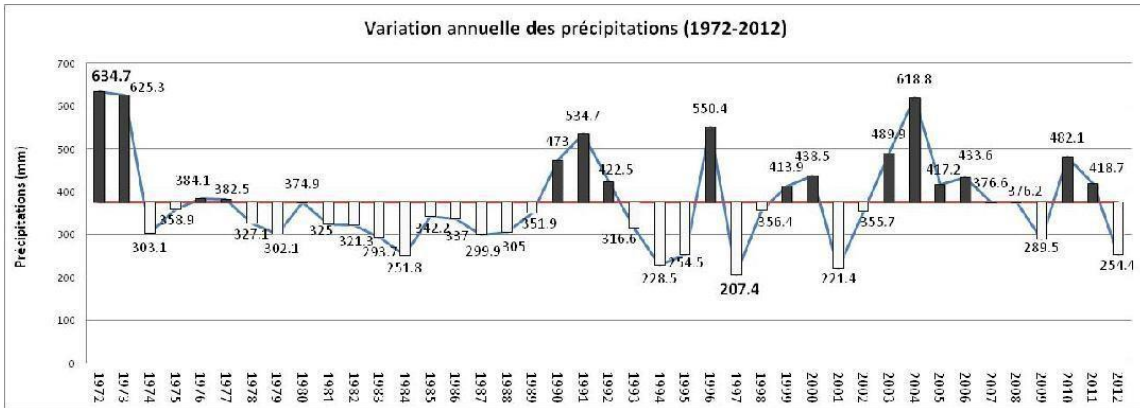


Figure 26: Interannual variation of precipitation at the Tébessa station (1972/2012).

Table 6 summarizes the wet years exceeding the average annual rainfall module. It is very remarkable that the wet and dry periods are very far apart, a characteristic element of semi-arid climates, thereby accentuating the swelling-shrinkage phenomenon.

Table 6: Wet years during the period (1972-2012).

Wet years	1972	1973	1976	1977	1980	1990	1991	1992	1996	1999
	2000	2003	2004	2005	2006	2007	2008	2010	2011	

II.6.2. Temperatures

Temperature is a determining factor of the climate which allows the calculation of the water balance and specifies periods of drought where the phenomenon of clay shrinkage is to be feared.

Table 7 and Figure 27 represent the monthly average temperature distribution. The month of January is the coldest with an average monthly temperature of 6.65°C, but the hottest month is July with an average monthly temperature of 26.28°C. This considerable thermal difference is characteristic of a semi-arid climate and is responsible for the thermoclasty of surface rocks and soils. For clays, the increase in temperature is responsible for the desiccation in a polygonal shape on the dehydrated surface.

Table 7: Température moyenne mensuelle 1972/2012.

Months	Sep	Oct	Nov	Dec	Jan	Feb	Mar	Apr	May	Jun	Jul	Aug
T°C	21.53	17.14	11.10	7.88	6.65	7.82	10.47	13.41	18.62	23.43	26.28	25.55



Figure 27: Monthly temperature distribution 1972/2012.

II.7. Conclusion

The overview of the different geological formations of the studied region has allowed for the identification of areas where the main formations are clays and marls, based on a lithostratigraphic description of the existing ages in the region. Among these formations, we note: the Lower Maastrichtian, mainly composed of gray marls and marl-limestones; the Paleogene, which features clay and gypsum formations; the Pliocene, characterized by the abundance of red clays; and the alluvial formations marked by the presence of clays, silty clays, sand and silt deposits.

Thus, the consultation of maps and geological cross-sections derived from core drillings carried out in the studied region confirms the existence of fine-grained soil, clayey and marl-clay formations at shallow depths. Despite their heterogeneity on a metric scale, they can be considered homogeneous on the scale of the study region. The degradation of clay and marl formations directly produces fine plastic soils, which are prone to volume changes due to changes in their water content or due to external loading. This mechanism can cause ground instability problems in the short or long term.

Hydrogeological and climatic study has highlighted the contribution of precipitation to surface watercourses and groundwater, especially during the months of January, February, and March. During months with below-average rainfall, the water supply is compensated by an increase in humidity. When potential evapotranspiration depletes all surface and subsurface water reserves (easily usable reserves), soil fine grain compression comes into play, especially during the summer period. During this dry period, the reduction in volume of clayey and silty soils, coupled with loading and external charges, leads to the formation of characteristic polygonal-shaped desiccation cracks. This underscores the soil's susceptibility to deformation under loading conditions.

Chapter III:
Geotechnical Data
Investigation

III.1. Introduction

The identification and characterization of soils play a fundamental role in geotechnical engineering, providing crucial insights into their properties and behavior under various loading and environmental conditions (Razmyar, A., & Eslami, A. 2017). In the context of the Tebessa region, where diverse geological formations and environmental factors influence soil composition, understanding the characteristics of local soils is paramount for informed decision-making in geotechnical engineering projects. This chapter focuses on the comprehensive investigation and characterization of soils sampled from the Tebessa region. And samples taken from the studied area to conduct a series of laboratory tests, including Oedometer tests, Atterberg limits analysis, and other geotechnical tests, to elucidate their engineering properties and behavior. By conducting these tests, we aim to establish a robust understanding of soil composition, density, moisture content and compressibility characteristics prevalent in the studied area. This study will contribute to the development of accurate geotechnical models and also will be used in validation of the obtained models and equations in the next chapter.

III.2. Presentation of geotechnical soil data in the studied region

For the determination of geotechnical properties of soils related to soil compression-recompression phenomenon in the study area, it is possible to identify the compressibility by determining a number of simple geotechnical parameters that are related to the compressibility character of the soils and are determined, for the most part, during the preliminary reconnaissance phase. Thus, we can suspect the compression and recompression characters of a soil through particularly interesting tests: We cite in particular the identification tests (Atterberg limits, particle size analysis, methylene blue value and hydrometer analysis) and mechanical tests (Oedometer swelling test and Oedometric compressibility test).

At this stage of recognition, classifications available in the literature can be used to qualitatively identify the soils studied. In this chapter we will present the geotechnical identification and characterization of the soils of the studied region, as well as the application of different indirect methods based on the available data.

III.2.1. Implementation of boreholes

For all geotechnical studies, soil studies are obtained from core boreholes, carried out in the area under study. In our case, more than 110 boreholes, with a depth ranging from 2 to 20 m were used (Figure 28), other samples were recovered from excavations and excavations. The necessary data were sorted and selected to facilitate their exploitation. They are spread over an area of about 100km² on four sectors (Route El-kouif, El-Merdja, Route de Constantine and the center of the city) where the thickness of the clay and marl layers is important; these formations can reach 200m thick according to (Durozoy. Gy 1948; Bles J.L, Fleury J.J 1970), the geological nature of the majority of the formations can be described as marly clays and greyish marl to greenish gypsum with little compactness.

The physical and mechanical properties measured for the studied sites are:

- Sieving and hydrometer analysis according to NF P94-056 and NFP94-057 respectively,
- Atterberg limits (liquidity limits and plasticity index) according to NFP94-051;
- Natural water content according to NF P94-050;
- Dry volume weight according to NF P94-053;
- Methylene blue value NF P 94-068;
- Compression pressure at the Oedometer according to XP P 94-090-1;
- Oedometer swelling pressure according to XP P 94-091.

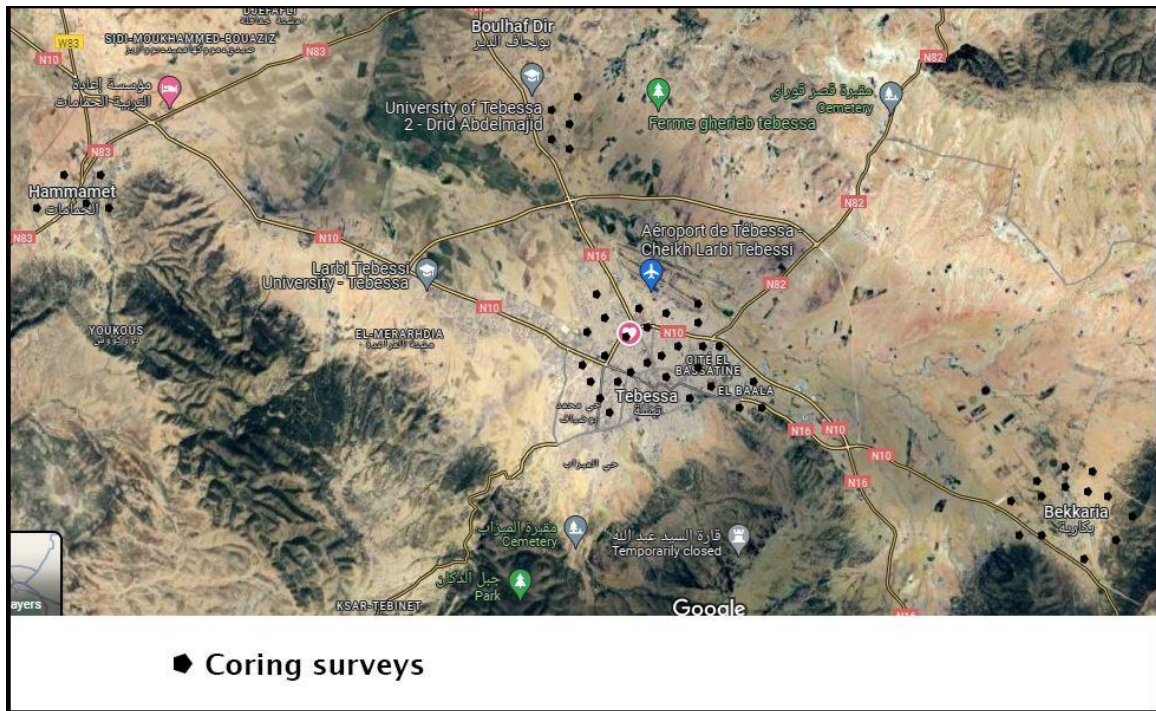


Figure 28: Implementation of boreholes in the studied area.

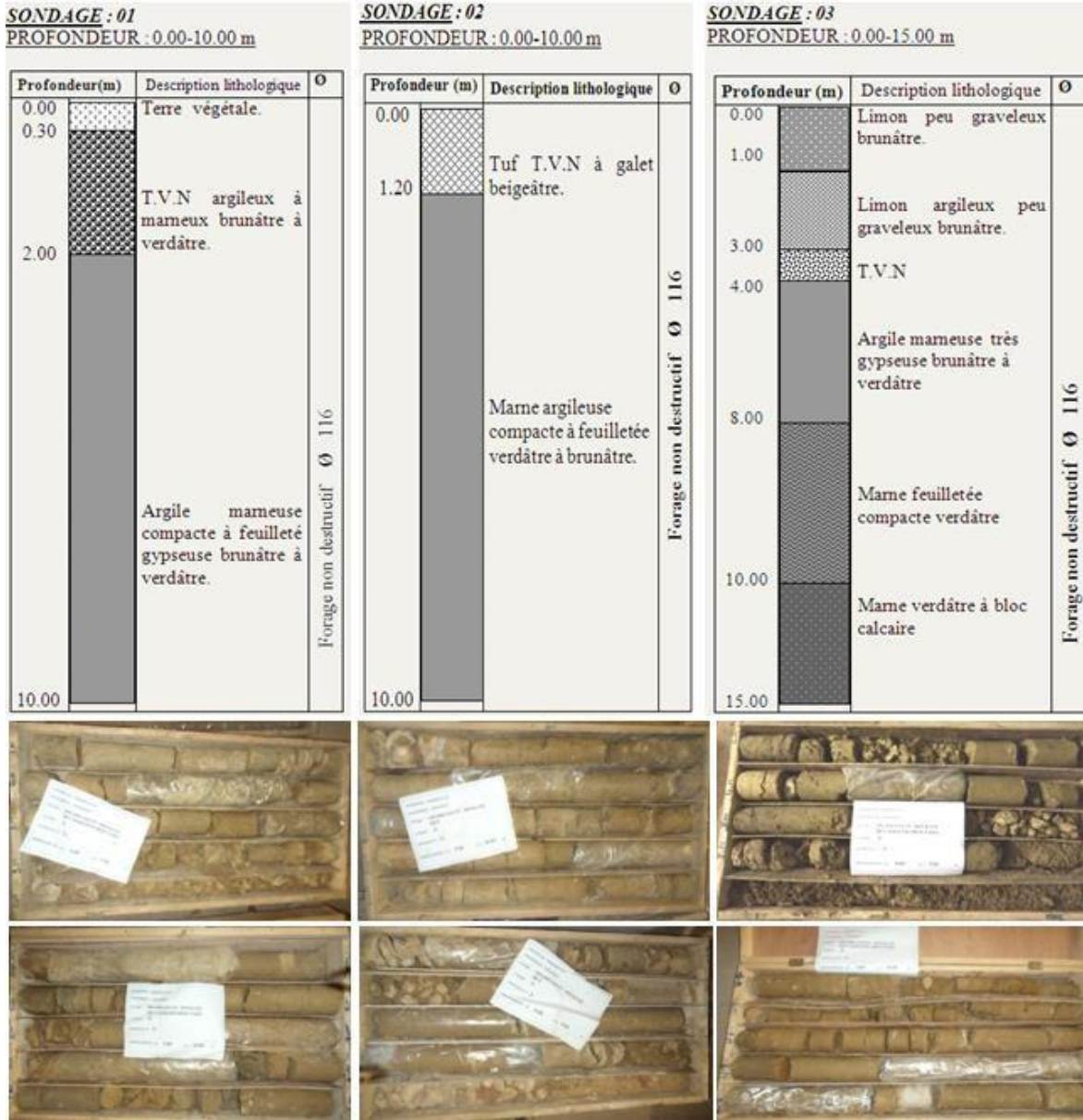


Figure 29: Logs of representative surveys taken in the study area (LTPE).

Physical, mechanical and chemical tests are conducted on all samples. Table 8 below summarize all the results:

Table 8: Synthesis of soil geotechnical characteristics of the study area.

Symbol	Description	Values / classification
γ_d (kN/m^3)	Dry unit weight	10,1 - 19,5
w (%)	Water content %	8.43 - 46,2
F_f (%) < $80\mu m$	Fine friction < 0,08mm	29.64 – 99
F_c (%) < 0,02	Fine friction < 0,02mm	26,64 – 56,16

LL (%)	Liquid limit	28 – 150
PI (%)	Plasticity index %	11 – 85
A	Activity ($I_p / < \text{fraction } 0,02\mu\text{m}$)	0,4 – 2,13
VBS	Methylene blue value	2,2 – 10,84 (g/100g de sol sec)
Cc	Compression index	0,044 - 0,582
Cs	Swelling index	0,023 - 0,307
Pc (kPa)	Preconsolidation pressure	37,5 – 270
Ps (kPa)	Swelling pressure	60 – 670
CaCo3 (%)	Percentage of Calcium Carbonate	68,1 - 1,53
Gypse (%)	Gypsum percentage	60,86 - 1,51

III.3. Identification and classification of the soils studied

In the field of geotechnics, clay soil is considered to be a loose material, the largest proportion of which consists of elements smaller than 2 μm . these elements are mostly made of clay minerals, the few remaining are not clay such as carbonates, feldspars, quartz, etc. the proportion and nature of clay minerals largely characterize the mechanical behaviour of the soil and the extent of water exchange.

The classification systems (USCS, LPC or GTR) detail more precisely the characteristics of a clay soil. For example, in LPC clay soils correspond to the fine soil classes of more than 50% element less than 80 μm with a portion of organic matter (OM).

III.3.1. Granulometry of the studied soils (grain size)

Grain size is the description of the solid or skeleton phase of the soil; it aims to determine the percentage of different granular fractions according to their size to allow a classification of soils and provide an order of magnitude of some of these properties. The grain size is very simple to implement; sieving is used for the fraction $> 0.08\text{mm}$. If more than 50% of the soil have grain dimensions $> 0.08\text{mm}$, the soil is said to be coarse. If more than 50% of the soil is of fraction $< 0.08\text{mm}$, they are classified as fine soils and are classified according to their plastic behavior.

Several classifications are used to identify soils according to their grain sizes. In this study the LPC and GTR classification were adopted to classify soil in the region.

The LPC classification (Laboratoire des Ponts et Chaussées) is based on the USCS classification (United States). On the one hand it uses particle size analysis for coarse matrix soils and on the other hand on the Atterberg limits for fine matrix soils. According to this classification (Figure 30), Tebessa clay corresponds to very plastic clays (**At** in French, **CH** in English) and medium plastic clays (**Ap** in French, **CI** in English).

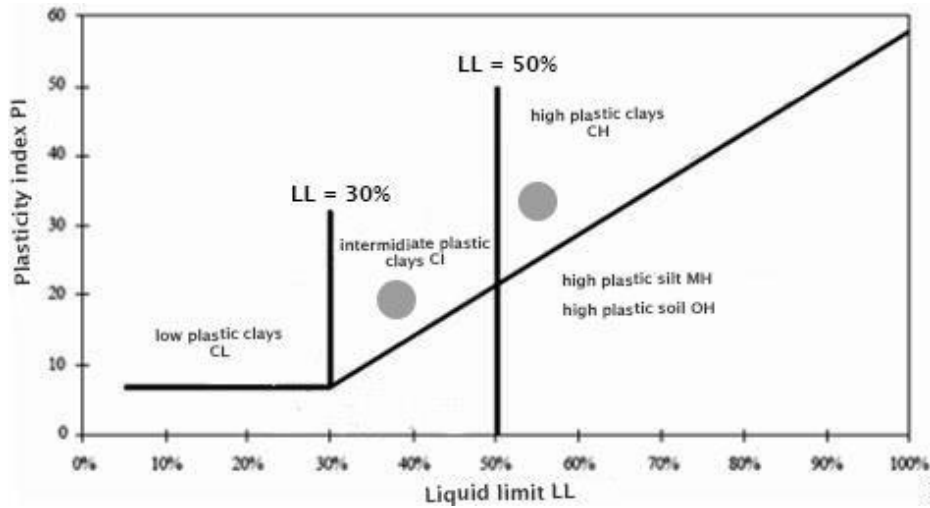


Figure 30: LPC classification of fine soils, the gray dot identifies the clay of the study area.

The GTR classification (Guide des Terrassement Routier) according to the standard (NF P 11-300) which replaces the RTR, used in particular in earthworks and embankments, the classification is based on two synoptic tables (Figure 31 and Table 9) is aimed at characterizing not only the granulometric nature of a soil but also its sensitivity to water and its natural water state.

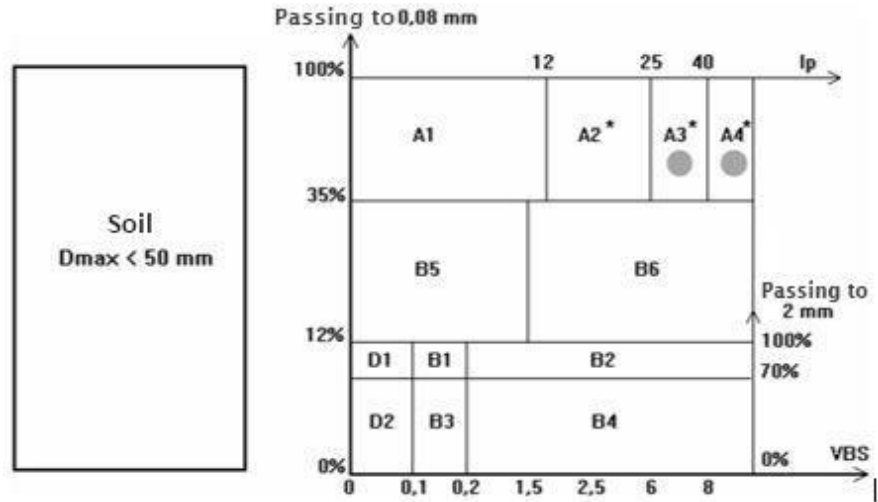


Figure 31: GTR soil classification with $D_{max} < 50$ mm. Source: NF P 11-300.

According to the GTR classification Tebessa clay is of class A3, corresponds to clays and marly clays, very plastic silts and A4 corresponds to very plastic clays and marly clays.

There is agreement between the LPC soil geotechnical classification (based on USCS) and the GTR classification. Soil behaviour indicates that both classifications are most relevant. These soils are also visually described as marly clays, silty clays and marls (Figure 29).

Table 9: Fine Soil Classification (GTR) Standard NF P 11 – 300.

Classement selon la nature				Classement selon l'état hydrique		
Paramètres de nature Premier niveau de classification	Classe	Paramètres de nature Deuxième niveau de classification	Sous classe fonction de la nature	Paramètres d'état	Sous classe fonction de l'état	
D _{max} ≤ 50 mm et Tamisat à 80 μm > 35%	A	VBS ≤ 2,5 ⁽¹⁾ OU I _p ≤ 12	A₁ Limons peu plastiques, loess, sils alluvionnaires, sables fins peu pollués, arènes peu plastiques...	IPI ⁽¹⁾ ≤ 3 OU W _n ≥ 1,25 W _{OPN}	A ₁ th	
				3 < IPI ⁽¹⁾ ≤ 8 OU 1,10 ≤ W _n < 1,25 W _{OPN}	A ₁ h	
				8 < IPI ≤ 25 OU 0,9 W _{OPN} ≤ W _n < 1,1 W _{OPN}	A ₁ m	
				0,7 W _{OPN} ≤ W _n < 0,9 W _{OPN}	A ₁ s	
				W _n < 0,7 W _{OPN}	A ₁ ts	
		12 < I _p ≤ 25 ⁽¹⁾ OU 2,5 < VBS ≤ 6	A₂ Sables fins argileux, limons, argiles et marnes peu plastiques arènes...	IPI ⁽¹⁾ ≤ 2 OU I _c ⁽¹⁾ ≤ 0,9 OU W _n ≥ 1,3 W _{OPN}	A ₂ th	
				2 < IPI ⁽¹⁾ ≤ 5 OU 0,9 ≤ I _c ⁽¹⁾ < 1,05 OU 1,1 W _{OPN} ≤ W _n < 1,3 W _{OPN}	A ₂ h	
				5 < IPI ≤ 15 OU 1,05 < I _c ≤ 1,2 OU 0,9 W _{OPN} ≤ W _n < 1,1 W _{OPN}	A ₂ m	
				1,2 < I _c ≤ 1,4 OU 0,7 W _{OPN} ≤ W _n < 0,9 W _{OPN}	A ₂ s	
				I _c > 1,3 OU W _n < 0,7 W _{OPN}	A ₂ ts	
		25 < I _p ≤ 40 ⁽¹⁾ OU 6 < VBS ≤ 8	A₃ Argiles et argiles marnées, limons très plastiques...	IPI ⁽¹⁾ ≤ 1 OU I _c ⁽¹⁾ ≤ 0,8 OU W _n ≥ 1,4 W _{OPN}	A ₃ th	
				1 < IPI ⁽¹⁾ ≤ 3 OU 0,8 ≤ I _c ⁽¹⁾ < 1 OU 1,2 W _{OPN} ≤ W _n < 1,4 W _{OPN}	A ₃ h	
				3 < IPI ≤ 10 OU 1 < I _c ≤ 1,15 OU 0,9 W _{OPN} ≤ W _n < 1,2 W _{OPN}	A ₃ m	
				1,15 < I _c ≤ 1,3 OU 0,7 W _{OPN} ≤ W _n < 0,9 W _{OPN}	A ₃ s	
				I _c > 1,3 OU W _n < 0,7 W _{OPN}	A ₃ ts	
		I _p > 40 ⁽¹⁾ OU VBS > 8	A₄ Argiles et argiles marnées, très plastiques...	Valeurs seuils des paramètres d'état, à définir à l'appui d'une étude spécifique		A ₄ th
						A ₄ h
						A ₄ m
						A ₄ s

III.3.2. Atterberg limits

The liquidity limit LL and the plasticity index PI are used to determine not only the plastic nature of the soils but also gives an idea of their swelling potential using the Casagrande abacus. The exploitation of the test results gives a point cloud following the Casagrande abacus (Figure 30, Figure 32) following the transfer of the limit values of liquidity LL and the plasticity index I_p. This abacus gives a soil called clay of medium to high plasticity.

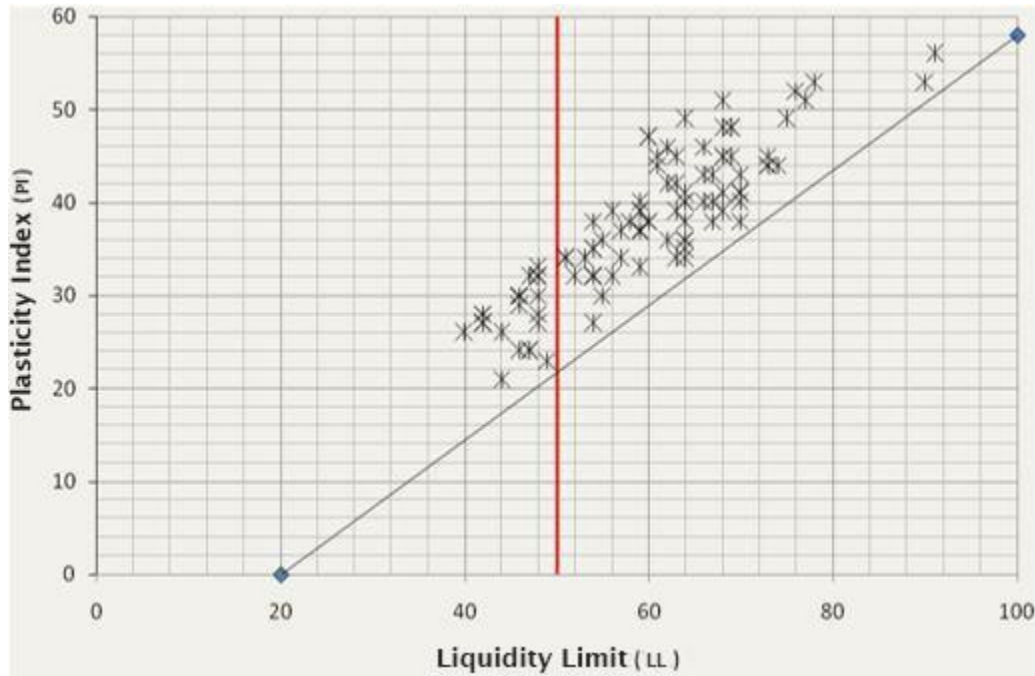


Figure 32: Projection of measurements of (LL and PI) soils studied on Casagrande abacus.

III.4. Tests and results

Soil samples were gathered and analyzed in a specific laboratory to obtain their physical and index properties. Key parameters like C_c and C_s underwent testing via Oedometer tests. Subsequently, the data underwent statistical scrutiny utilizing the principles of Design of Experiments (DOE). Various screening designs, including two-level full factorial design, and also central composite design (CCD) was employed for process optimization using Response Surface Methodology (RSM), demonstrating the core principles and applications of DOE. Equations were formulated to predict the compression and recompression indexes C_c and C_s based on soil index properties, which are relatively simple to assess in the laboratory. The impact of each parameter on compressibility was examined through extensive literature review. By identifying factors influencing compressibility and fitting equations to optimize responses via maximization or minimization functions in the full factorial and RSM methods, attained superior models compared to existing published ones.

After obtaining these equations for the C_c and C_s coefficients, we need to verify them, by taking samples from the studied area and performing all the necessary tests, in order to test the equations, and compare the results obtained from the tests with the results obtained from the equations.

The equations obtained after treating previous collected data with the design expert software carry the following parameters: (Water content w (%), dry unit weight (kN/m^3), degree of saturation (%), liquid limit LL , fine friction F_f , void ratio e_0), so we need to perform the tests to get these parameters. Two sample of fine-grained soil collected from the studied area (Figures 33 and 34).



Figure 33: Sample 1 location (UTM: zone 32, easting 416801, and northing 3916741).



Figure 34: Sample 2 location (UTM: zone 32, easting 415225, and northing 3920853).

a- Water content:

NFP 94-050 might refer to a specific method or standard used for measuring the water content of soil samples in geotechnical engineering. Typically, the water content of soil is determined by comparing the initial and final weights of a soil sample before and after drying it to remove all the water. This method is often referred to as the oven-drying method.

Here's a basic outline of how the NFP 94-050 method might work:

1. Obtain a representative soil sample from the site.
2. Weigh the sample accurately (initial weight).
3. Place the sample in an oven at a specified temperature (usually around 105°C to 110°C) for a specified duration (typically 24 hours).
4. After drying, weigh the sample again (final weight).
5. Calculate the water content using the formula: $\text{Water Content (\%)} = \frac{(\text{Initial Weight} - \text{Final Weight})}{\text{Final Weight}} * 100$.

Table 10: Water content results.

N° Samples	1				2			
	I		II		I		II	
P.H Tare (g)	55.41	66.98	67.74	63.13	54.40	61.85	48.56	51.16
P.S Tare (g)	50.83	60.37	61	57.39	50.33	57	44.85	47.37
P. Tare (g)	23.10	21.63	21.17	23.29	23.66	24.66	24.05	25.04
P. Water (g)	4.58	6.61	6.74	5.74	4.07	4.85	3.71	3.79
P. Dry soil (g)	27.73	40.52	39.83	34.10	27.27	32.34	23.80	28.66
Water content (%)	16.51	16.31	16.92	15.18	14.92	14.99	15.58	13.22
Water content (%)	16.41		16.05		14.95		14.4	

b- Unit weight:

NFP 94-053 likely refers specifically for determining the unit weight of soil. Unit weight, also known as density, is a critical parameter in soil mechanics and geotechnical engineering as it influences soil behavior.

The unit weight of soil can be determined using various methods, including laboratory tests and in-situ measurements. NFP 94-053 could specify a particular laboratory test method for measuring the unit weight of soil samples.

NFP 94-053, the method likely involves measuring the weight and volume of a soil sample to calculate its unit weight. Here's a general outline of how such a method might work:

1. **Sample Preparation:** Obtain a representative soil sample from the site and prepare it for testing. This may involve removing large particles, rocks, or organic materials and ensuring the sample is adequately compacted.
2. **Weight Measurement:** Weigh the soil sample accurately using a laboratory balance (weight of the sample without and with paraffin, also sample weight in the water using hydrostatic balance).
3. **Volume Measurement:** Measure the volumes (gross, paraffin and net volume).

4. Calculate Unit Weight: Calculate the unit weight (density), Calculation method below the table 11.



Figure 35: Paraffined and weighed samples.

Table 11: Unit weight results.

N° Samples	1		2	
	I	II	I	II
P.H Paraffin (g)	624.50	142.94	181.72	341.69
Wet weight (g)	608.22	137.58	174.63	333.77
Paraffin weight	16.28	5.36	7.09	7.92
weight of soil in water (g)	308.64	68.61	84.39	167.31
Gross volume (cm ³)	315.86	74.33	93.33	174.38
Paraffin volume (cm ³)	18.5	6.1	8.05	9
Net volume (cm ³)	297.36	68.23	85.28	165.38

Wet unit weight (t/m ³)	1.99	2	2.07	2.08
Water content (%)	16.41	16.05	14.95	14.4
Dry unit weight (t/m ³)	1.71	1.72	1.81	1.82

Gross volume = Wet weight with paraffin – Weight of soil in water

$$\text{Paraffin volume} = \frac{\text{Paraffin weight}}{0.88}$$

Net volume = Gross volume – Paraffin volume

$$\text{Wet unit weight} = \frac{\text{Wet weight}}{\text{Net volume}}$$

$$\text{Dry unit weight} = \frac{\text{Wet unit weight}}{\text{Water content} + 100} * 100$$

c- Atterberg limits (Liquid limit):

In geotechnical engineering, the Atterberg limits refer to specific water content thresholds that define the consistency and behavior of fine-grained soils, particularly clays. The Atterberg limits are determined through standardized laboratory tests according to specific procedures outlined in standards like NFP 94-051.

Liquid Limit (LL) is the water content at which a soil transitions from a liquid to a plastic state. This transition is determined using the Casagrande method or a cone penetrometer test, where the soil is progressively mixed with water until it just begins to flow along a groove. The water content at this point is the liquid limit. The liquid limit helps classify soils for engineering purposes and provides insight into their behavior under different moisture conditions.

Determining the liquid limit of a soil sample in the laboratory involves following a standardized procedure to identify the water content at which the soil transitions from a

liquid to a plastic state. The test is typically conducted using the Casagrande method. Here are the key steps involved in determining the liquid limit:

1. Preparation of Sample: Take a representative soil sample (typically passing through a 0.4mm sieve) and air-dry it if necessary. Break down any aggregates to ensure uniformity. Mix the soil sample thoroughly with distilled water to form a uniform paste. The moisture content of the sample should initially be above the expected liquid limit.



Figure 36: Washing the samples through a 0.4mm sieve.

2. Setting up the Casagrande Apparatus: Set up the liquid limit device (Casagrande apparatus) on a flat, stable surface. Ensure that the cup can be raised and dropped smoothly.
3. Preparation of Test Portions: Take a portion of the moist soil sample and place it in the cup of the Casagrande apparatus. Level and smooth the soil surface.



Figure 37: portion of the moist soil sample in the cup of the Casagrande.

4. Grooving Process: Use the grooving tool to create a groove in the soil sample. The groove should be made by lowering the cup through a standardized distance and then cutting a groove with a standardized tool.



Figure 38: Grooving the Portion in the cup of the Casagrande.

5. Lift and drop the cup by turning crank at the rate of two revolutions per second until the two halves of soil cake come in contact with each other, and record the number of blows, N.
6. Take a representative portion of soil from the cup (portion from each side) for moisture content determination.



Figure 39: Determination of moisture content

7. Repeat the test with different moisture contents at least to get three points.

Table 12: Liquid limit results for sample 1.

tests	1		2		3	
N° of blows	33		24		15	
Total wet weight (g)	35	37	32.04	37.69	38.25	31.89
Total dry weight (g)	31.02	32.32	28.13	33.55	31.99	27.76
Tare weight (g)	24.61	24.82	22.29	27.33	23.23	22.04
Water weight (g)	3.98	4.68	3.91	4.14	6.26	4.13
Dry soil weight (g)	6.41	7.5	5.84	6.22	8.76	5.72
Water content (%)	62.1	62.4	66.95	66.55	71.46	72.2
Water content (%)	62.25		66.75		71.83	

Table 13: Liquid limit results for sample 2.

tests	1		2		3	
N° of blows	35		27		18	
Total wet weight (g)	33.5	35.3	33	36	37.5	33.9
Total dry weight (g)	29	31	28.13	31.55	31.4	28.6
Tare weight (g)	22.3	23.42	20.8	26.33	21.53	20.6
Water weight (g)	4.5	4.3	4.87	4.45	6.1	5.3
Dry soil weight (g)	7.69	7.15	7.33	5.22	8.87	8.05
Water content (%)	58.5	60.1	64	62.2	67.3	65.9
Water content (%)	59.3		63.1		66.6	

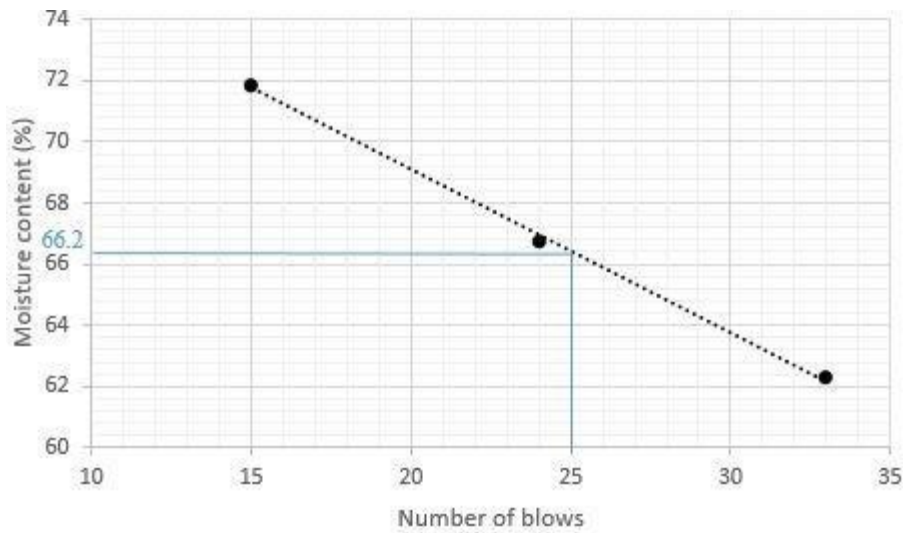


Figure 40: Liquid limit for sample 1 (LL= 66.2).

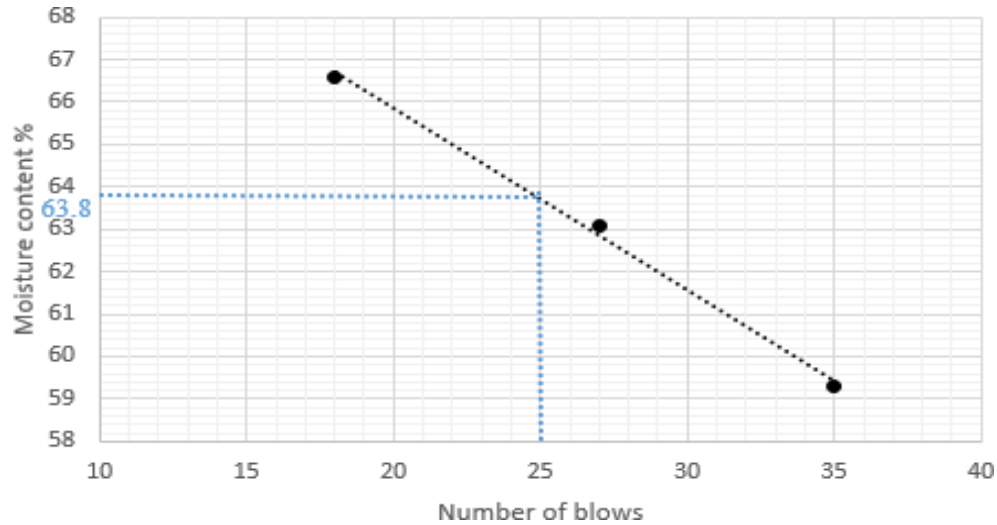


Figure 41: Liquid limit for sample 2 (LL= 63.8).

d- Oedometer test:

The NFP 94-090-1 standard in geotechnical engineering likely pertains to Oedometer tests, which are commonly used to determine the consolidation properties of soils. Consolidation refers to the process by which soil particles rearrange themselves under an applied load, resulting in a decrease in volume. Oedometer tests are crucial for assessing the compressibility and settlement characteristics of soils, which are essential considerations in the design of foundations and other geotechnical structures.

Here's an outline of how Oedometer tests typically work, based on the NFP 94-090-1 standard:

1. **Sample Preparation:** Obtain undisturbed or disturbed soil samples from the field at the desired depth. The samples are carefully handled to minimize disturbance.
2. **Sample Trimming:** Trim the soil sample to the desired dimensions using cutting tools to fit into the Oedometer test apparatus. For undisturbed samples, special care is taken to maintain the natural structure and fabric of the soil.



Figure 42: Sample trimming.

3. Sample Saturation: Fully saturate the soil sample with water to ensure that it is completely saturated before testing. This may involve immersion in water or vacuum saturation techniques to remove entrapped air.



Figure 43: Sample saturation.

4. Assembly of Oedometer Apparatus: Set up the Oedometer test apparatus, which typically consists of a loading frame with a loading platform, a porous stone or membrane to distribute the load uniformly, and a dial gauge or displacement transducer to measure vertical displacement.



Figure 44: Set the loading frame with a loading platform.

5. Loading: Place the saturated soil sample into the Oedometer cell and apply a vertical load incrementally using the loading frame. The load is typically applied in stages to allow for the measurement of settlement at each stage.

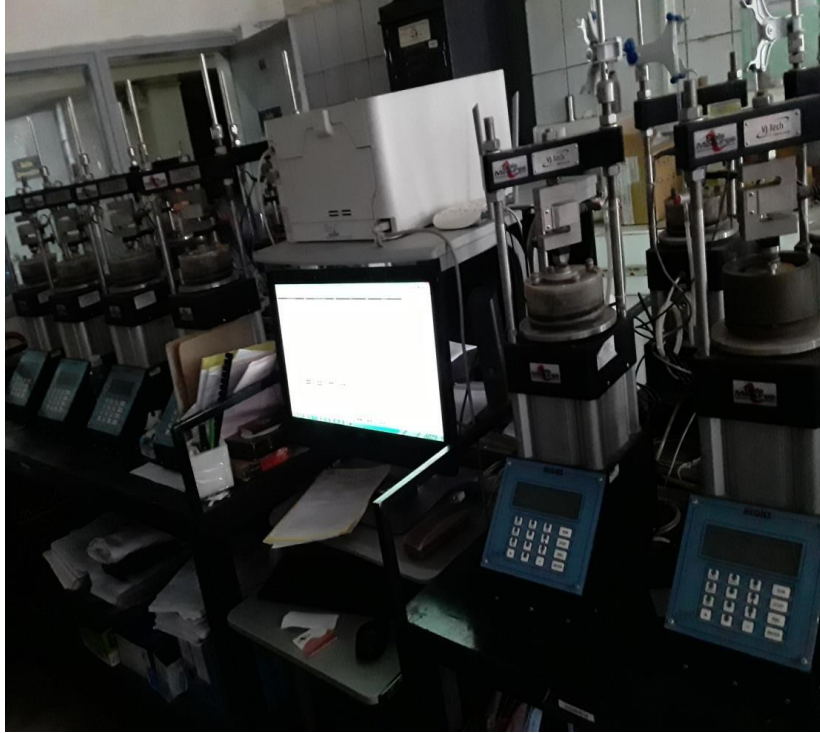


Figure 45: The loads are applied using air pressure via a computer.

6. Settlement Measurements: Measure the vertical settlement of the soil sample at regular time intervals or load increments using the dial gauge or displacement transducer. The settlement data are recorded and used to plot a settlement-time curve.
7. Data Analysis: Analyze the settlement-time curve to determine the consolidation characteristics of the soil, including the compression index (C_c) and recompression index (C_s), and the preconsolidation pressure (σ_p). These parameters are essential for predicting settlement and estimating the time required for consolidation to occur under different loading conditions.

Table 14: Oedometer test results for sample 1.

P. Kg/cm ²	P. kPa	Settlement Δh (mm)	Specimen height $H_i - \Delta h$ (mm)	Void ratio e_0
0	0	0	19	0.646
0.25	24.5	0.19	18.81	0.630
0.5	49	0.29	18.71	0.621

1	98	0.48	18.16	0.610
2	196	1.08	17.92	0.575
4	392	1.49	17.51	0.517
2	196	1.12	17.88	0.545
1	98	0.61	18.39	0.574
4	392	1.4	17.6	0.540
8	784.5	1.9	17.1	0.475
16	1569	2.42	16.58	0.365
8	784.5	2.05	16.95	0.39
4	392	1.65	17.35	0.43

Table 15: Oedometer test results for sample 2.

P. Kg/cm ²	P. kPa	Settlement Δh (mm)	Specimen height $H_i - \Delta h$ (mm)	Void ratio e_0
0	0	0	19	0.87
0.25	24.5	0.19	18.81	0.85
0.5	49	0.29	18.71	0.835
1	98	0.48	18.16	0.815
2	196	1.08	17.92	0.767
4	392	1.49	17.51	0.705
2	196	1.12	17.88	0.735
1	98	0.61	18.39	0.777
4	392	1.4	17.6	0.713
8	784.5	1.9	17.1	0.646
16	1569	2.42	16.58	0.51
8	784.5	2.05	16.95	0.54
4	392	1.65	17.35	0.586

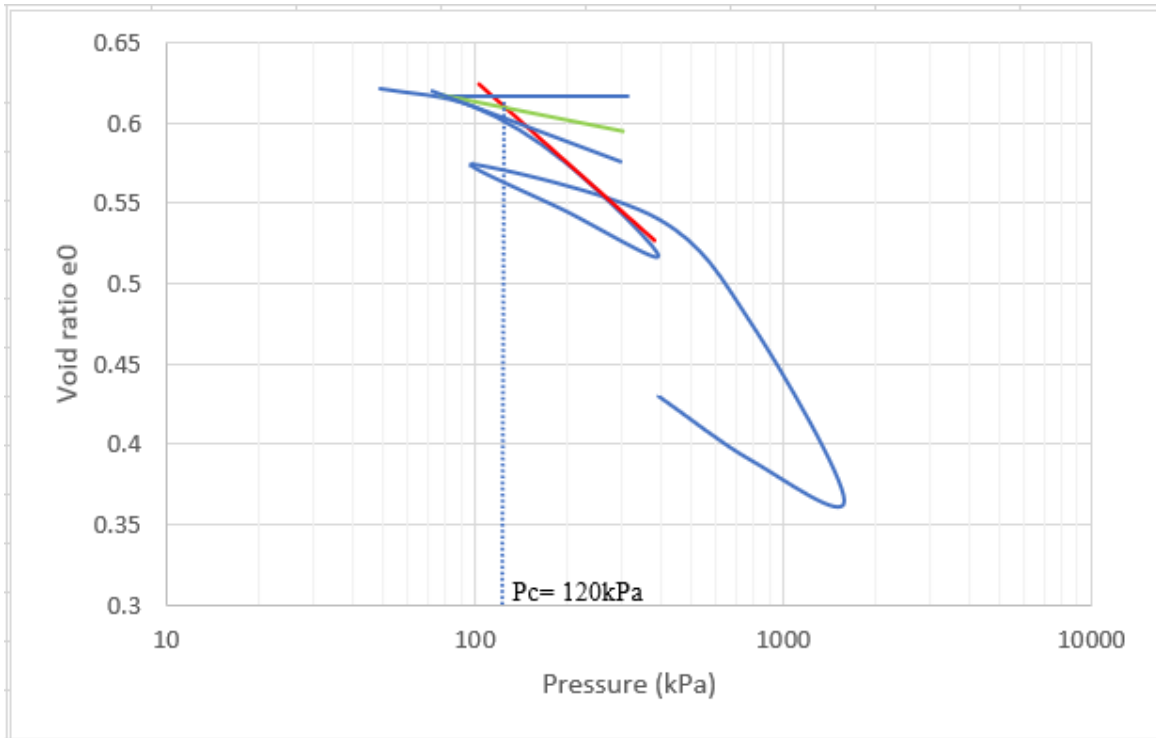


Figure 46: e - log(P) curve for sample 1.

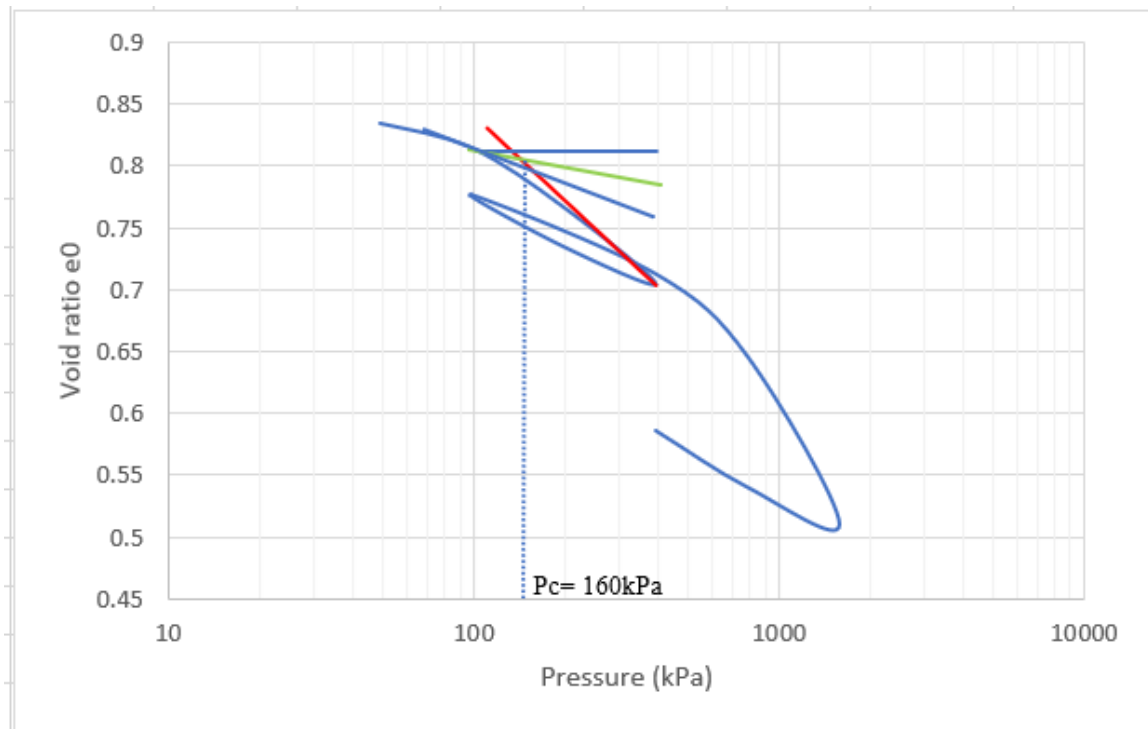


Figure 47: e - log(P) curve for sample 2.

Table 16: Needed results of all tests.

Sample N°	1	2
Dry unit weight (kN/m ³)	16.47	17.75
Wet unit weight (kN/m ³)	19.49	20.35
Sat unit weight (kN/m ³)	20.32	22.31
Water content (%)	16.23	14.66
Degree of saturation (%)	74.5	68.5
Fine friction (%)	90	88
Liquid limit (%)	66.2	63.8
Void ratio	0.646	0.87
Pressure in field -P ₀ - (kPa)	35	40
Compression index -C _c -	0.282	0.371
Recompression index -C _s -	0.107	0.126
Preconsolidation pressure -P _c - (kPa)	120	160
Overconsolidation ratio -OCR-	3.43	4

Where:

- Sample 1:

$$C_c = -\frac{\Delta e}{\log\left(\frac{P_2}{P_1}\right)} = -\frac{0.365 - 0.54}{\log(1569/392)} = 0.282$$

$$C_s = \frac{\Delta e}{\log\left(\frac{P_2}{P_1}\right)} = \frac{0.43 - 0.365}{\log(1569/392)} = 0.107$$

$$OCR = P_c/P_0 = 120/35 = 3.43$$

- Sample 2:

$$C_c = -\frac{\Delta e}{\log\left(\frac{P_2}{P_1}\right)} = -\frac{0.51 - 0.7}{\log(1569/500)} = 0.371$$

$$C_s = \frac{\Delta e}{\log\left(\frac{P_2}{P_1}\right)} = \frac{0.586 - 0.51}{\log(1569/392)} = 0.126$$

$$\text{OCR} = P_c/P_0 = 160/40 = 4$$

III.5. Conclusion

In conclusion, the comprehensive investigation and characterization of soils in the Tebessa region presented in this chapter are crucial for informing geotechnical engineering projects in the area. By conducting a series of laboratory tests, including Oedometer tests, Atterberg limits analysis, and other geotechnical tests, we have gained insights into the engineering properties and behavior of local soils under various conditions. The implementation of over 110 boreholes, along with additional samples from excavations, has provided a robust dataset for analysis.

Through the identification and classification of soils using methods such as LPC and GTR classifications, we have elucidated the granulometry and plasticity of the soils in the study area. The Atterberg limits, including liquidity limit (LL) and plasticity index (PI), have been instrumental in understanding soil plasticity and swelling potential. The obtained soil geotechnical characteristics, including compression and swelling indexes, preconsolidation pressure, and swelling pressure, offer valuable insights into soil behavior.

Furthermore, the application of statistical analysis techniques, such as Design of Experiments (DOE) and Response Surface Methodology (RSM), has facilitated the formulation of predictive equations for compression and recompression indexes (C_c and C_s). These equations, based on soil index properties, provide a means to optimize geotechnical models and better understand soil compressibility.

Moving forward, validation of these equations through field tests and comparison with laboratory results will be essential to ensure their accuracy and reliability. Overall, this study contributes to the development of accurate geotechnical models and enhances our understanding of soil behavior in the Tebessa region, thereby facilitating informed decision-making in geotechnical engineering projects.

Chapter IV:
Experimental Design and
Data Analysis in Predictive
Modeling

IV.1. Introduction

The essence of scientific inquiry lies in its structured approach to unraveling the mysteries of the natural world. At the heart of this approach lies the design of experiments, a meticulous framework that orchestrates targeted changes to input variables while meticulously measuring their effects on the response variable. This methodology, applicable across both physical processes and computer simulation models, stands as a beacon of efficiency, enabling researchers to extract maximal information while minimizing data collection efforts.

Against the backdrop of 190 meticulously collected soil samples from diverse locales within the Tebessa province, our research endeavors to elucidate the intricate relationships between these indices and a plethora of soil physical parameters. From the dry and wet unit weight to the degree of saturation, from the moisture content to the preconsolidation pressure, each parameter serves as a vital piece in the intricate puzzle of soil compressibility.

In tandem with our experimental endeavors, we navigate the terrain of optimization, seeking to identify optimal process conditions that maximize our desired outcomes. With a keen eye on overconsolidation ratio and preconsolidation pressure, we strive to unravel the complex web of interactions that underpin soil behavior.

Through meticulous experimentation, rigorous analysis, and a steadfast commitment to scientific inquiry, our study endeavors to shed light on the enigmatic realm of soil compressibility. By unraveling the intricate relationships between input parameters and response variables, we pave the way for enhanced engineering practices and sustainable infrastructure development, thus leaving an indelible mark on the landscape of geotechnical engineering.

IV.2. Materials and methods

IV.2.1. Principal component analysis

Principal component analysis is performed to obtain a small number of linear combinations of the variables that account for most of the variability in the data. From the table of eigenvalues given in Table 17-a and the scree plot in Figure 48, we can see that there are two components with eigenvalues greater than or equal to 1.0, which together account for 66.75% of the variability in the original data. The first and second principal components are the result of the linear combination

of the 12 studied variables, and both explain 50.51% and 16.24% of the variance respectively. For the other components, as shown in Table 17-b, the values in bold for each variable correspond to the factor for which the cosine squared is greatest.

Table 17-a: Eigenvalue table and accumulated proportion of principal component analysis of 190 data samples.

	F1	F2	F3	F4	F5	F6	F7	F8	F9	F10	F11	F12
Eigenvalue	6.06	1.94	1.32	1.09	0.84	0.36	0.14	0.08	0.07	0.03	0.02	0.002
Variability (%)	50.51	16.23	11.07	9.15	7.03	3.01	1.2	0.67	0.59	0.25	0.22	0.02
Cumulative %	50.51	66.75	77.82	86.98	94.01	97.02	98.23	98.9	99.5	99.75	99.98	100.00

Table 17-b: Squared cosines of the variables.

	F1	F2	F3	F4	F5
γ_d (kN/m ³)	0.795	0.001	0.135	0.028	0.010
γ_h (kN/m ³)	0.781	0.043	0.017	0.113	0.004
w %	0.578	0.050	0.322	0.027	0.012
Sr %	0.078	0.294	0.215	0.385	0.005
Ff %	0.019	0.213	0.061	0.084	0.611
LL %	0.710	0.050	0.117	0.093	0.009
PI%	0.585	0.040	0.162	0.126	0.024
e ₀	0.843	0.004	0.101	0.010	0.004
Pc (Kg/cm ²)	0.003	0.707	0.011	0.077	0.013
Cc	0.872	0.018	0.011	0.012	0.012
Cs	0.792	0.000	0.099	0.034	0.014
OCR	<u>0.006</u>	<u>0.529</u>	<u>0.076</u>	<u>0.111</u>	<u>0.127</u>

Table 18: Factor loadings correlations between variables and factors.

	F1	F2	F3	F4	F5
γ_d (kN/m ³)	-0.891	-0.036	-0.368	0.168	-0.100
γ_h (kN/m ³)	-0.884	-0.207	-0.129	0.336	-0.060
w %	0.760	-0.225	0.568	0.163	0.109
Sr %	-0.279	-0.542	0.464	0.620	0.071
Ff %	0.137	0.461	-0.247	0.289	0.781
LL %	0.843	-0.223	-0.342	0.304	-0.095
PI%	0.765	-0.199	-0.402	0.355	-0.154
e ₀	0.918	0.067	0.318	-0.101	0.065
Pc (Kg/cm ²)	-0.054	0.841	0.104	0.278	-0.115

Cc	0.934	0.133	-0.107	-0.108	-0.109
Cs	0.890	-0.004	-0.315	0.183	-0.118
<u>OCR</u>	<u>-0.075</u>	<u>0.727</u>	<u>0.276</u>	<u>0.334</u>	<u>-0.357</u>

According to the circle of correlation and factor loadings (Figure 49, Table 18) the variables with a negative contribution are respectively the factors F1, F2 (γ_d , γ_h (kN/m³), Sr %, Pc (Kg/cm²), and OCR), the other factors represented by (w %, Ff %, LL %, PI%, e₀, Cc, Cs) have a positive contribution in this analysis, it is important to note the strong correlation between the two index parameters (LL, PI), as well as the good correlation between (Cc, Cs and e₀), is because these methods take into account neither the position of the points in space, nor the degrees of similarity between the parameters.

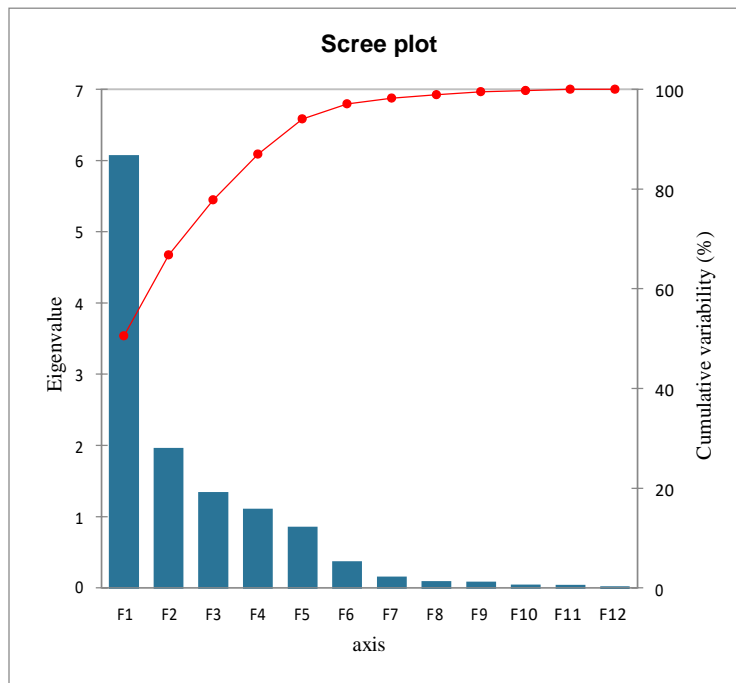


Figure 48: Scree plot of the data.

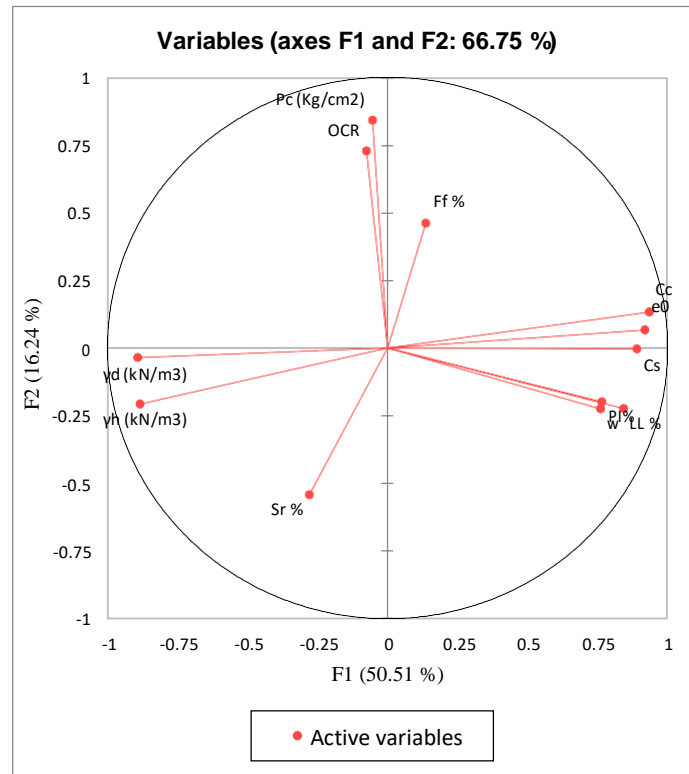


Figure 49: The variables circle of correlation.

The results of the principal component analysis use ten soil parameters of twelve. They show strong correlation on the first principal axes, which absorb around 66.75 % of the total variance. The PCA enabled the best correlated parameters to be grouped as the first group, made up of Cc, Cs, e0 and Atterberg limits on positive F1 F2 axis, and the second group composed unit weights, preconsolidation pressure have negative contribution or affection on the studied phenomena as second group, the last group is presented by the fine fraction and saturation degree as shown on figure 49.

IV.2.2. Design of experiments

An experimental design is a series of tests that make targeted changes to the input variables of a system or process and measure the effects on the response variable. Experimental design applies to both physical processes and computer simulation models. Experimental design is an effective tool for maximizing the amount of information obtained from a study while minimizing the amount of data to be collected. Factorial designs examine the effects of many different factors by varying them simultaneously, rather than just one factor at a time. Factorial designs allow estimation of

sensitivity to each factor and to the combined effect of two or more factors other factors. Experimental design methods have been successfully used in many studies in various fields to maximize the amount of information with the minimum number of computer simulation runs. In the competitive world of testing and evaluation, an efficient method for testing many factors is needed. (Telford, J. K. 2007).

Experimental design methods investigate how common conditions can be varied using empirical processes to increase the likelihood of detecting significant changes in response. In this way, more knowledge about the behavior of the process of interest can be obtained. In order for the experimental design method to be effective, it is important that the experiment is well designed, whether it is to identify the main cause of a change in the response for any of the following reasons, or to find the experimental condition variable that reaches an extreme value or the response of interest to compare different observations of the controlled variable levels of response, or to obtain statistical mathematical models that allow predictions of future responses.

This work consists in studying the compressibility of soils based on compression index C_c and recompression index C_s used in settlement measuring of fine-grained soils. Therefore, C_c and C_s are linked to soil physical parameters as input parameters that may directly or indirectly affect the process of the compression and recompression indexes as output parameters, the different input parameters taken in this treatment are (dry and wet unit weight γ_d (kN/m³), γ_h (kN/m³), water content w (%), degree of saturation S_r , fine fraction F_f (%), liquid limit LL (%), plasticity index PI (%), initial void ratio e_0 and preconsolidation pressure P_c (kg/cm²)).

IV.2.2.1. Input and output parameters

The purpose of this study was to estimate the compression index (C_c) and recompression index (C_s) as a function of basic soil properties, since its determination is relatively simple. 190 samples will be collected from different locations in Tebessa province to study their geotechnical parameters. All data sets were analyzed descriptively using classical statistics, the minimum and maximum values were determined, and the mean and standard deviation were calculated as shown in table 19.

In the first step, statistical tests are performed to obtain a general overview and to examine parameters known to be related to compression and recompression coefficients (C_c , C_s). These

variables were selected as independent variables: dry and wet weight (γ_d , γ_h), moisture content (w), degree of saturation (S_r), fines (F_f) ($\% < 80 \mu\text{m}$), plasticity index (PI), liquid limit (LL), void content (e_0) and preconsolidation pressure (P_c).

Table 19: Summary statistics of the collected data set.

Variable	Observations	Obs. without missing data	Minimum	Maximum	Mean
γ_d (kN/m)	190	190	10.100	19.500	15.739
γ_h (kN/m)	190	190	14.700	21.070	19.002
w %	190	190	8.430	46.200	21.503
S_r %	190	190	55.000	100.000	82.741
F_f %	190	190	29.640	99.000	85.059
LL %	190	190	28.000	150.000	62.575
PI %	190	190	11.000	85.000	39.487
e_0	190	190	0.355	1.616	0.711
P_c (kg/cm)	190	190	0.220	3.100	1.352
C_c	190	190	0.044	0.582	0.256
C_s	190	190	0.023	0.307	0.089
OCR	190	190			

The experiment was conducted simultaneously with nine factors at two levels (i.e., low level and high level). These two levels were chosen to cover the practical range of the parameters considered (Table 20).

Table 20: Factors for response study.

<i>Factor</i>	<i>Name</i>	<i>Units</i>	<i>Low Level</i>	<i>High Level</i>
A	γ_d	kN/m ³	10.10	19.5

<i>B</i>	γ_h	kN/m ³	14.70	21.07
<i>C</i>	w	%	8.43	46.20
<i>D</i>	Sr	%	55.00	100.00
<i>E</i>	Ff	%	29.64	99.00
<i>F</i>	LL	%	28.00	150.00
<i>G</i>	PI	%	11.00	85.00
<i>H</i>	e0		0.35	1.61
<i>I</i>	Pc	Kg/cm ²	0.22	3.1

Factorial designs find broad application in experiments encompassing multiple factors, facilitating the examination of their collective influence on a response variable. This method constitutes a versatile array of statistical techniques utilized in scientific experiment design. When employing factorial designs, researchers can effectively explore the impact of diverse factors on one or more response variables. Each factor is typically treated as an independent variable and investigated across various discrete subdivisions or levels, representing distinct values within a predetermined range tailored to the specific requirements of each experiment. (Shahabadi, S. M. S., & Reyhani, A. 2014).

The response surface methodology RSM in DOE techniques is used for machining processes and relate to the determination of response surface based on the general equation. (Myers, R. H. et al 2016).

$$y = A_0 + A_1x_1 + \dots + A_kx_k + A_{12}x_1x_2 + A_{13}x_1x_3 + A_{11}x_1^2 + A_{kk}x_k^2 \quad (1)$$

Where A_0 , A_i , A_{ij} are respectively interaction, linear, quadratic and intercept coefficients, and x_i are input independent variables. Continuous factors affect the quantitative response which is analyzed by response surface methodology (RSM).

IV.3. DOE and data implementation

The number of runs needed for the full factorial DOE where the two levels of factors variation are considered. Factors are the variables that you believe may affect the outcome of your experiment. Each factor should have different levels. Using the design expert software, input the

factors, their levels, and the responses you want to measure. Then, select the option for a full factorial design, Figure 50.

Factors: 9 Horizontal
 Vertical

	Name	Units	Type	Low	High
A [Numeric]	yd	kN/m3	Numeric	10.1	19.5
B [Numeric]	yh	kN/m3	Numeric	14.7	21.07
C [Numeric]	w	%	Numeric	8.43	46.2
D [Numeric]	Sr	%	Numeric	55	100
E [Numeric]	FF	%	Numeric	29.64	99
F [Numeric]	LL	%	Numeric	28	150
G [Numeric]	PI	%	Numeric	11	85
H [Numeric]	e0		Numeric	0.354695	1.616
J [Numeric]	Pc	kg/cm2	Numeric	0.22	3.1

Figure 50: Definition of different parameters in full factorial design.

For response surface methodology RSM, central composite design is chosen and CCD-Rotatable was selected, in which standard error remains the same at all the points which are equidistant from the center of the region. Figure 51.

Numeric factors: 9 (2 to 50) Horizontal Enter factor ranges in terms of ± 1 levels
Categoric factors: 0 (0 to 10) Vertical Enter factor ranges in terms of alphas

	Name	Units	Low	High	-alpha	+alpha
A [Numeric]	yd	kN/m3	10.1	19.5	-7.55709	37.1571
B [Numeric]	yh	kN/m3	14.7	21.07	2.7345	33.0355
C [Numeric]	w	%	8.43	46.2	-62.5177	117.148
D [Numeric]	Sr	%	55	100	-29.5286	184.529
E [Numeric]	FF	%	29.64	99	-100.647	229.287
F [Numeric]	LL	%	28	150	-201.167	379.167
G [Numeric]	PI	%	11	85	-128.003	224.003
H [Numeric]	e0		0.354695	1.616	-2.01456	3.98525
J [Numeric]	Pc	kg/cm2	0.22	3.1	-5.18983	8.50983

Type: Full Blocks: 1

Points:
Non-center points: 530
Center points: 64
alpha = 4.75683 Options... 594 Runs

CCD Options

Replication
Replicates of factorial points: 1 (1 to 100)
Replicates of axial (star) points: 1 (1 to 100)
Center points: 64 (0 to 1000)

Alpha
 Rotatable (k < 6) 4.75683
 Spherical 3
 Orthogonal quadratic 4.44286
 Practical (k > 5) 1.73205
 Face centered 1
 Other 1.73205

594 Runs

OK Cancel Help

Figure 51: Definition of different parameters in RSM.

CCD is composed of a core factorial that forms a cube with sides that are two coded units in length, from -1 to $+1$. The distance out of the cube, designated as distance “Alpha” and measured in terms of coded factor levels. The upper and lower limits parameters, their units and levels are put with respect to all chosen parameters.

IV.4. Results and discussion

IV.4.1. Full factorial design

One thing about factorial design, it’s quite unique in such a way that you need to select the factors before proceeding to ANOVA, the reason for this is that when you want to create ANOVA table, you need to have what we call the sum replication within the design, in order to calculate the F ratio. In this case the most effect factors (the significant terms) are selected from the plot (Figures 52 and 53).

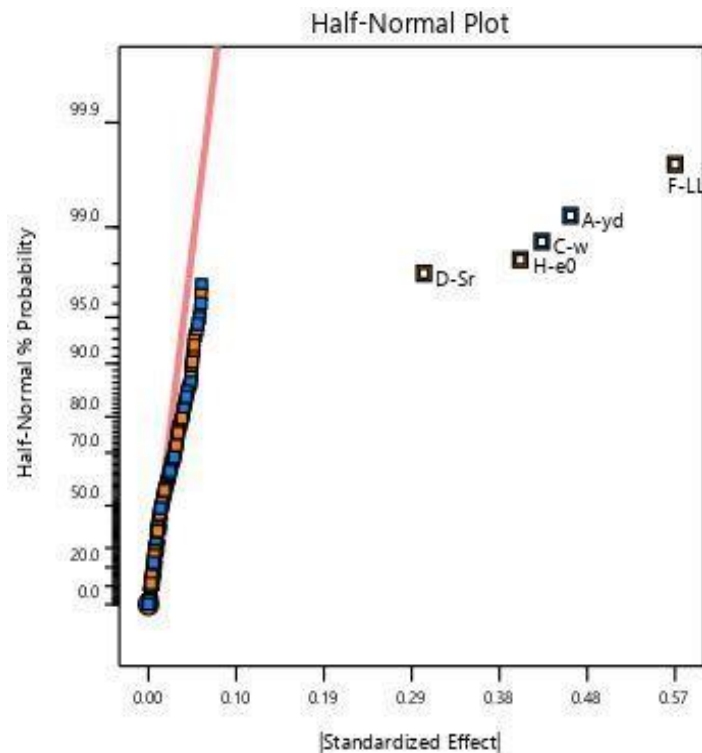


Figure 52: Select the most effect factors for compression index.

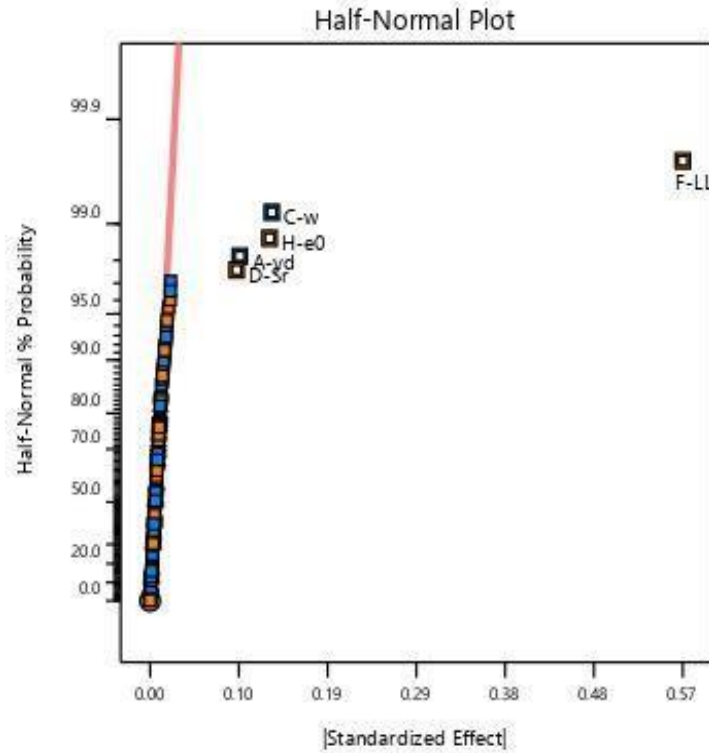


Figure 53: Select the most effect factors for recompression index.

Also, the Pareto chart is used to select the effects (Figures 54 and 55), the effects that cross the red line (Bonferroni limit) are significant, but those below the black line (t-value limit) are not significant. As for those falling between the two lines, selecting them depends on experience, without forgetting that whatever effect is selected affects the ANOVA, and ANOVA essentially builds the model obtained later.

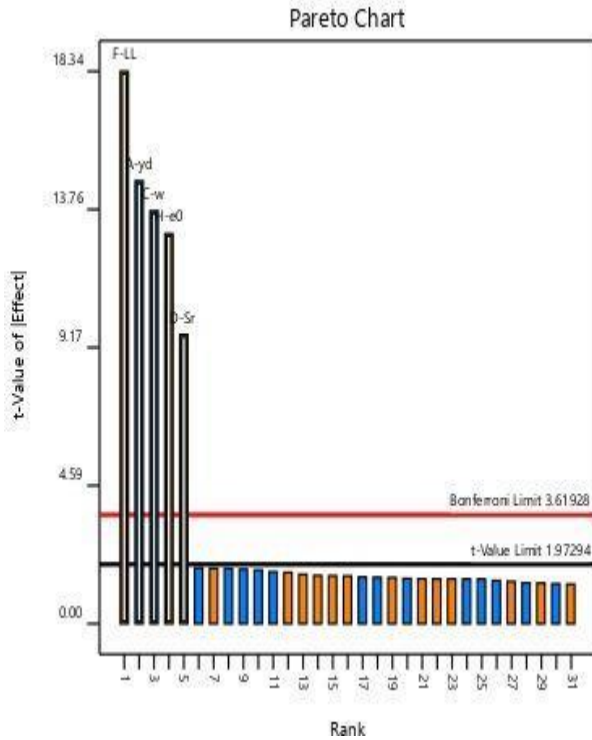


Figure 54: Pareto chart for Cc.

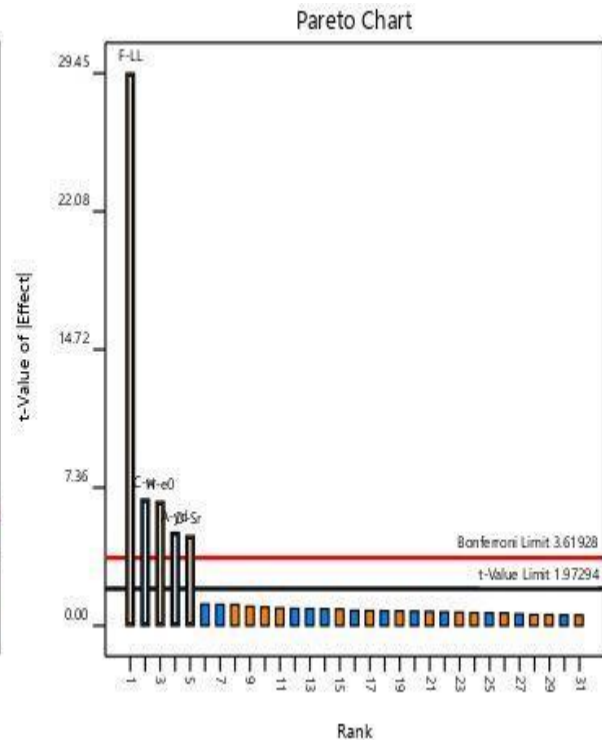


Figure 55: Pareto chart for Cs.

Once the effects selected only then ANOVA will be available, tables 21 and 22 show that all models are depending on the effects selected before, which each term is significant according to p-value (by default p-value < 0.05 indicate model terms are significant).

Table 21: Results of ANOVA model for compression index.

Source	Sum of Squares	df	Mean Square	F-value	p-value	
Model	1.02	5	0.2043	556.44	< 0.0001	Significant
A- γd	0.0793	1	0.0793	215.99	< 0.0001	
C-w	0.0689	1	0.0689	187.68	< 0.0001	
D-Sr	0.0338	1	0.0338	92.03	< 0.0001	
F-LL	0.1235	1	0.1235	336.36	< 0.0001	
H-e0	0.0615	1	0.0615	167.64	< 0.0001	
Residual	0.0675	184	0.0004			

Lack of Fit	0.0593	126	0.0005	3.30	< 0.0001	Significant
Pure Error	0.0083	58	0.0001			
Cor Total	1.09	189				

Table 22: Results of ANOVA model for recompression index.

Source	Sum of Squares	df	Mean Square	F-value	p-value	
Model	0.2790	5	0.0558	393.54	< 0.0001	Significant
A- γ d	0.0035	1	0.0035	24.60	< 0.0001	
C-w	0.0064	1	0.0064	45.28	< 0.0001	
D-Sr	0.0032	1	0.0032	22.88	< 0.0001	
F-LL	0.1229	1	0.1229	867.10	< 0.0001	
H-e0	0.0062	1	0.0062	43.67	< 0.0001	
Residual	0.0261	184	0.0001			
Lack of Fit	0.0246	126	0.0002	7.84	< 0.0001	Significant
Pure Error	0.0014	58	0.0000			
Cor Total	0.3051	189				

The models also significant, based on the obtained results the ANOVA will make a regression line (prediction), the analysis of the experimental data was performed to identify statistical significance of the input parameters, on the measured responses the results are summarized in Tables 23 and 24.

Table 23: Regression statistics for compression index.

Std. Dev.	0.0192	R²	0.9380
Mean	0.2573	Adjusted R ²	0.9363
C.V. %	7.45	Predicted R ²	0.9321
		Adeq Precision	133.8012

The **Predicted R²** of 0.9321 is in reasonable agreement with the **Adjusted R²** of 0.9363; i.e. the difference is less than 0.2, **Adeq Precision** measures the signal to noise ratio. A ratio greater than 4 is desirable. The model ratio of 133.8012 indicates an adequate signal. This model can be used to navigate the design space.

Table 24: Regression statistics for recompression index.

Std. Dev.	0.0119	R²	0.9145
Mean	0.0890	Adjusted R ²	0.9122
C.V. %	13.38	Predicted R ²	0.9075
		Adeq Precision	117.3554

The **Predicted R²** of 0.9075 is in reasonable agreement with the **Adjusted R²** of 0.9122; i.e. the difference is less than 0.2, **Adeq Precision** measures the signal to noise ratio. A ratio greater than 4 is desirable. The model ratio of 117.355 indicates an adequate signal. This model can be used to navigate the design space.

These statistics would give the final equations in terms of actual factors:

$$Cc = 0.627 - 0.05\gamma d - 0.029w + 0.0053Sr + 0.0018LL + 0.65e0 \quad (2)$$

$$Cs = 0.042 - 0.01\gamma d - 0.009w + 0.0017Sr + 0.0018LL + 0.21e0 \quad (3)$$

The equations in terms of actual factors can be used to make predictions about the response for given levels of each factor. Here, the levels should be specified in the original units for each factor. These equations should not be used to determine the relative impact of each factor because the coefficients are scaled to accommodate the units of each factor and the intercept is not at the center of the design space.

To assess the effectiveness of the adopted model, it's essential to examine if the predicted response points align randomly with the actual values along the 45° line, as illustrated in Figures 56 and 57.

Such alignment indicates the adequacy of the proposed model and suggests no apparent violation of the assumptions regarding independence or constant variance.

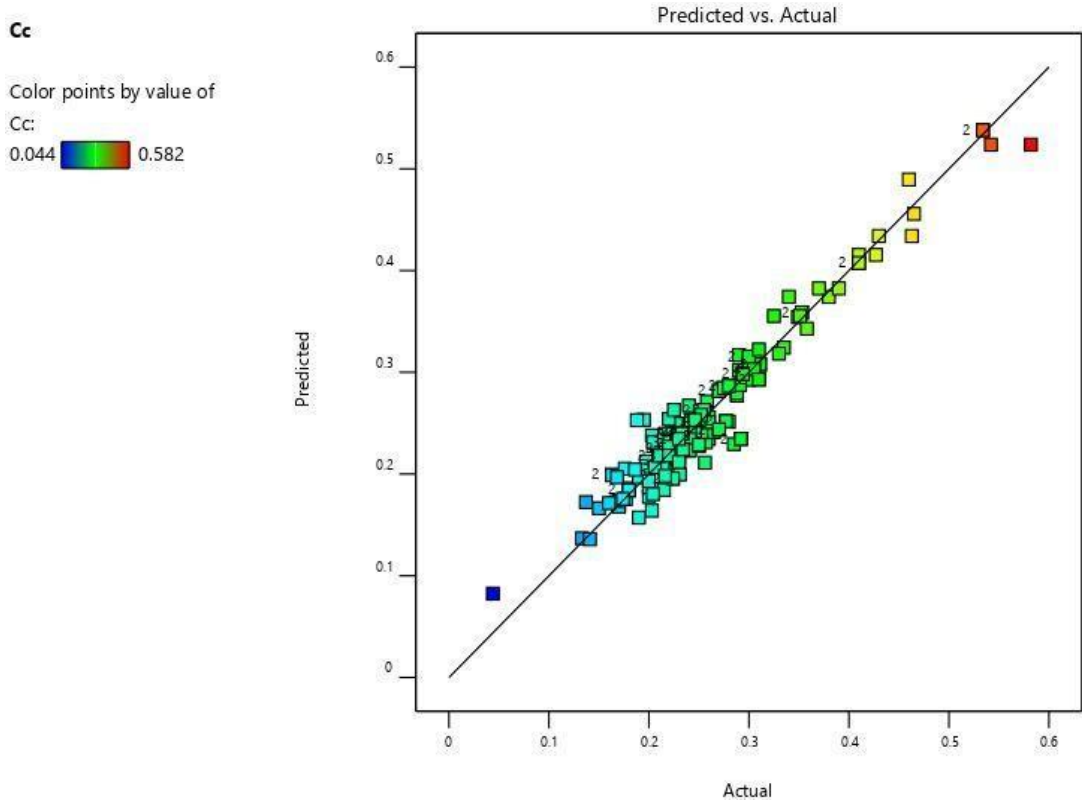


Figure 56: Predicted response versus actual for compression index.

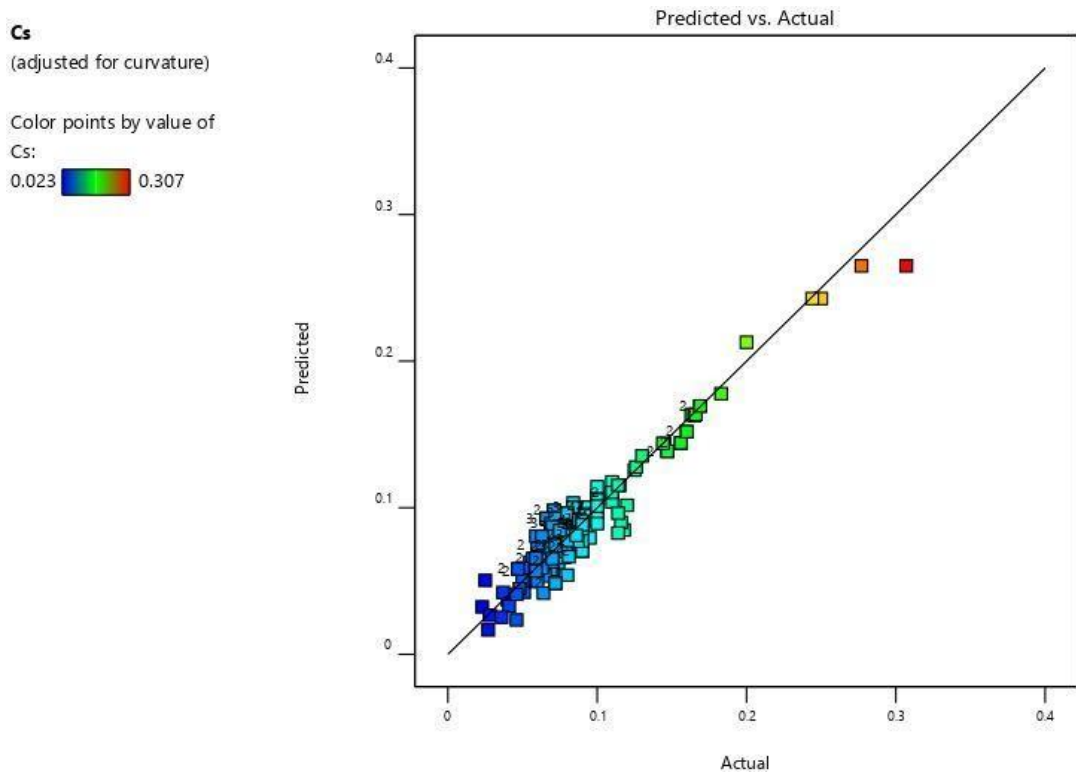


Figure 57: Predicted response versus actual for recompression index.

The following 3D figures depict the response surfaces illustrating the relationship between the compressibility index (C_c) and various factors: γ_d (kN/m³) and w (%), liquid limit (%) and e_0 , these figures numbered 58 and 59. Also the swelling index (C_s) and various factors: γ_d (kN/m³) and w (%), liquid limit (%) and e_0 , these figures numbered 60 and 61. These figures demonstrate the interaction between two process variables as a function of factors.

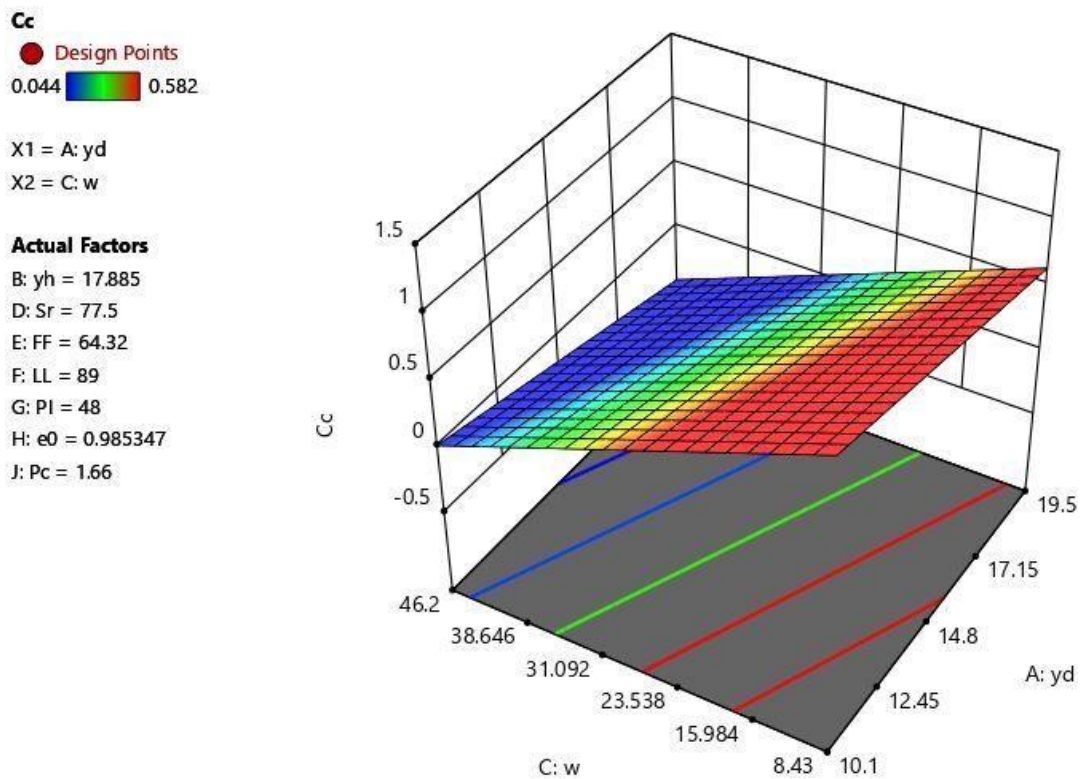


Figure 58: Response surface 3D representing the compressibility index (C_c) vs dry unit weight γ_d and water content w .

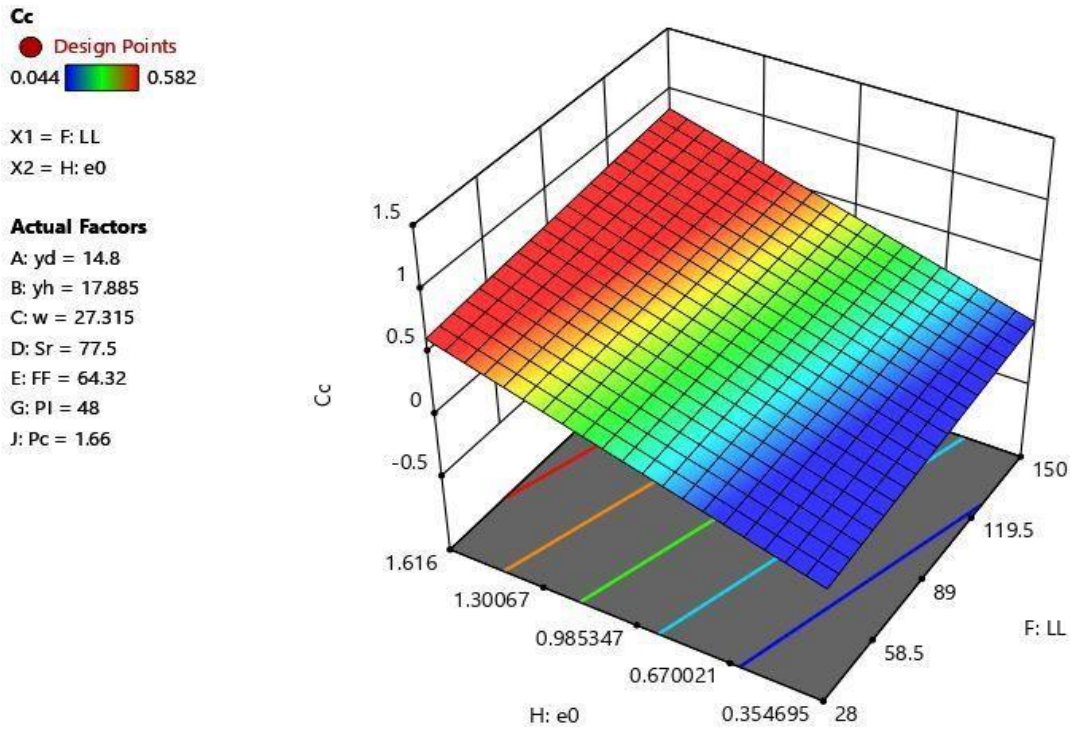


Figure 59: Response surface 3D representing the compressibility index (C_c) vs liquid limit LL and the void ratio e_0 .

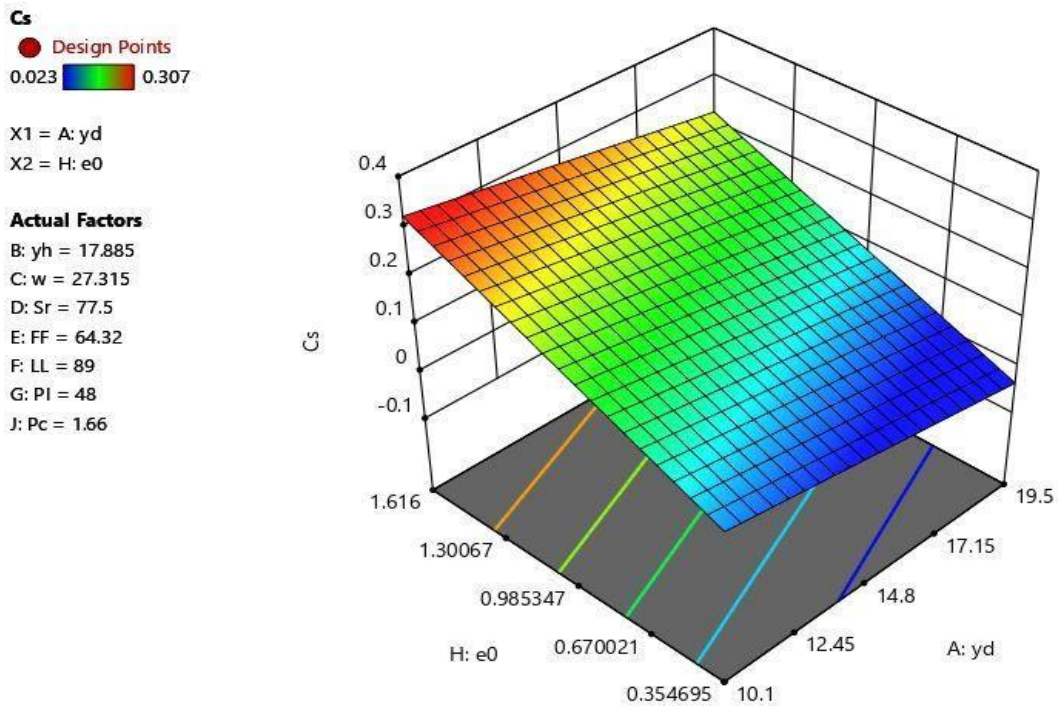


Figure 60: Response surface 3D representing the swelling index (C_s) vs dry unit weight and void ratio e_0 .

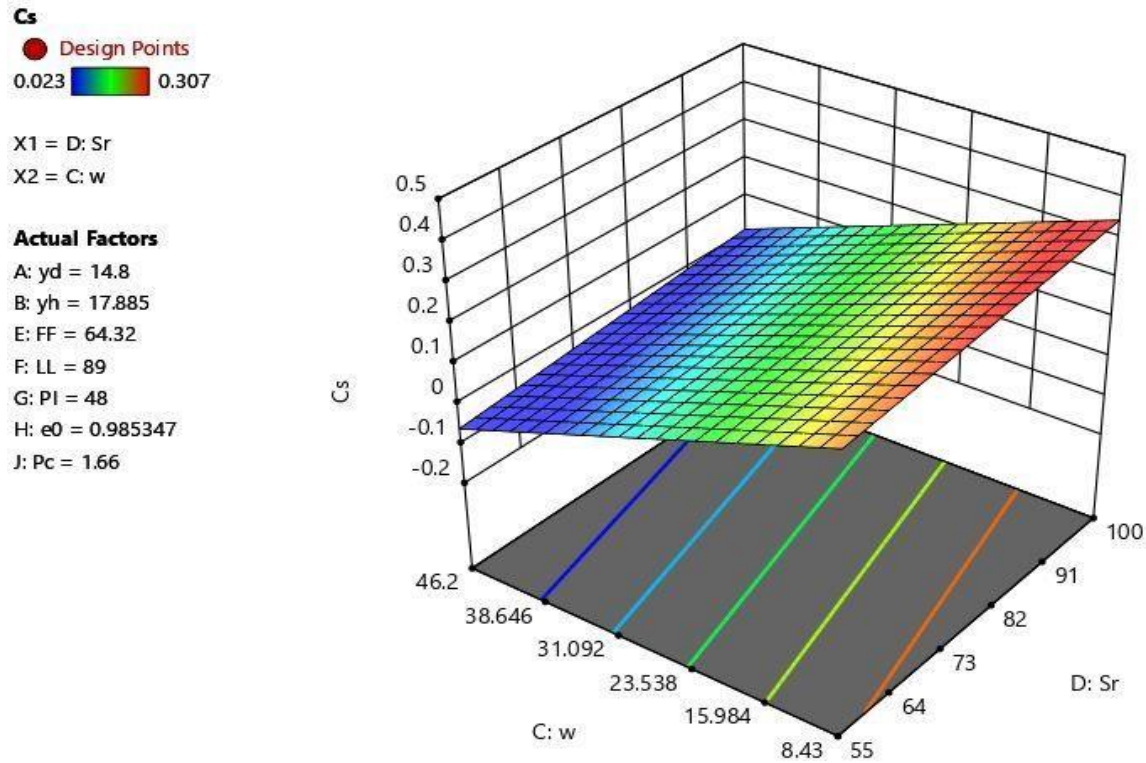


Figure 61: Response surface 3D representing the swelling index (C_s) vs saturation degree S_r and water content w .

IV.4.2. Response surface methodology

Starting with numerical analysis of the responses, Design-Expert offers an extensive range of response transformations. At this juncture, Design-Expert employs linear, two-factor interaction (2FI), quadratic, and cubic polynomials to fit the response. The central composite matrix, by design, offers a limited number of unique design points, making it insufficient to ascertain all terms in the cubic model. Tables 25 and 26 represent the best process order for each response.

Table 25: Model fit summary for C_c .

Source	Model p-value	Lack of Fit p-value	Adjusted R^2	Predicted R^2	
Linear	< 0.0001	< 0.0003	0.9532	0.9487	
2FI	0.3396	< 0.0002	0.9541	0.9035	
Quadratic	0.0005	< 0.0024	0.9604	0.8712	Suggested

Cubic	< 0.0024	0.9753	Aliased
-------	----------	--------	---------

Table 26: Model fit summary for Cs.

Source	Model	Lack of Fit	Adjusted R ²	Predicted R ²	
	p-value	p-value			
Linear	< 0.0001	< 0.0001	0.9323	0.9272	Suggested
2FI	0.0192	< 0.0001	0.9402	0.8470	Suggested
Quadratic	0.0621	< 0.0001	0.9433	0.8058	
Cubic	< 0.0001		0.9845		Aliased

For each term source (linear, etc.), assess the probability (Prob > F) to determine if it is below the chosen statistical significance level, typically 0.05. So far, Design-Expert highlights the quadratic model as the most favorable for Cc, but linear and 2FI model as the most favorable for Cs (bold highlighting indicates significance). While these terms hold significance, incorporating cubic order terms wouldn't notably enhance the fit. Even if significant, the cubic terms would be aliased and wouldn't contribute meaningfully to modeling. The Lack of Fit Tests pane can be adjusted to explore alternative suggested models by conducting lack of fit tests across various model orders.

The ANOVA results are employed to assess the impact of the constructed RSM model and its statistically significant terms. The ANOVA analysis is conducted by testing the hypothesis of equal variance, typically at a confidence level of 95% or a significance level of 0.05. ANOVA is frequently utilized to summarize the significance test of the regression model and to assess the significance of individual model coefficients. The summary statistics for the models are presented in Tables 27 and 28.

Table 27: ANOVA for response surface quadratic model for compressibility index.

Source	Sum of Squares	df	Mean Square	F-value	p-value	
Model	0.9875	4	0.2469	450.75	< 0.0001	Significant
A- γ d	0.0459	1	0.0459	83.72	< 0.0001	

C-w	0.1185	1	0.1185	216.41	<	0.0001
F-LL	0.1293	1	0.1293	236.02	<	0.0001
H-e0	0.0327	1	0.0327	59.77	<	0.0001
Residual	0.1013	185	0.0005			
Lack of Fit	0.0931	127	0.0007	5.14	<	Significant 0.0001
Pure Error	0.0083	58	0.0001			
Cor Total	1.09	189				

Table 28: ANOVA for response surface quadratic model for recompression index.

Source	Sum of Squares	df	Mean Square	F-value	p-value	
Model	0.2757	4	0.0689	434.78	<	Significant 0.0001
A- γ d	0.0010	1	0.0010	6.11	0.0143	
C-w	0.0103	1	0.0103	65.26	<	0.0001
F-LL	0.1249	1	0.1249	787.59	<	0.0001
H-e0	0.0036	1	0.0036	22.59	<	0.0001
Residual	0.0293	185	0.0002			
Lack of Fit	0.0279	127	0.0002	8.80	<	Significant 0.0001
Pure Error	0.0014	58	0.0000			
Cor Total	0.3051	189				

To achieve this objective, the F-values in the ANOVA table are computed by dividing the mean square of the factor by the mean square of the residual. These values are then compared to the F-values from the Fisher distribution, which are suggested for a significance level of 0.05. In the Fisher distribution, the F-values are determined based on the degrees of freedom of the associated factors and residuals, along with the chosen significance level. The contribution of each parameter in enhancing the UCS performance of the mixture in the constructed RSM model is assessed by dividing the F-value of each parameter by the sum of F-values of all parameters.

The experimental data analysis aimed to determine the statistical significance of various physical parameters: dry unit weight (ρ_d) in kN/m³, wet unit weight (ρ_h) in kN/m³, water content (w) in %, fine fraction (Ff) in %, Liquidity limits (WL) in %, plasticity index (IP) in %, void ratio (e_0), Saturation degree (Sr) in %, on the measured response compressibility index (C_c). The model was constructed with a confidence level of 95%, and the findings are presented in Tables 29 and 30.

Table 29: Regression statistics for recompression index.

Std. Dev.	0.0234	R²	0.9069
Mean	0.2573	Adjusted R ²	0.9049
C.V. %	9.10	Predicted R ²	0.9012
		Adeq Precision	106.1962

Table 30: Regression statistics for recompression index.

Std. Dev.	0.0126	R²	0.9049
Mean	0.0890	Adjusted R ²	0.9022
C.V. %	14.15	Predicted R ²	0.9001
		Adeq Precision	124.0219

For the analyzed studies, the final equations in terms of actual factors were determined, which present the compressibility index (C_c) and swelling index from the input factors:

$$C_c = 0.65 - 0.03\gamma_d - 0.009w + 0.002LL + 0.29e_0 \quad (4)$$

$$C_s = 0.048 - 0.004\gamma_d - 0.003w + 0.002LL + 0.075e_0 \quad (5)$$

The equations expressed in terms of actual factors are suitable for predicting the response for specific levels of each factor. It's important to note that the levels should be defined in the original units for each factor. However, these equations should not be utilized to assess the relative impact of each factor. This is because the coefficients are scaled to accommodate the units of each factor, and the intercept is not positioned at the center of the design space.

To assess the adequacy of the adopted model, it's essential to examine if the predicted response points versus the actual values exhibit random scattering along the 45° line, as depicted in Figures 62 and 63. Such a pattern indicates that the proposed model is fitting well, and there are no apparent violations of the assumptions of independence or constant variance.

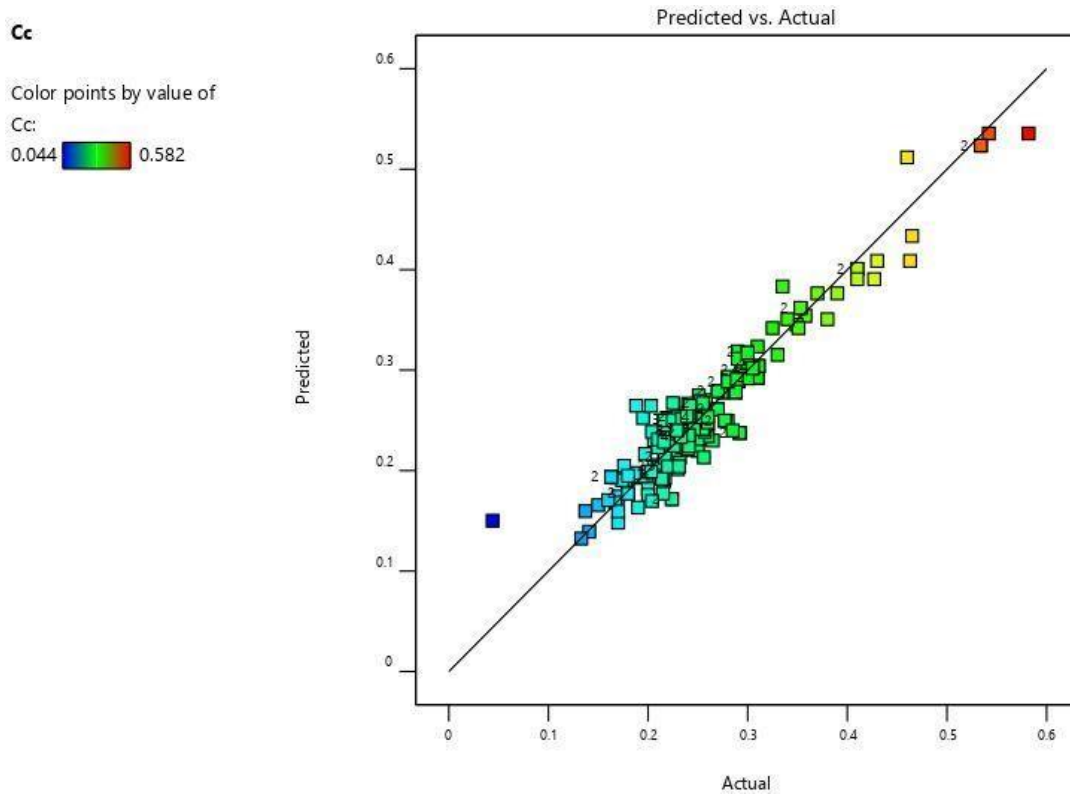


Figure 62: Predicted response versus actual for compression index.

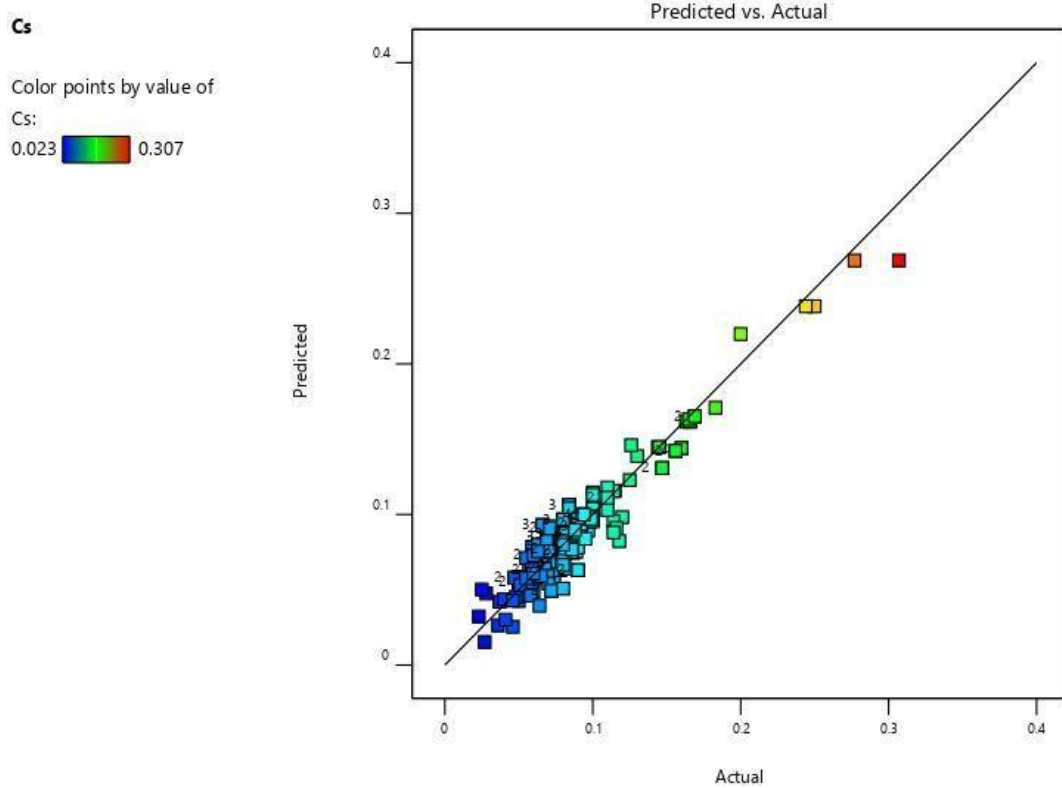


Figure 63: Predicted response versus actual for recompression index.

Figure 64 and 65 showcase 3D plots representing the response surfaces, elucidating the correlation between the compressibility index (C_c) and several factors: γ_d (kN/m^3) and w (%), LL (%) and e_o . Similarly, Figures 66 and 67 exhibit the swelling index (C_s) in relation to various factors: LL (%) and w (%), LL (%) and e_o . These figures effectively illustrate the interaction between two process variables as influenced by the factors under consideration.

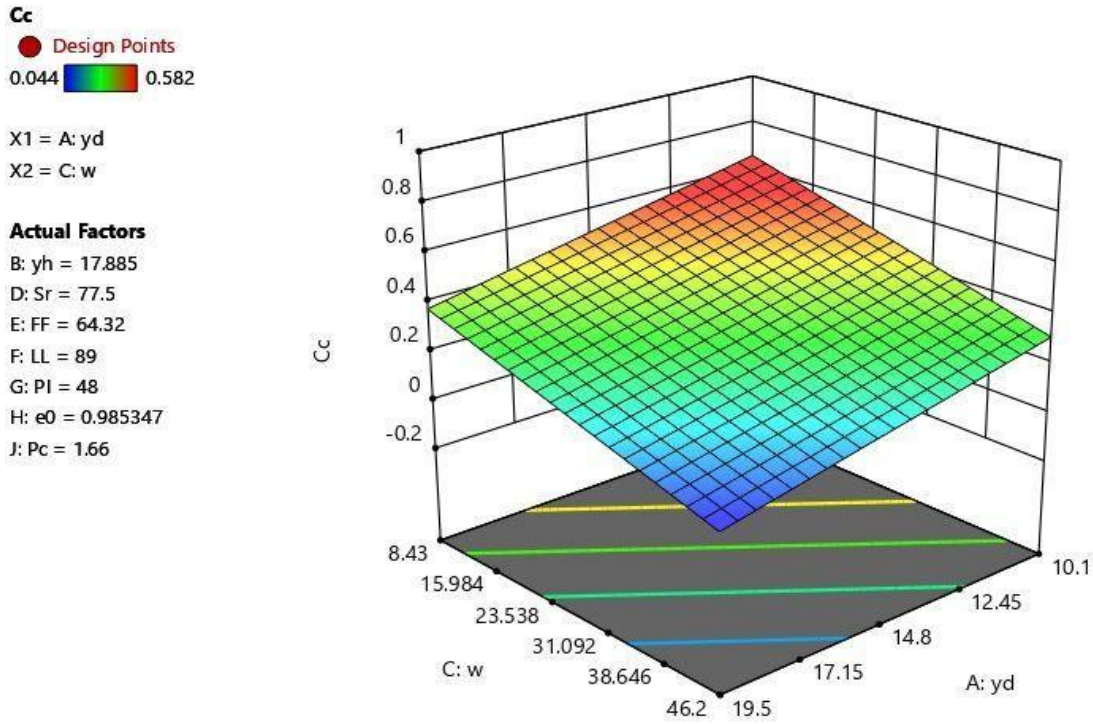


Figure 64: Response surface 3D representing the compressibility index (C_c) vs dry unit weight γ_d and water content w .

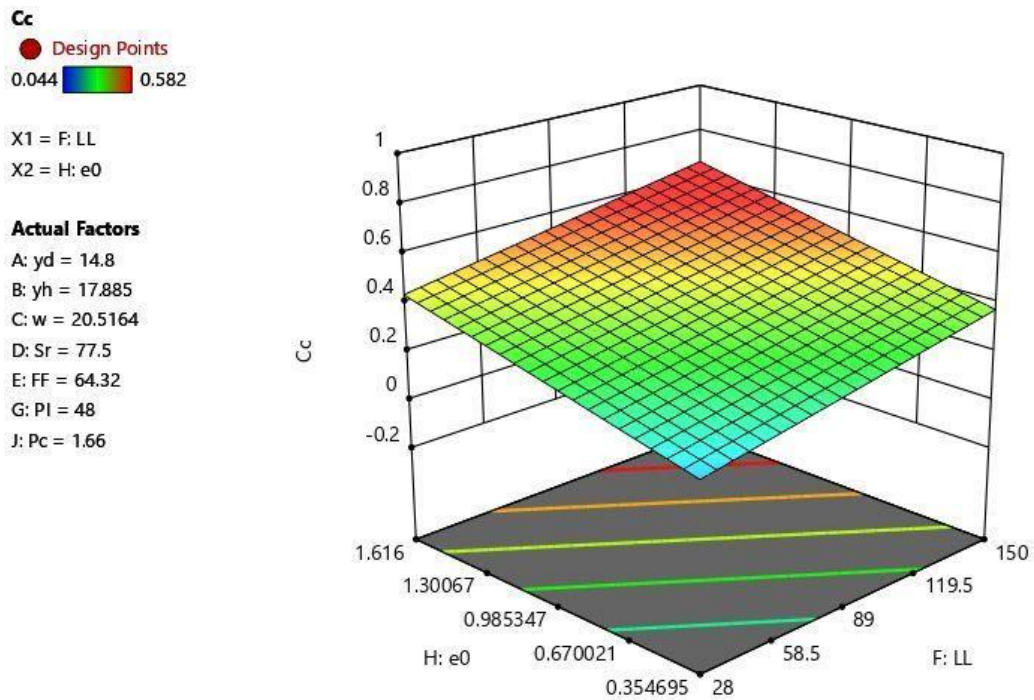


Figure 65: Response surface 3D representing the compressibility index (C_c) vs liquid limit LL and void ratio e_0 .

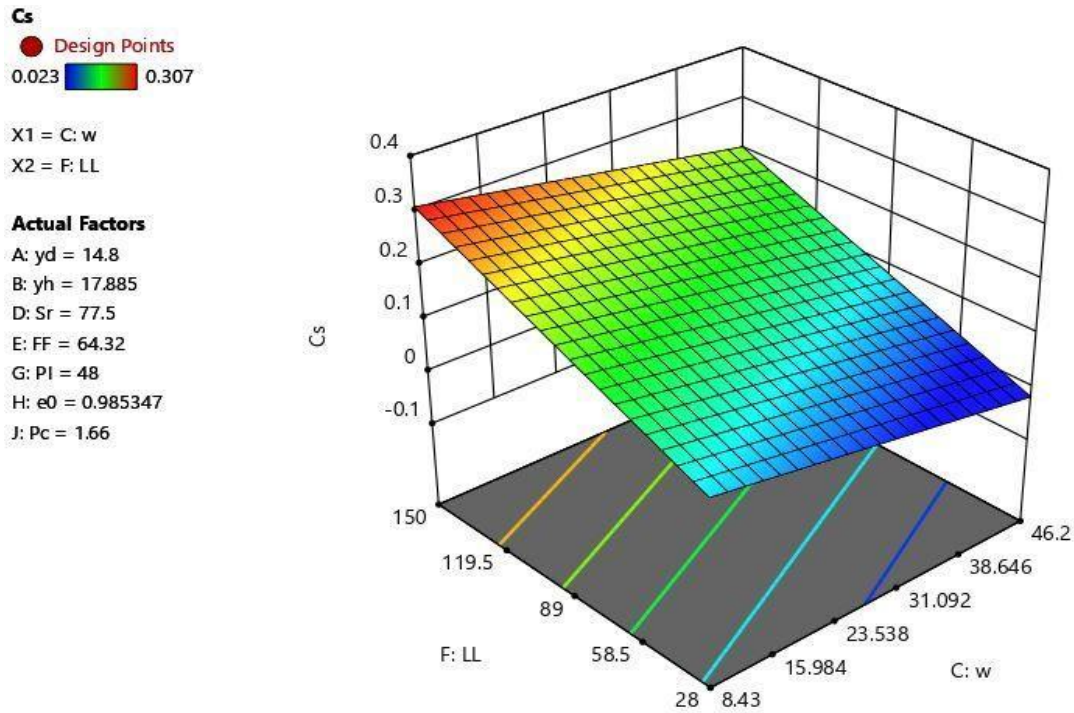


Figure 66: Response surface 3D representing the swelling index (C_s) vs water content w and liquid limit LL .

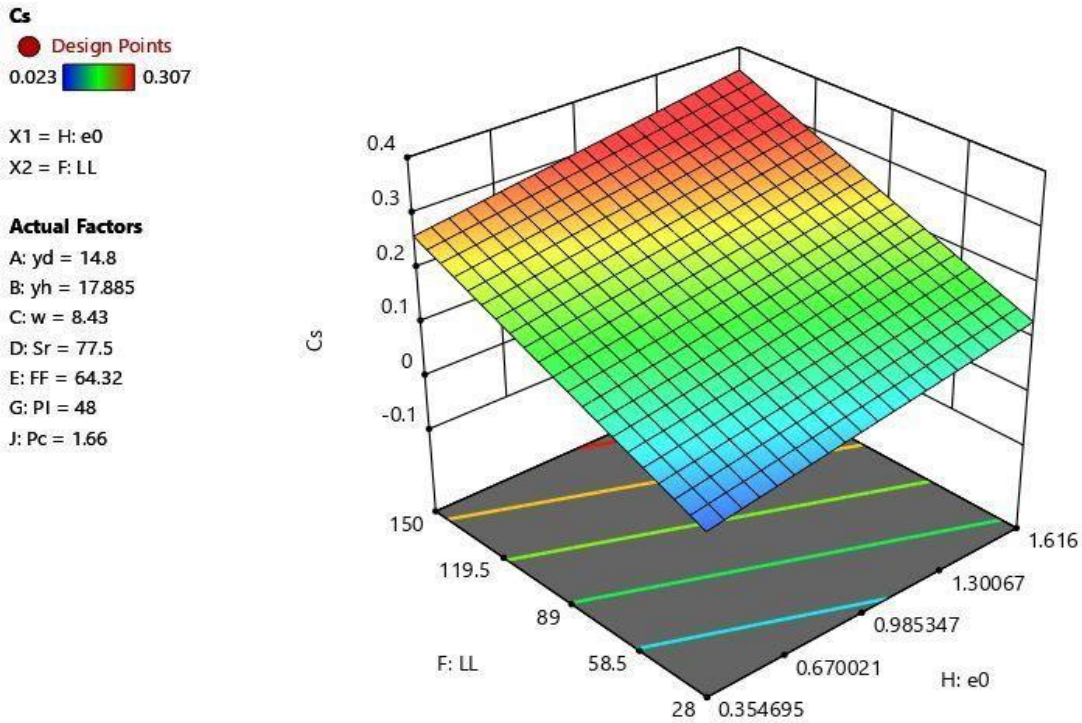


Figure 67: Response surface 3D representing the swelling index (C_s) vs liquid limit LL and void ratio e_0 .

IV.4.3. Optimisation

The experimental approach for exploring the parameter space of the process or independent variables involves employing FFD or RSM as a practical statistical modeling technique to establish a suitable approximating relationship. This relationship delineates the compressibility index (C_c) and swelling index (C_s) as the outputs responses and various input variables, including dry unit weight γ_d (kN/m^3), wet unit weight γ_h (kN/m^3), water content w (%), fine fraction F_f (%), Liquidity limits WL (%), plasticity index IP (%), void ratio e_0 , Saturation degree S_r (%) and preconsolidation pressure P_c (kg/cm^2). Optimization methods are then utilized to determine the values of the process variables that yield desirable responses. These methods identify points on the quadratic and linear response surface, whether they represent the surface's minimum or maximum. In this case, a straightforward method involves visual inspection, wherein the surfaces are analyzed to identify the design space that optimizes the entire range of response studies.

Randomly selecting a set of initial conditions to start the search for desirable outcomes can yield varying results. Conducting multiple cycles enhances the likelihood of discovering multiple local optimums, some of which may possess greater desirability than others.

The ramp display integrates individual graphs to facilitate interpretation, as depicted in Figures 68 and 69. Each ramp features a colored dot representing the factor setting or responses prediction for a particular solution. The height of the dot indicates its level of desirability.

The below optimal solutions denote the formulation that effectively maximizes the compressibility and swelling coefficients, reaching the target value of 0.594 and 0.307, also minimizes the coefficients to 0.034 and 0.02. Simultaneously, it identifies the point with minimal error transmitted to the responses. Consequently, these process conditions should exemplify robustness against slight variations in factor parameters.

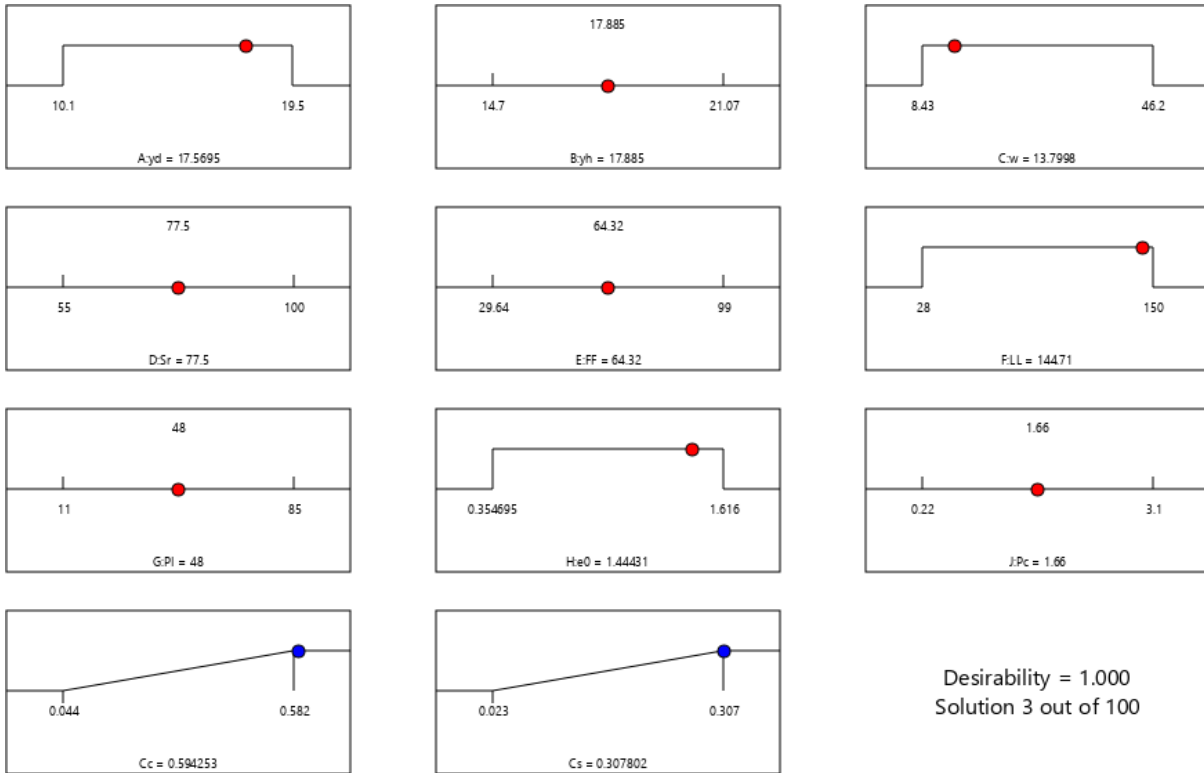


Figure 68: Maximization of the responses.

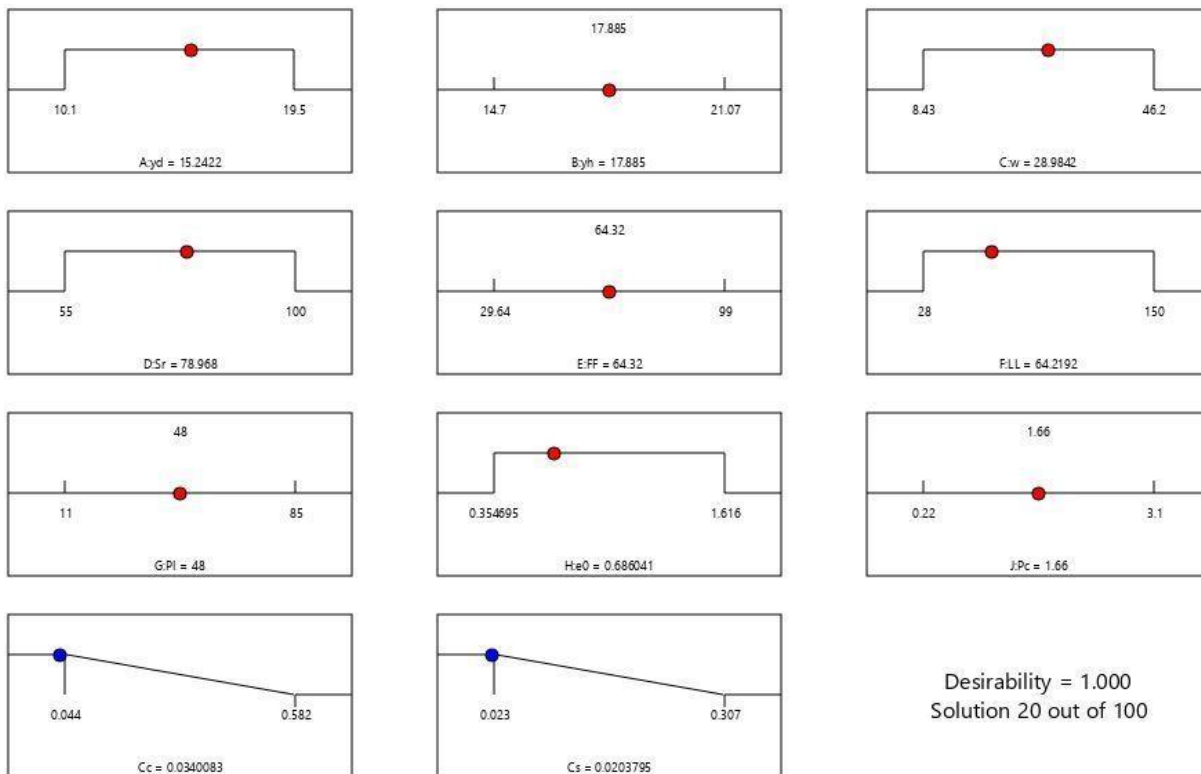


Figure 69: Minimization of the responses.

Notable observation when comparing the maximized and minimized solutions is that there are slight changes observed in all the parameters. However, it is evident that the void ratio (e_0) and liquid limit (LL %) exhibit opposing contributions to the compressibility and swelling indexes.

IV.4.4. Overconsolidation ration and preconsolidation pressure predicting

Although the equations for the C_c and C_s coefficients have been found, this is not enough, because the calculation of soil settlement does not depend only on these two coefficients, but overconsolidation (OCR) and preconsolidation pressure (P_c) must also be known. Therefore, the relationship must be found between one of the remaining coefficients and the inputs parameters.

The experiment was conducted simultaneously with nine factors at two levels which the taken response is OCR. These two levels were chosen to cover the practical range of the parameters considered (Table 31).

Table 31: Factors for response study.

<i>Factor</i>	<i>Name</i>	<i>Units</i>	<i>Low Level</i>	<i>High Level</i>
<i>A</i>	γ_d	kN/m ³	10.10	19.5
<i>B</i>	γ_h	kN/m ³	14.70	21.07
<i>C</i>	w	%	8.43	46.20
<i>D</i>	Sr	%	55.00	100.00
<i>E</i>	Ff	%	29.64	99.00
<i>F</i>	LL	%	28.00	150.00
<i>G</i>	PI	%	11.00	85.00
<i>H</i>	e_0		0.35	1.61
<i>I</i>	P_0	kPa	17.65	203.96

Starting with numerical analysis of the responses, Design-Expert offers an extensive range of response transformations. At this juncture, Design-Expert employs linear, two-factor interaction

(2FI), quadratic, and cubic polynomials to fit the response. As you can see, in table 32 the suggested models are linear and quadratic.

Table 32: Model fit summary for Cc.

Source	Model	Lack of Fit	Adjusted R ²	Predicted R ²	
	p-value	p-value			
Linear	< 0.0001	0.2497	0.8671	0.8521	Suggested
2FI	0.3735	0.2512	0.8296	0.7144	
Quadratic	0.0002	0.2716	0.8551	0.8299	Suggested
Cubic	0.2534	0.2998	0.9571		Aliased

The ANOVA results are employed to assess the impact of the constructed model and its statistically significant terms. The ANOVA analysis is conducted by testing the hypothesis of equal variance, typically at a confidence level of 95% or a significance level of 0.05. ANOVA is frequently utilized to summarize the significance test of the regression model and to assess the significance of individual model coefficients. The summary statistics for the models are presented in Tables 33 and 34.

Table 33: ANOVA for response surface quadratic model for OCR.

Source	Sum of Squares	df	Mean Square	F-value	p-value	
Model	169.07	4	42.27	163.69	< 0.0001	Significant
C- w	8.28	1	8.28	32.06	< 0.0001	
G-P0	147.16	1	147.16	569.9	< 0.0001	
EF	15.47	1	15.47	59.9	< 0.0001	
EH	12.97	1	12.97	50.21	< 0.0001	
Residual	48.55	188	0.2582			
Lack of Fit	48.53	187	0.2595	12.97	0.2184	Not Significant
Pure Error	0.02	1	0.02			
Cor Total	217.61	192				

Table 34: Regression statistics for OCR.

Std. Dev.	0.5082	R²	0.8475
Mean	2.05	Adjusted R²	0.8344
C.V. %	24.75	Predicted R²	0.8298
		Adeq Precision	61.88

For the analyzed studies, the final equation in terms of actual factors was determined, which present the overconsolidation ratio OCR from the input factors:

$$OCR = 4.8 - 0.07 * w - 0.027P0 - 0.0002 * Ff * LL + 0.03 * Ff * e0 \quad (6)$$

The equations expressed in terms of actual factors are suitable for predicting the response for specific levels of each factor. It's important to note that the levels should be defined in the original units for each factor. However, these equations should not be utilized to assess the relative impact of each factor. This is because the coefficients are scaled to accommodate the units of each factor, and the intercept is not positioned at the center of the design space.

To assess the adequacy of the adopted model, it's essential to examine if the predicted response points versus the actual values exhibit random scattering along the 45° line, as depicted in Figure 70. Such a pattern indicates that the proposed model is fitting well, and there are no apparent violations of the assumptions of independence or constant variance.

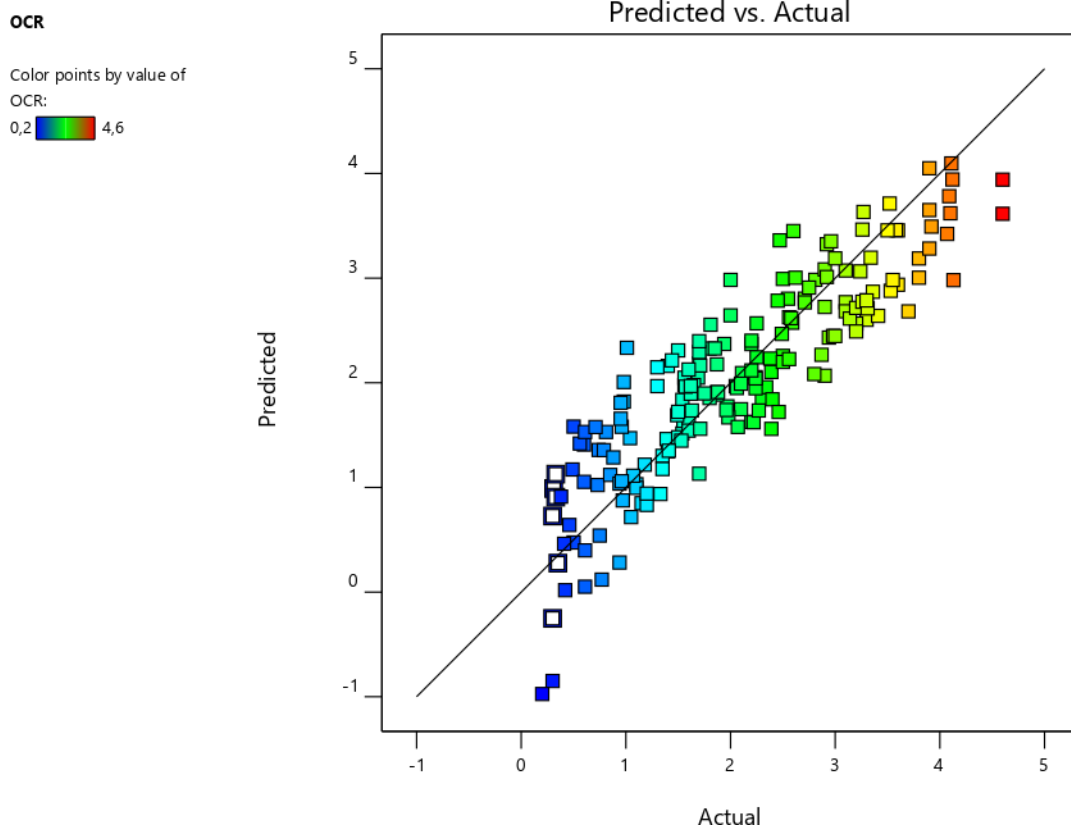


Figure 70: Predicted response versus actual for OCR.

Figure 71 and 72 showcase 3D plots representing the response surfaces, elucidating the correlation between the overconsolidation ratio (OCR) and several factors: F_f (%) and LL (%), e_0 and F_f (%). These figures effectively illustrate the interaction between two process variables as influenced by the factors under consideration.

OCR
 ● Design Points
 0.2 4.6

X1 = E: Ff
 X2 = F: LL

Actual Factors

A: yd = 14.8
 B: yh = 17.885
 C: w = 27.315
 D: Sr = 77.5
 G: PI = 48
 H: e0 = 0.985347
 J: P0 = 1.13

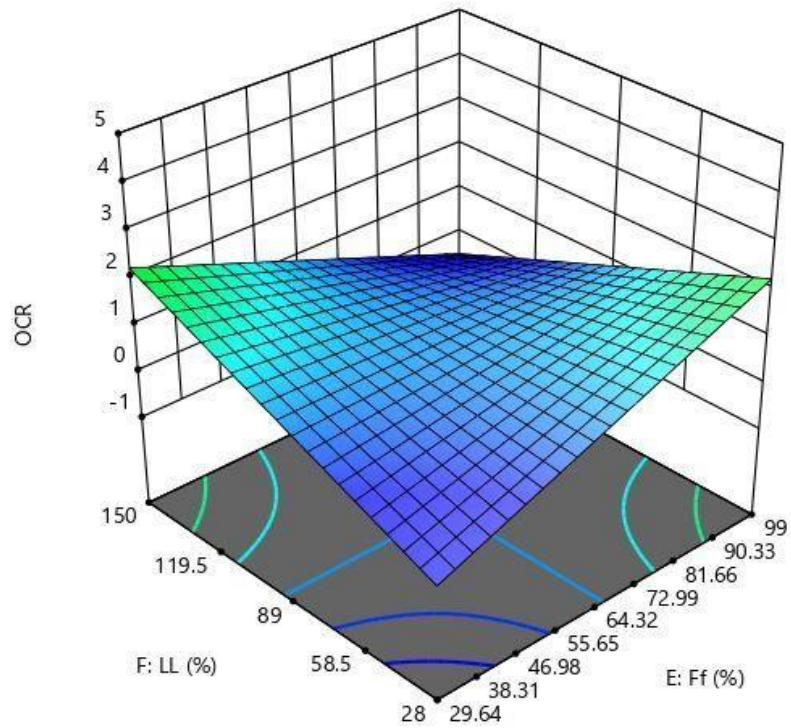


Figure 71: Response surface 3D representing the OCR vs liquid limit LL and fine friction Ff.

OCR
 ● Design Points
 0.2 4.6

X1 = E: Ff
 X2 = H: e0

Actual Factors

A: yd = 14.8
 B: yh = 17.885
 C: w = 27.315
 D: Sr = 77.5
 F: LL = 28
 G: PI = 48
 J: P0 = 0.598

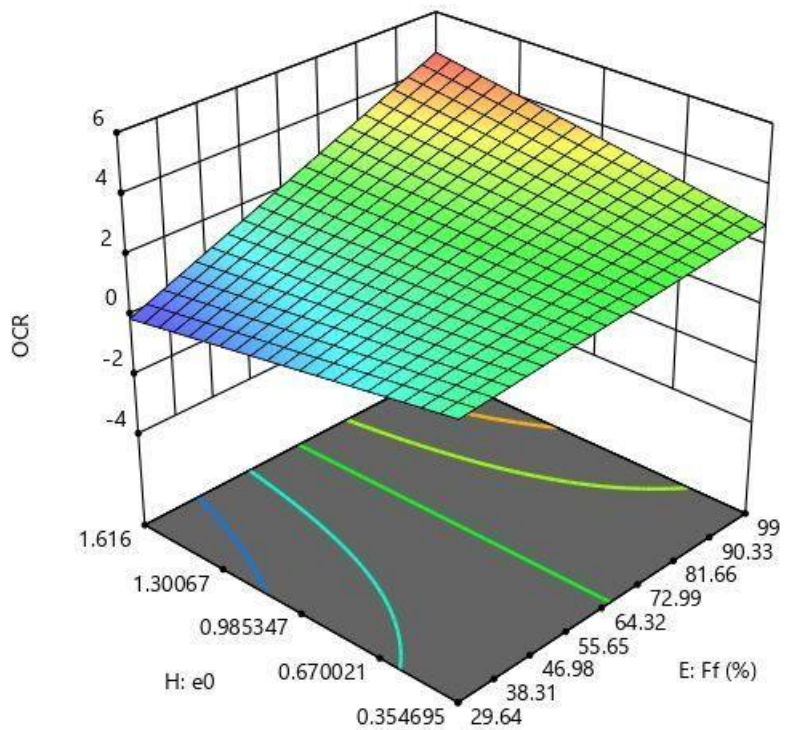


Figure 72: Response surface 3D representing the OCR vs fine friction Ff and void ratio e0.

IV.4.5. Validation of the equations

Focus on the validation of the derived equations for compression, swelling indexes and overconsolidation ratio through a comprehensive comparison with experimental results obtained from laboratory tests and numerical simulations performed using PLAXIS 3D software. The primary objective is to ensure the reliability and accuracy of the proposed equations by comparing them with empirical data and advanced computational models. Initially, we will outline the experimental procedures and results, followed by a detailed application of the equations to these experimental conditions. Subsequently, numerical simulations will be conducted using PLAXIS 3D, replicating the laboratory test scenarios to generate theoretical predictions. Finally, a comparative analysis will be presented, highlighting the consistency and discrepancies among the laboratory tests, analytical equations, and numerical simulations.

After using equations (2) and (3) from compression and recompression indexes and equation (6) for overconsolidation ratio, the obtained results are in table 35.

Table 35: Obtained results from the equations

Sample N°	1	2
Compression index –Cc-	0.267	0.358
Recompression index –Cs-	0.113	0.136
Overconsolidation ratio -OCR-	3.27	3.87
Preconsolidation pressure -Pc- (kPa)	114.45	154.8

Where:

- Sample 1:

$$C_c = 0.627 - 0.05 * 16.47 - 0.029 * 16.23 + 0.0053 * 74.5 + 0.0018 * 66.2 + 0.65 * 0.646 = 0.267$$

$$C_s = 0.042 - 0.01 * 16.47 - 0.009 * 16.23 + 0.0017 * 74.5 + 0.0018 * 66.2 + 0.21 * 0.646 = 0.113$$

$$OCR = 4.8 - 0.07 * 16.23 - 0.027 * 35 - 0.0002 * 90 * 66.2 + 0.03 * 90 * 0.646 = 3.27$$

$$P_c = OCR * P_0 = 3.27 * 35 = 114.5 \text{ kPa}$$

- Sample 2:

$$C_c = 0.627 - 0.05 * 17.75 - 0.029 * 14.66 + 0.0053 * 68.5 + 0.0018 * 63.8 + 0.65 * 0.87 = 0.358$$

$$C_s = 0.042 - 0.01 * 17.75 - 0.009 * 14.66 + 0.0017 * 68.5 + 0.0018 * 63.8 + 0.21 * 0.87 = 0.136$$

$$OCR = 4.8 - 0.07 * 14.66 - 0.027 * 40 - 0.0002 * 88 * 63.8 + 0.03 * 88 * 0.87 = 3.87$$

$$P_c = OCR * P_0 = 3.87 * 40 = 154.8 \text{ kPa}$$

Table 36: Comparison between calculated and predicted results.

	Cc		Cs		OCR		Pc	
	Calc	Pred	Calc	Pred	Calc	Pred	Calc	Pred
Sample 1	0.282	0.267	0.107	0.113	3.43	3.27	120	114.5
Sample 2	0.371	0.358	0.126	0.136	4	3.87	160	154.8

There is only a slight difference between the two results, as the difference does not exceed 5 percent (± 5).

IV.4.5.1. Settlement calculation

Since both samples are OCC, we suppose that $\Delta P = 150 \text{ kPa}$, which is will be the second condition because $P_0 + \Delta P > P_c$, so the settlement will be:

$$S = \frac{(C_s \cdot H)}{(1 + e)} \log\left(\frac{P_c}{P_0}\right) + \frac{(C_c \cdot H)}{(1 + e)} \log\left(\frac{P_0 + \Delta P}{P_c}\right)$$

Where, H is the layer's thickness, and e is the initiale void ratio.

After using the settlement equation with the calculated and predicted parameters, the settlement results is presented in table 37.

Table 37: Settlement results.

N°	Sample 1	Sample 2
Settlement with calculated parameters (cm)	13.3	10.6
Settlement with predicted parameters (cm)	13.8	11.3

The difference in settlement is a few millimeters, and this is considered negligible.

IV.4.5.2. Plaxis Modeling

PLAXIS 3D is a sophisticated and powerful software tool, widely used in geotechnical engineering for the analysis of soil mechanics and much more. It provides advanced capabilities for simulating the behavior of soil structures under various conditions, including static and dynamic loading, excavation and many.

IV.4.5.2.1. Data Introduction

The geometry is 2 meters of the layer thickness and vertical load applied on a surface 8*8 meter (The average social housing is set at 63.5 m² plus or minus 1.5%).

IV.4.5.2.1.1. The geometric model

Before everything, we need to look at the general settings and we choose what is consistent with the case studied. (Figure 73).

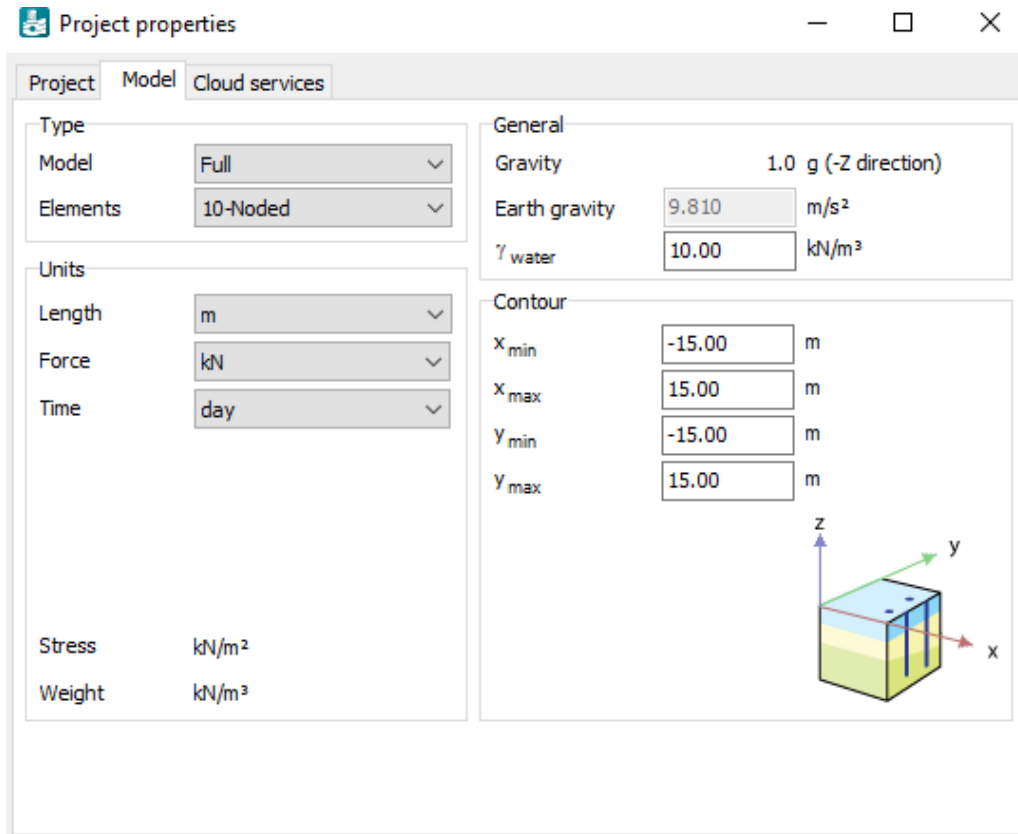


Figure 73: General settings.

So, as you can see the previous figure, I will try to embody what exists in reality (what we described in data introduction part) in all its details, and you can see it on Figure 74.

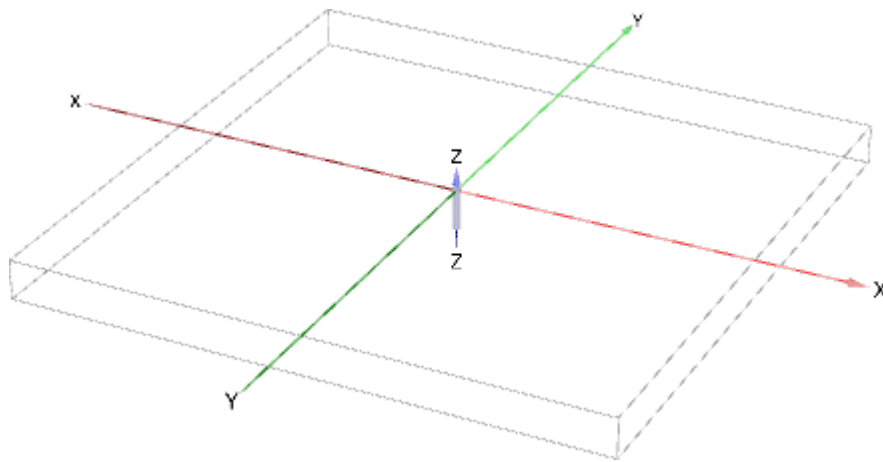



Figure 74: The geometric model.

IV.4.5.2.1.2. Material properties

The layer is modeled with soft soil model. The behavior is considered drained. The properties of the soil are taken from table 13 (Chapter 3).

Property	Unit	Value
Material set		
Identification		Clayey
Soil model		Soft Soil ▼
Drainage type		Drained ▼
Colour		 RGB 240, 155, 51
Comments		
Unit weights		
γ_{unsat}	kN/m ³	16.47
γ_{sat}	kN/m ³	20.30
Void ratio		
e_{init}		0.6460
n_{init}		0.3925

General				Mechanical				Groundwater				Interfaces				Initial			
Property		Unit		Value															
Stiffness																			
λ^* (lambda*)				0.07441															
κ^* (kappa*)				0.05646															
ν_{ur}				0.1500															
Alternatives																			
Use alternatives				<input checked="" type="checkbox"/>															
C_c				0.2820															
C_s				0.1070															
e_{init}				0.6460															
Strength																			
Shear																			
c'_{ref}		kN/m ²		50.00															
ϕ' (phi)		°		22.00															
ψ (psi)		°		0.000															

Figure 75: Material properties of the soil.

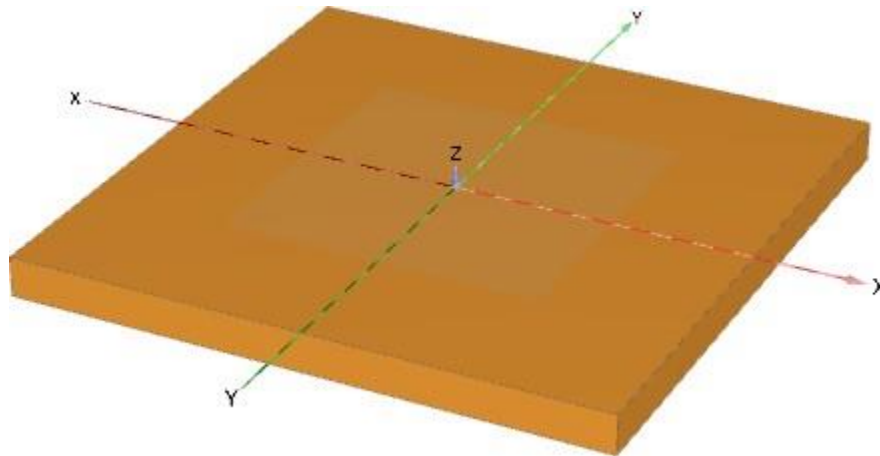


Figure 76: Model of adding material properties.

Now surface load is applied on the soil layer.

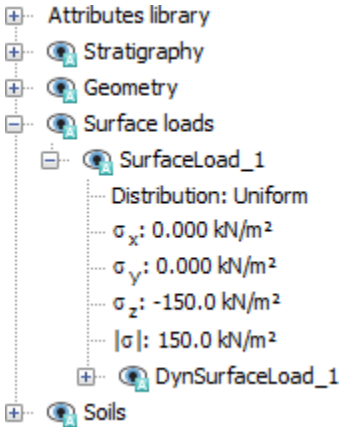


Figure 77: Surface load $\Delta P = 150\text{kPa}$.

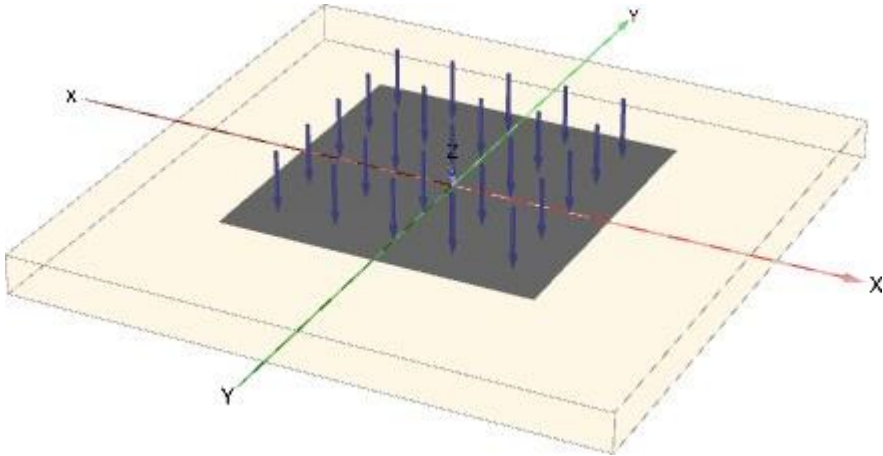


Figure 78: Surface load applied.

IV.4.5.2.2. Mesh Generation

The mesh is generated with a global coarseness set to medium. A local refinement is made. The result of the mesh generation is plotted in Figure 79.

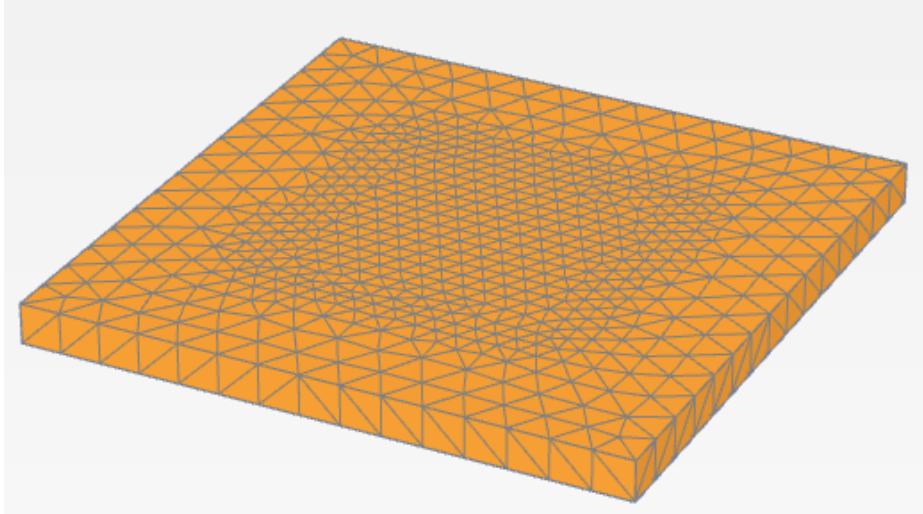


Figure 79: Mesh generation.

IV.4.5.2.3. Phasing

The analysis is composed of one calculation phase, which is applying the surface load on the soil layer

Phase 1:

1. Select plastic calculation in the general tab sheet.
2. Select the staged construction of the sheet from the settings tab.
3. Activate the surface load.

Note: you can add one more phase which can be consolidation phase and give it a specific time.

- All the previous steps are also applied for the sample 2.

IV.4.5.2.4. Output

The following results obtained after the calculation stage:

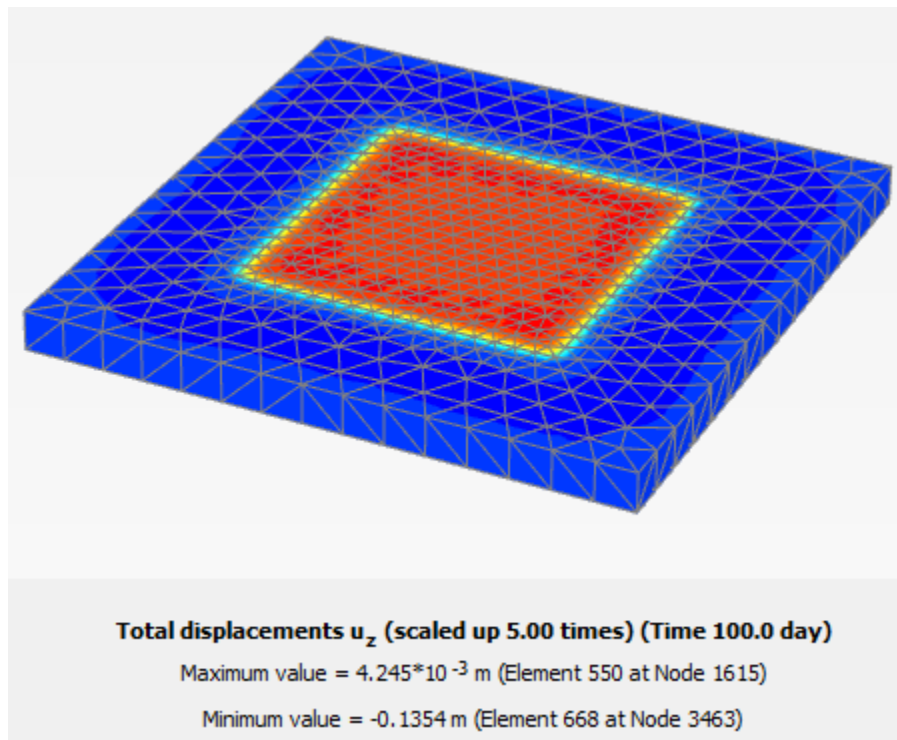


Figure 80: Vertical displacement $U_z = 13.54\text{cm}$ for sample 1.

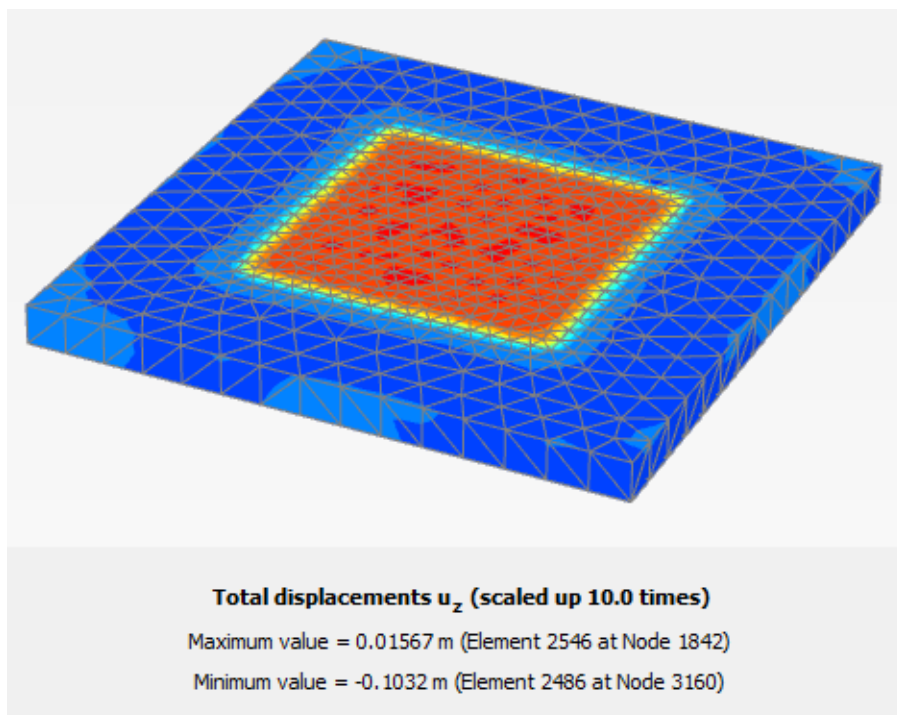


Figure 81: Vertical displacement $U_z = 10.32\text{cm}$ for sample 2.

IV.4.5.2.5. Curves

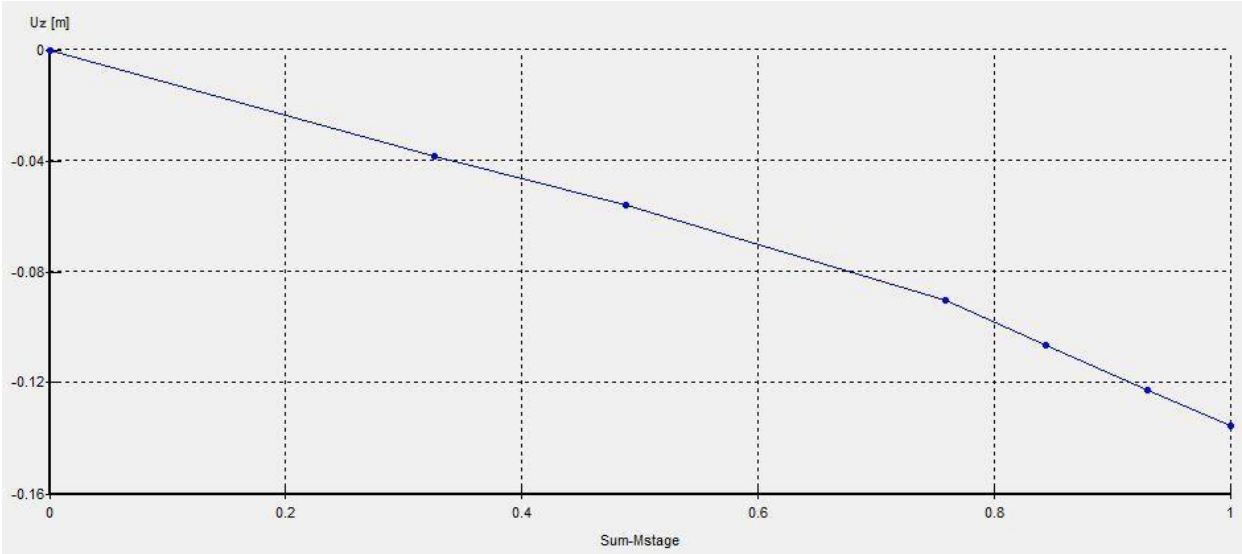


Figure 82: Vertical displacement curve for sample 1.

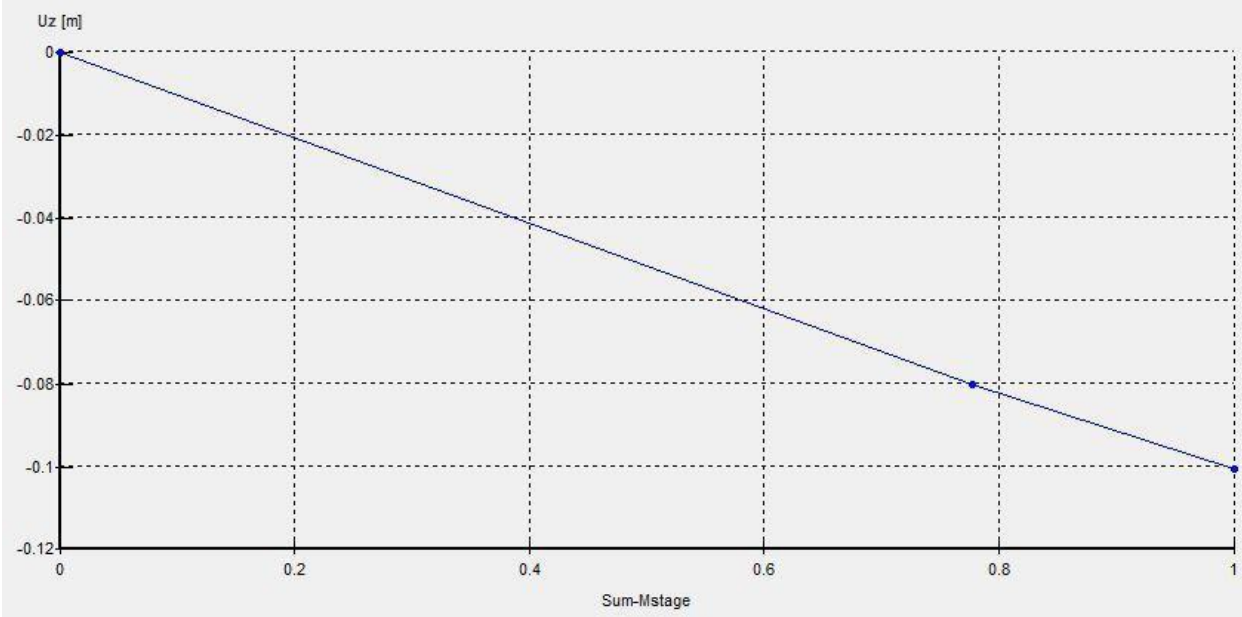


Figure 83: Vertical displacement curve for sample 2.

After modeling and simulating the case, the final settlement results is in table 38. Which represent various obtained results.

IV.4.6. Results interpretation

The study aimed to develop predictive equations for compression index, recompression index, and overconsolidation ratio using a dataset treated with Design of Experiments (DOE) software. To validate these equations, several tests were conducted on two samples from the studied area. The settlement was calculated for both cases. Additionally, a 3D Plaxis simulation was performed to further evaluate the settlement predictions. This interpretation discusses the results from the predictive equations, the experimental tests, and the Plaxis simulation, highlighting the consistency and reliability of the predictive models.

IV.4.6.1. Predictive Equations and Validation

Using the DOE software, equations were formulated to predict the compression index, recompression index, and overconsolidation ratio. These equations are essential for understanding the soil behavior under various load conditions and are critical in geotechnical engineering for predicting settlement.

To validate these equations, laboratory tests were performed on two samples from the study area. The experimental results for the compression index, recompression index, and overconsolidation ratio were compared with the values predicted by the equations. The comparison showed a high degree of correlation, indicating that the predictive models accurately represent the soil behavior.

IV.4.6.2. Settlement Analysis

Settlement calculations were performed based on both the predictive equations and the experimental test results. The settlements derived from the predictive models were consistent with those obtained from the laboratory tests, further validating the reliability of the predictive equations.

IV.4.6.3. Plaxis Simulation

To provide an additional layer of validation, a 3D Plaxis simulation was conducted. The Plaxis model simulated the same conditions and parameters as those used in the laboratory tests and predictive equations. The settlement results from the Plaxis simulation closely matched the settlements calculated from both the predictive equations and the experimental tests.

IV.4.6.4. Comparison of Results

The comparison between the results from the predictive equations, experimental tests, and 3D Plaxis simulation revealed the following:

- Compression Index: The predicted compression index values were very close to those obtained from the experimental tests and the Plaxis simulation. This consistency indicates that the predictive model for the compression index is robust and reliable.

- Recompression Index: Similar to the compression index, the recompression index values predicted by the equations matched well with the experimental and simulation results, demonstrating the accuracy of the predictive model.

- Overconsolidation Ratio: The predictive model for the overconsolidation ratio showed excellent agreement with the experimental results and the Plaxis simulation, confirming its validity.

- Settlement: The settlement calculations from all three approaches (predictive equations, experimental tests, and Plaxis simulation) were in close agreement, providing strong evidence that the predictive equations are capable of accurately estimating settlement.

Table 38: Finale settlement results.

N°	Sample 1	Sample 2
Settlement with calculated parameters (cm)	13.3	10.6
Settlement with predicted parameters (cm)	13.8	11.3
Settlement with 3D Plaxis	13.5	10.3

IV.5. Conclusion

In this study, Design of Experiments (DOE) has been utilized for the development and optimization of the compressibility index (Cc), recompression index (Cs) and overconsolidation ratio (OCR) as outputs process function. This involved employing a matrix consisting of various input parameters, including dry unit weight (γ_d) in kN/m³, wet unit weight (γ_h) in kN/m³, water

content (w) in percentage, saturation degree (S_r) in percentage, fine fraction (F_f) in percentage, Liquidity limits (LL) in percentage, plasticity index (PI) in percentage, initial void ratio (e_0), preconsolidation pressure (P_c) in kg/cm² and pressure in field P_0 in kPa. For this geotechnical hazards case study, focusing on an important output parameters, can help engineers to calculate the settlement of fine-grained soil. Additionally, the DOE enables the establishment of various correlations among the input parameters. These correlations are easily derived from laboratory tests, aiding in understanding their effects on the response parameter.

The study successfully developed and validated predictive equations for the compression index, recompression index, and overconsolidation ratio. The close agreement between the results from the predictive models, experimental tests, and 3D Plaxis simulation indicates that the equations are reliable and accurate for predicting soil behavior in the studied area. This validation confirms that the predictive equations can be confidently used in geotechnical engineering applications to estimate settlement and other critical parameters, providing a valuable tool for future projects in similar soil conditio

General conclusion

This study investigated the compressibility of clayey soils in Tebessa province, focusing on understanding soil behavior and its implications for engineering projects. Through empirical testing, statistical analysis, and numerical modeling, valuable insights were gained into soil properties and compression indices evaluation. Various tests were conducted to measure physical and mechanical soil properties such as dry and wet unit weights, water content, degree of saturation, Atterberg limits, fine fraction, void ratio, preconsolidation pressures, compression index (C_c), swelling or recompression index (C_s), overconsolidation ratio (OCR); providing essential data for understanding soil behavior under different conditions. Statistical methods embedded under the design of experiment methodology such as Full Factorial Design (FFD) and Response Surface Methodology (RSM) were used to develop and optimize predictive models for soil compression indices and overconsolidation ratio yielded high correlation coefficients (R^2) for compression indices (C_c and C_s) and OCR, related to liquid limits, void ratio and unit weights and vertical in-situ stress. The high correlation coefficients obtained demonstrate the accuracy of these models in predicting parameters and estimating soil settlement. Numerical simulations using 3D Plaxis software confirmed the validity of the predictive models, with settlement results closely matching both calculated and predicted parameters, validating the accuracy of the models. The findings have practical implications for engineering practice, enabling engineers to anticipate and mitigate settlement issues in construction projects. The identification of preconsolidation pressure through OCR values enhances soil stability assessment and foundation design. In conclusion, this study contributes to advancing knowledge in geotechnical engineering and provides practical tools for addressing settlement issues in construction projects, achieving a comprehensive approach to understanding and predicting soil compressibility.

This study yielded several key findings regarding the compressibility of clayey soils in Tebessa province.

Statistical Analysis and Modeling Results:

- Full Factorial Design (FFD) and Response Surface Methodology (RSM) yielded high correlation coefficients (R^2) for compression indices (C_c and C_s) and OCR.

- Predictive models derived from FFD and RSM showed promising accuracy in predicting soil behavior.
- The validation of these models through numerical simulations confirmed their reliability in predicting settlement behavior.

Numerical Modeling Results:

- Settlement results obtained from numerical simulations closely aligned with both calculated and predicted parameters, validating the accuracy of the predictive models.
- Settlement values ranged from 10.3 cm to 13.8 cm, indicating variations in settlement behavior across different soil samples.

These findings provide valuable insights into the compressibility of clayey soils in Tebessa province and lay the foundation for improved engineering practices in construction projects in the region.

References

- [1] Abdi, H., & Williams, L. J. (2010). Principal component analysis. *Wiley interdisciplinary reviews: computational statistics*, 2(4), 433-459.
- [2] Alzabeebee, S., & Al-Taie, A. (2022). Development of new models to predict the compressibility parameters of alluvial soils. *Geomech Eng*, 30, 437-448.
- [3] Akan, R., Keskin, S. N., & Uzundurukan, S. (2015). Multiple regression model for the prediction of unconfined compressive strength of jet grout columns. *Procedia Earth and Planetary Science*, 15, 299-303.
- [4] Arjwech, R., Somchat, K., Pondthai, P., Everett, M., Schulmeister, M., & Saengchomphu, S. (2020). Assessment of geological, hydrogeological and geotechnical characteristics of a proposed waste disposal site: A case study in Khon kaen, Thailand. *Geosciences*, 10(3), 109.
- [5] Ameratunga, J., Sivakugan, N., & Das, B. M. (2016). Correlations of soil and rock properties in geotechnical engineering.
- [6] Balasubramaniam, A. S., & Brenner, R. P. (1981). Consolidation and settlement of soft clay.
- [7] Balasubramani, A., Dasgupta, S., & Freund, Y. (2013). The fast convergence of incremental PCA. *Advances in neural information processing systems*, 26.
- [8] Been, K., & Sills, G. C. (1981). Self-weight consolidation of soft soils: an experimental and theoretical study. *Geotechnique*, 31(4), 519-535.
- [9] Benz, T., & Nordal, S. (2010). *Numerical methods in geotechnical engineering*. Boca Raton, FL: CRC Press.
- [10] Berrah, Y., Chegrouche, A., Brahmi, S., & Boumezbeur, A. (2022). Land clayey deposits compressibility investigation using principal component analysis and multiple regression tools. *Geomatics, Landmanagement and Landscape*, (4).
- [11] Beattie, J. R., & Esmonde-White, F. W. (2021). Exploration of principal component analysis: deriving principal component analysis visually using spectra. *Applied Spectroscopy*, 75(4), 361-375.
- [12] Budhu, M. (2010). *Soil mechanics and foundations*. John Wiley and Sons.

- [13] Bouzenoune A. (1993). Peridiapiric mineralization of the Aptian limestone: iron carbonates from the hematite deposit of Ouenza (Eastern Algeria). Doctoral thesis, University Paris VI, 209 p.
- [14] Das, B. M., & Sobhan, K. (2012). Principles of geotechnical engineering, 8th Edition.
- [15] Durakovic, B. (2017). Design of experiments application, concepts, examples: State of the art. Periodicals of Engineering and Natural Sciences, 5(3).
- [16] Dubourdieu G. (1956). Geological study of the Ouenza region (Algerian-Tunisian borders). Publications of the geological map service of Algeria, Algiers, N.S., 10, 659 p.
- [17] Elhaik, E. (2022). Principal component analyses (PCA)-based findings in population genetic studies are highly biased and must be reevaluated. Scientific Reports, 12(1), 14683.
- [18] Emerson, R. W., & Cavazzuti, M. (2017). Design of Experiments. Design for Six Sigma: a practical approach through innovation.
- [19] Erzin, Y., MolaAbasi, H., Kordnaeij, A., & Erzin, S. (2020). Prediction of compression index of saturated clays using robust optimization model. Journal of Soft Computing in Civil Engineering, 4(3), 1-16.
- [20] Fathi, B., & Smail, B. (2021). Contribution to the estimation of current reserves of the Tebessa-Morsott-NE Algerian aquifer complex (Doctoral dissertation, Larbi Tebessi Tebessa University).
- [21] Fox, G. A., & Metla, R. (2005). Soil property analysis using principal components analysis, soil line, and regression models. Soil Science Society of America Journal, 69(6), 1782-1788.
- [22] Gunduz, Z., & Arman, H. (2007). Possible relationships between compression and recompression indices of a low-plasticity clayey soil. Arabian Journal for science and engineering, 32(2), 179.
- [23] Hemaili I. (2020). Updates of hydrogeological and hydrochemical data from the Tebessa-Morsott watershed, Larbi Tebessi university- Tebessa.
- [24] Hüeber, S. (2008). Discretization techniques and efficient algorithms for contact problems.

- [25] Ivosev, G., Burton, L., & Bonner, R. (2008). Dimensionality reduction and visualization in principal component analysis. *Analytical chemistry*, 80(13), 4933-4944.
- [26] Jackson, J. E. (2005). *A user's guide to principal components*. John Wiley & Sons.
- [27] Khan, M. I., & Wang, S. (2021). Slope Stability Analysis to Develop Correlations between Different Soil Parameters and Factor of Safety Using Regression Analysis. *Polish Journal of Environmental Studies*, 30(5).
- [28] Kim, Y., Nam, B. H., Park, K. W., Shamet, R., & Horhota, D (2022). Estimation of Soils' Compression and Recompression Index Using Soil Index Properties—Florida Case Study. In *Geo-Congress* (pp. 92-102).
- [29] Kurnaz, T. F., Dagdeviren, U., Yildiz, M., & Ozkan, O. (2016). Prediction of compressibility parameters of the soils using artificial neural network. *SpringerPlus*, 5, 1-11.
- [30] Kurmi, P., Rai, H. K., Patel, R., Pandey, R., Agrawal, K., & Raghuwanshi, S. Prediction of related Soil Properties using Empirical Modelling Approach in Vertisols.
- [31] Kumar, V., Singh, K. P., Mangaraj, S., Chandel, N. S., Kumar, M., & Singh, K. (2023). Study of Advanced Techniques to Predict the Soil Properties. *Int. J. Environ. Clim. Change*, 13(5), 69-74.
- [32] LaValley, M. P. (2008). Logistic regression. *Circulation*, 117(18), 2395-2399.
- [33] Le, T. H., & Shin, S. (2018). A literature review on RSM-based robust parameter design (RPD): Experimental design, estimation modeling, and optimization methods. *Journal of Korean Society for Quality Management*, 46(1), 39-74.
- [34] Legget, R. F. (1979). Geology and geotechnical engineering. *Journal of Geotechnical and Geoenvironmental Engineering*, 105(ASCE 1444 Conf Paper).
- [35] Long, T., He, B., Ghorbani, A., & Khatami, S. M. H. (2023). Tree-Based Techniques for Predicting the Compression Index of Clayey Soils. *Journal of Soft Computing in Civil Engineering*, 7(3), 52-67.

- [36] Masse J.P. & Chikhi-Aouimeur F. (1982). The Ouenza carbonate platform (South Constantine, Algeria). Organization and dynamics during the Upper Aptian. Geol. Mediate, Marseille, Vol, IX, n°3, p 259-267.
- [37] Montgomery, D. C. (2017). Design and analysis of experiments. John Wiley & sons.
- [38] Myers, R. H., Montgomery, D. C., & Anderson-Cook, C. M. (2016). Response surface methodology: process and product optimization using designed experiments. John Wiley & Sons.
- [39] Naqvi, M. W., Kc, D., & Hu, L. (2023). Numerical Modelling and Sensitivity Analysis of the Pitztal Valley Debris Flow Event. Geosciences, 13(12), 378.
- [40] Niedoba, T. (2014). Multi-parameter data visualization by means of principal component analysis (PCA) in qualitative evaluation of various coal types. physicochemical problems of Mineral processing, 50(2), 575-589.
- [41] Ostertagová, E. (2012). Modelling using polynomial regression. Procedia Engineering, 48, 500-506.
- [42] Potts, D. M., Zdravković, L., Addenbrooke, T. I., Higgins, K. G., & Kovačević, N. (2001). Finite element analysis in geotechnical engineering: application (Vol. 2, p. 427). London: Thomas Telford.
- [43] Razmyar, A., & Eslami, A. (2017). Geotechnical characterization of soils in the eastern and western areas of tehran. Engineering, Technology & Applied Science Research, 7(4), 1802-1810.
- [44] Stewart, G. W. (1993). On the early history of the singular value decomposition. SIAM review, 35(4), 551-566.
- [45] Schölkopf, B., Smola, A., & Müller, K. R. (1997, October). Kernel principal component analysis. In International conference on artificial neural networks (pp. 583-588). Berlin, Heidelberg: Springer Berlin Heidelberg.
- [46] Scholz, M. (2012). Validation of nonlinear PCA. Neural processing letters, 36, 21-30.
- [47] Shahabadi, S. M. S., & Reyhani, A. (2014). Optimization of operating conditions in ultrafiltration process for produced water treatment via the full factorial design methodology. *Separation and Purification Technology*, 132, 50-61.

- [48] Smith, D. K. (2021). The Role of Hydrogeological Investigation in Geotechnical Engineering. *Science Insights*, 37(4), 288-291.
- [49] Tang, K., Wang, J., & Li, L. (2020). A prediction method based on Monte Carlo simulations for finite element analysis of soil medium considering spatial variability in soil parameters. *Advances in Materials Science and Engineering*, 2020, 1-10.
- [50] Telford, J. K. (2007). A brief introduction to design of experiments. *Johns Hopkins apl technical digest*, 27(3), 224-232.
- [51] Villa, A., Carrión García, A., & San Matías Izquierdo, S. (2012). Modeling response variables in Taguchi design parameters using CART and random forest based systems. *Communications in Dependability and Quality Management*, 15(4), 5-15.
- [52] Vinod, P., & Bindu, J. (2010). Compression index of highly plastic clays—an empirical correlation. *Indian Geotechnical Journal*, 40(3), 174-180.
- [53] Yu, J., Kim, J. E., Lee, J. H., & Kim, T. W. (2021). Development of a PCA-based vulnerability and copula-based hazard analysis for assessing regional drought risk. *KSCE Journal of Civil Engineering*, 25(5), 1901-1908.
- [54] Yune, C. Y., & Olgun, C. G. (2016). Analysis of consolidation settlement of normally consolidated soil by layering under 3D conditions. *KSCE Journal of Civil Engineering*, 20, 2280-2288.
- [55] Zienkiewicz, O. C., & Taylor, R. L. (2005). *The finite element method for solid and structural mechanics*. Elsevier.
- [56] Zou, K. H., Tuncali, K., & Silverman, S. G. (2003). Correlation and simple linear regression. *Radiology*, 227(3), 617-628.